



**DIAGENETIC EFFECTS AT EROSIONAL BOUNDARIES IN THE TRIASSIC WOLFVILLE  
FORMATION AT RAINY COVE, NOVA SCOTIA**

**Erin Anderson**

SUBMITTED IN PARTIAL FULFILLMENT OF THE REQUIREMENTS FOR  
THE DEGREE OF BACHELOR OF SCIENCES, HONOURS  
DEPARTMENT OF EARTH SCIENCES  
DALHOUSIE UNIVERSITY, HALIFAX, NOVA SCOTIA

April 2017

## Distribution License

DalSpace requires agreement to this non-exclusive distribution license before your item can appear on DalSpace.

### NON-EXCLUSIVE DISTRIBUTION LICENSE

You (the author(s) or copyright owner) grant to Dalhousie University the non-exclusive right to reproduce and distribute your submission worldwide in any medium.

You agree that Dalhousie University may, without changing the content, reformat the submission for the purpose of preservation.

You also agree that Dalhousie University may keep more than one copy of this submission for purposes of security, back-up and preservation.

You agree that the submission is your original work, and that you have the right to grant the rights contained in this license. You also agree that your submission does not, to the best of your knowledge, infringe upon anyone's copyright.

If the submission contains material for which you do not hold copyright, you agree that you have obtained the unrestricted permission of the copyright owner to grant Dalhousie University the rights required by this license, and that such third-party owned material is clearly identified and acknowledged within the text or content of the submission.

If the submission is based upon work that has been sponsored or supported by an agency or organization other than Dalhousie University, you assert that you have fulfilled any right of review or other obligations required by such contract or agreement.

Dalhousie University will clearly identify your name(s) as the author(s) or owner(s) of the submission, and will not make any alteration to the content of the files that you have submitted.

If you have questions regarding this license please contact the repository manager at [dalspace@dal.ca](mailto:dalspace@dal.ca).

Grant the distribution license by signing and dating below.

---

Name of signatory

---

Date





Department of Earth Sciences  
Halifax, Nova Scotia  
Canada B3H 4R2  
(902) 494-2358

DATE: 28 April 2017

AUTHOR: Erin Anderson

TITLE: Diagenetic effects at erosional boundaries in the Triassic Wolfville Formation at Rainy Cove, Nova Scotia

Degree: B. Sc. Honours Earth Sciences      Convocation: May      Year: 2017

Permission is herewith granted to Dalhousie University to circulate and to have copied for non-commercial purposes, at its discretion, the above title upon the request of individuals or institutions.

**Redacted for Privacy**

---

Signature of Author

THE AUTHOR RESERVES OTHER PUBLICATION RIGHTS, AND NEITHER THE THESIS NOR EXTENSIVE EXTRACTS FROM IT MAY BE PRINTED OR OTHERWISE REPRODUCED WITHOUT THE AUTHOR'S WRITTEN PERMISSION.

THE AUTHOR ATTESTS THAT PERMISSION HAS BEEN OBTAINED FOR THE USE OF ANY COPYRIGHTED MATERIAL APPEARING IN THIS THESIS (OTHER THAN BRIEF EXCERPTS REQUIRING ONLY PROPER ACKNOWLEDGEMENT IN SCHOLARLY WRITING) AND THAT ALL SUCH USE IS CLEARLY ACKNOWLEDGED.

## Abstract

Fluid flow and reservoir quality are affected by lithologic heterogeneities that cause permeability changes in sedimentary successions. Determining the style and timing of cementation within siliciclastic sedimentary outcrops is of paramount importance when addressing the controls on lithologic heterogeneity. This is important in ancient fluvial deposits since they often form aquifers and hydrocarbon reservoirs.

At Rainy Cove (Minas Basin, Nova Scotia), lithological heterogeneity in the siliciclastic sedimentary successions of the Upper Triassic Wolfville Formation is expressed by the preferential erosion and preservation of the coastline. I hypothesize that observed variations in erosion at the study location were a result of differences in cementation texture between sandstone lithofacies. To test my hypothesis, I investigate the lithologic characteristics (measured sections, facies analysis, gamma ray and permeability measurements) and cementation textures (microscopy and cathodoluminescence) in a series of coarse-grained, vertically stacked alluvial and fluvial successions from the Wolfville Formation. The discussion on the cause of lithological heterogeneity can be expanded to address fluid flow and reservoir quality.

Six lithofacies were identified: (F1) matrix-supported clastic breccias from alluvial debris flows, (F2) clast to matrix supported conglomerates, (F3) pebbly to clean sandstones, (F4) silty sandstones, (F5) clays, and (F6) paleosols. All lithofacies are cemented by carbonate with blocky, granular, and dogtooth textures and exhibit dull cathodoluminescence. Cements are interpreted to have precipitated in a burial diagenetic environment. The samples have relatively low permeability, ranging from 32.78 to 276.53 mD. The cements have the same overall characteristics between samples and the observed textures are not limited to any single lithofacies. This suggests that cementation style is not the main control on the differential preservation of outcrop sections at Rainy Cove. Pervasive cementation contributes to the poor reservoir quality of the Wolfville Formation at Rainy Cove.

Key words: Wolfville Formation, Rainy Cove, Triassic, fluvial braided channel systems, carbonate cementation, reservoir quality.

## Table of Contents

<b>Abstract .....</b>	<b>ii</b>
<b>Table of Contents .....</b>	<b>iii</b>
<b>List of Figures .....</b>	<b>v</b>
<b>List of Tables .....</b>	<b>vii</b>
<b>Acknowledgements.....</b>	<b>viii</b>
<b>Chapter 1: Introduction .....</b>	<b>1</b>
<b>1.1 Statement of Problem .....</b>	<b>1</b>
<b>1.2 Scope of Project .....</b>	<b>2</b>
<b>1.3 Previous Research .....</b>	<b>2</b>
<b>Chapter 2: Geologic Background.....</b>	<b>5</b>
<b>2.1 Study Location .....</b>	<b>5</b>
<b>2.2 Regional Setting .....</b>	<b>5</b>
<b>2.3 Fundy Basin Tectonic Setting.....</b>	<b>6</b>
<b>2.4 Stratigraphy .....</b>	<b>10</b>
2.4.1 Stratigraphic Descriptions .....	10
2.4.2 Sequence Stratigraphy .....	13
<b>2.5 Fluvial Channel Deposits .....</b>	<b>16</b>
<b>2.6 Hierarchy of Sedimentary Structures .....</b>	<b>18</b>
<b>2.7 Sediment Paragenesis .....</b>	<b>18</b>
<b>Chapter 3: Methods .....</b>	<b>21</b>
<b>3.1 Sample Collection.....</b>	<b>21</b>
<b>3.2 Measured Section Logs.....</b>	<b>23</b>
<b>3.3 Gamma Ray Spectrometer Measurements .....</b>	<b>25</b>
<b>3.4 Hand Held Permeameter Measurements.....</b>	<b>26</b>
<b>3.5 Thin Section Microscopy.....</b>	<b>29</b>
<b>3.6 Cathodoluminescence .....</b>	<b>30</b>
<b>Chapter 4: Results .....</b>	<b>32</b>
<b>4.1 Lithofacies descriptions.....</b>	<b>32</b>
<b>4.2 Measured Sections .....</b>	<b>37</b>

<b>4.3 Gamma Scintillometer Readings.....</b>	<b>43</b>
<b>4.4 Permeability.....</b>	<b>46</b>
<b>4.5 Grain Size Measurements.....</b>	<b>47</b>
<b>4.6 Cement Textures .....</b>	<b>49</b>
<b>4.7 Cathodoluminescence Photomicrographs.....</b>	<b>55</b>
<b>Chapter 5: Discussion .....</b>	<b>57</b>
<b>5.1 Lithologic Characteristics.....</b>	<b>57</b>
<b>5.2 Carbonate Cementation .....</b>	<b>58</b>
5.2.1 Cementation Environment.....	58
5.2.2 Impact of Cementation on Erosion .....	62
<b>5.3 Fluid Flow Implications.....</b>	<b>62</b>
<b>5.4 Reservoir Quality Implications.....</b>	<b>64</b>
<b>5.5 Hydrocarbon Producing Analogue for a Braided Channel System .....</b>	<b>64</b>
<b>Chapter 6: Conclusions .....</b>	<b>67</b>
<b>6.1 Conclusions .....</b>	<b>67</b>
<b>6.2 Recommendations and Future Work .....</b>	<b>68</b>
<b>References .....</b>	<b>70</b>
<b>Appendix.....</b>	<b>74</b>

## List of Figures

<i>Figure 1.1. (a) Satellite image of Nova Scotia with the location of Rainy Cove marked by white star and (b) Satellite image of Rainy Cove with outcrop of interest marked.</i> .....	2
<i>Figure 2.1. (a) Satellite image of Rainy Cove field work location, (b) N-S outcrop section at Rainy Cove), and (c) E-W outcrop section of incised channel at Rainy Cove.</i> .....	6
<i>Figure 2.2. Map of the Fundy Basin, made up of the Fundy, Chignecto, and Minas Subbasins.</i> .....	7
<i>Figure 2.3. Paleogeographic reconstruction of the Atlantic margin in (a) the mid-Triassic and (b) the mid-Jurassic.</i> ...	7
<i>Figure 2.4. Map of the Eastern North American rift system, divided into Southern, Central, and Northern segments.</i> .	9
<i>Figure 2.5. Diagram of Steer's Head sedimentary basin geometry.</i> .....	10
<i>Figure 2.6. Fluvial-eolian system interaction in rift basins.</i> .....	12
<i>Figure 2.7. Geologic map and cross section of the Fundy Basin stratigraphy.</i> .....	14
<i>Figure 2.8. Fundy Basin stratigraphic column.</i> .....	15
<i>Figure 2.9. Schematic diagram of common fluvial channel morphologies.</i> .....	17
<i>Figure 2.10. Suggested paragenesis of diagenetic events in the Wolfville Formation at Rainy Cove, Nova Scotia.</i> .....	20
<i>Figure 3.1. Field work in Fall 2016.</i> .....	21
<i>Figure 3.2. Sample collection with chisel and hammer</i> .....	21
<i>Figure 3.3. Rainy Cove outcrop with major bounding surfaces and sample locations</i> .....	22
<i>Figure 3.4. Example of a grain card used to estimate grain size, shape, and sorting in the field.</i> .....	23
<i>Figure 3.5. Ruler held next to outcrop for measured section work, Fall 2016.</i> .....	23
<i>Figure 3.6. Wentworth grain-size scale chart for sediments</i> .....	24
<i>Figure 3.7. GEORADiS GT-40 Multipurpose Gamma Ray Spectrometer.</i> .....	26
<i>Figure 3.8. TinyPerm II handheld permeameter and data reporting screen from New England Research.</i> .....	28
<i>Figure 3.9. New England Research permeability calibration chart used to correlate TinyPerm II values to permeability values.</i> .....	28
<i>Figure 3.10. (left) Dalhousie University Basin and Reservoir Lab Olympus BX51 microscope and (right) University of Calgary Nikon 50iPOL microscope.</i> .....	29
<i>Figure 3.11. Acadia University Reliotron cold-cathode CL system.</i> .....	31
<i>Figure 3.12. Simplified diagram of cathodoluminescence.</i> .....	31
<i>Figure 4.1. Rainy Cove outcrop and locations of the three measured sections at (1) the Carboniferous-Triassic Unconformity, (2) the fluvial contacts, and (3) the intra-Triassic Unconformity.</i> .....	37
<i>Figure 4.2. Measured section of the Carboniferous-Triassic Unconformity beside an outcrop photo.</i> .....	38
<i>Figure 4.3. Measured section of erosional surfaces in the Triassic fluvial section beside an outcrop photo.</i> .....	40
<i>Figure 4.4. Measured section of the Intra-Triassic Unconformity (ITU) beside and outcrop photo.</i> .....	42

<i>Figure 4.5. Gamma ray scintillometer counts plotted against metres measured for Section 1 (Carboniferous-Triassic Unconformity).</i> .....	43
<i>Figure 4.6. Gamma ray scintillometer counts plotted against metres measured for Section 2 (Fluvial Contacts).</i> .....	44
<i>Figure 4.7. Gamma ray scintillometer counts plotted against metres measured for section 3 (Intra-Triassic Unconformity).</i> .....	45
<i>Figure 4.8. Histogram plots for frequency of grain sizes in phi scale for each of the Triassic sediment samples.</i> .....	48
<i>Figure 4.9. Photomicrograph in (a) plane-polarizing light and (b) cross-polarizing light showing the typical petrography of the Rainy Cove Triassic sediments.</i> .....	49
<i>Figure 4.10. Photomicrographs showing some textural features of the Rainy Cove Triassic sediments.</i> .....	50
<i>Figure 4.11. Simple drawings of blocky, granular, and dog tooth carbonate cement mosaics</i> .....	51
<i>Figure 4.12. Photomicrographs showing sparry cement textures</i> .....	52
<i>Figure 4.13. Photomicrographs showing dogtooth cement textures in the carbonate cements</i> .....	53
<i>Figure 4.14. Photomicrographs under plane-polarized light (left) and corresponding sections under cathodoluminescence (right)</i> .....	56
<i>Figure 5.1. Schematic diagram of the carbonate diagenetic environment</i> .....	59
<i>Figure 5.2. Characteristics of typical burial calcite cements</i> .....	61
<i>Figure 5.3. Map and geologic cross section of the location of the Prudhoe Bay field and its Permian-Triassic productin reservoir formation</i> .....	65
<i>Figure 5.4. Diagram depicting the correlation between grain size and sorting (governed by depositional environment) and permeability observed in the sandstone reservoirs of the Prudhoe Bay field</i> .....	66
<i>Figure 5.5. Photomicrographs from the Ivishak (left) and Wolfville (right) formations.</i> .....	66
<i>Figure 6.1. Satellite photographs showing circled examples of coastal promontories along the southern margin of the Minas Basin near (a) Rainy Cove and (b) Burntcoat Head</i> .....	69

## List of Tables

<i>Table 4.1. Descriptions, associations, and photographs of identified lithofacies in the Wolfville Formation at Rainy Cove.....</i>	<i>36</i>
<i>Table 4.2. TinyPerm II readings and calculated permeability values for collected hand samples. Reported readings are an average of three readings taken per sample. ....</i>	<i>46</i>
<i>Table 4.3. Grain size measurements. Average grain size and standard deviation in millimetres and in the phi scale (-log<sub>2</sub> of size in mm) readings. Grain size decreases with increasing phi value. ....</i>	<i>47</i>
<i>Table 4.4. Summary of results connecting cement textures to lithofacies and lithofacies associations. ....</i>	<i>54</i>

## **Acknowledgements**

I would first like to thank my supervisor, Professor Grant Wach, for his continued support and encouragement in all of my endeavors and for sharing his geologic knowledge and technical skill. Thank you to Darragh O'Connor for all of the support and interesting discussion this year. Thank you Dr. Ricardo Silva for sharing insight and for pointing me in the right direction with this project. Many thanks to Trevor Kelly and Kenneth Martyns-Yellowe for their help collecting samples and acquiring data, and to the Dalhousie University Basin and Reservoir Lab. I would also like to thank Dr. Peir Pufahl and Christa Pufahl at the Acadia University Department of Earth & Environmental Science for allowing me to complete the cathodoluminescence analysis in their lab and for lending their time and knowledge. Also, thanks to Elissa Lynn at the University of Calgary Department of Geoscience for use of the microscope lab and equipment, and to Joann Welton for her input and discussion. Thank you to the Dalhousie honours coordinator, Dr. Djordje Grujic, and thank you to Mike Young and Dr. Anne-Marie Ryan for their guidance and support this year. Special thanks to Sergei Ratchinski for his excellent work making thin sections from my very friable samples. Finally, thank you to my wonderfully supportive family and friends, who always brighten my days.

I would also like to acknowledge the generous research and travel funding from the Shell Experiential Learning Fund that made this learning opportunity possible for me, as well as the Dalhousie University Faculty of Science for providing conference funding.



## Chapter 1: Introduction

### 1.1 Statement of Problem

Fluvial deposits of the Wolfville Formation are well-preserved at Rainy Cove. The outcrops contain erosional surfaces of varying scale ranging from small intra-formational scour channels to basin scale angular unconformities. However, some sections of the outcrop appear to have eroded differently than others. Fluvial barforms are preserved within the intertidal zone, while the remainder of the successions have been eroded back to the present cliff location. At the northern end of the study section, the outcrop forms a large coastal promontory preserving the lowermost portion of the incised Triassic channel. The rocks in this location exhibit varied lithofacies character and all are well-cemented with carbonate.

Heterogeneities in lithologic character caused during deposition or subsequent diagenesis can impact porosity and permeability, and therefore fluid flow, throughout the rock. Erosional surfaces in particular often form baffles and barriers to flow because they may separate units of differing reservoir quality. Erosional surfaces represent missing sections created by erosion or non-deposition, so sediments above and below and erosive contacts may be laid down in different depositional environments. The erosional surfaces studied here display a range of scale and complexity that could be difficult to detect in the subsurface and pose problems to hydrocarbon production or water storage. The Wolfville Formation is the proposed reservoir component for a potential petroleum system in the Bay of Fundy, and braided channel complexes similar to the fluvial Wolfville Group are prolific reservoirs for oil and gas across the globe. The Wolfville Formation is also an important aquifer elsewhere in Nova Scotia, particularly in the Annapolis Valley. Some aspects of this research may be applicable for analogue studies of other braided channel reservoirs and aquifers. In this study I intend to investigate whether there are differences in cementation across erosional surfaces that could cause variable erodibility along the outcrop and to investigate heterogeneities across the erosional surfaces and their impact on fluid flow.

## 1.2 Scope of Project

This study investigates the lithologic characteristics and cementation variation within the Triassic fluvial successions in Rainy Cove, Nova Scotia, with special attention given to sediments above and below erosional surfaces between stratigraphic intervals in a 200 metre outcrop of the Wolfville Formation at Rainy Cove, Nova Scotia, on the southern margin of the Minas Basin in the Bay of Fundy (Figure 1.1).

The study objectives are:

- To describe the lithological and textural composition and depositional environments of the rocks above and below the erosional surfaces
- To describe the specific cement textures present and interpret the cementation environment and sediment paragenesis
- To look for differences in cementation style across erosional surfaces and between lithofacies that may affect outcrop erosion
- To apply results to reservoir quality and fluid flow in the formation

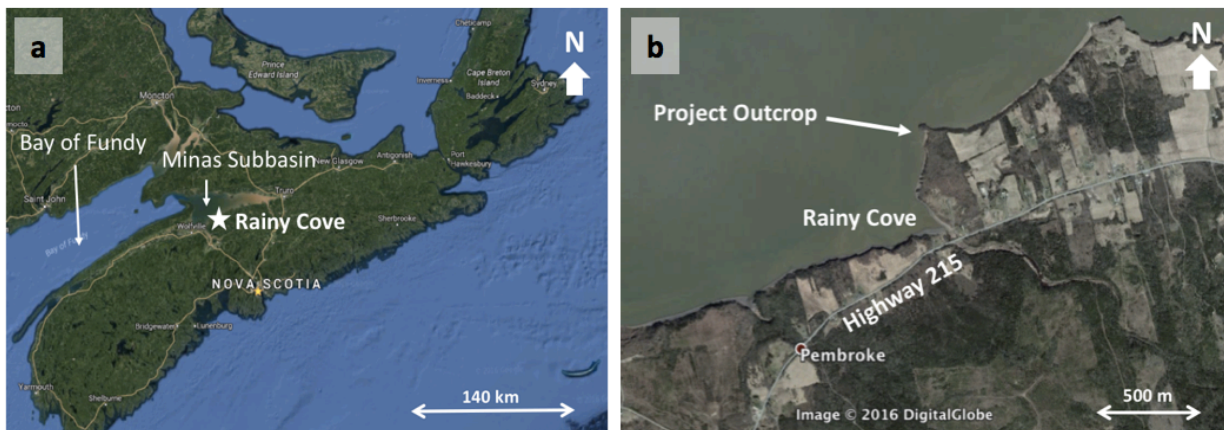


Figure 1.1. (a) Satellite image of Nova Scotia with the location of Rainy Cove marked by white star and (b) Satellite image of Rainy Cove with outcrop of interest marked (Google Earth Pro, 2016).

## 1.3 Previous Research

The Wolfville Formation represents early syn-rift sedimentation in the Fundy Basin and has been included in many regional studies (eg. Klein, 1962; Wade et al., 1996; Olsen, 1997; Withjack et al., 2009; Leleu and Hartley, 2010). Those most relevant to this project focus on the

depositional environment, lithologic character, paragenetic history, and reservoir quality of the sandstones. The majority of studies encompass the Wolfville Formation as a whole and only some include information specific to Rainy Cove. Recent research completed by O'Connor (2016) assessed the late Triassic syn-rift successions of the Fundy Basin and Orpheus Graben in Nova Scotia. His work at Rainy Cove includes identification of the Wolfville succession architectural elements in outcrop and lithologic characterization of the sandstones successions using X-ray fluorescence, point count analysis, and thin section micrograph descriptions. His work agreed with previous interpretations from Klein (1962), Wade et al. (1996), and LeLeu et al. (2009) that the Wolfville Formation at Rainy Cove was deposited in high-energy fluvial environments with episodic flooding separated by periods of extended aridity, and that sediments were sourced from the south and deposited in north-directed paleoflow regimes in a continental margin setting. He also found that the quartz-lithics-feldspar dominated sandstones at Rainy Cove were well cemented and had mixed reservoir quality (O'Connor, 2016). LeLeu et al. (2009), Kettanah et al. (2013) and O'Connor (2016) identified the presence of erosional surfaces and carbonate cements in the rocks at Rainy Cove, and while the erosional surfaces have been studied in great detail, the carbonates cements remain generally less studied.

Previous thesis projects at Dalhousie University have included studies of the architecture elements of the Wolfville braided channel complexes in Cambridge Cove, which is located just west of Rainy Cove, using field observations and high resolution radar stratigraphy (GPR). They determined that stratigraphic heterogeneities exert controls on lateral fluid flow by compartmentalizing lithologies with higher reservoir permeability (Mulcahy, 2006; Nickerson, 2010; Vaughan, 2011). This type of work has not been completed for the erosional surfaces at Rainy Cove, which have similar intra-formational fluvial barforms as well as the incised channel complex. A 2013 study by Kettanah et al. characterized the provenance and reservoir quality of the Wolfville sandstones using petrography and heavy mineral analysis of surface and subsurface samples. It concluded that the Wolfville Formation outcrops on the southern margin of the Bay of Fundy were deposited in a recycled orogen to collisional tectonic setting and showed porosities of ~6%, which is not encouraging for hydrocarbon development. As part of this study, Kettanah also suggested a multi-stage paragenetic history for the Wolfville

Formation that included cementation by carbonate as well as silica and iron grain coating (Kettanah et al., 2013).

Wade et al., (1996) assessed the hydrocarbon potential of the Fundy Basin sediments and determined that the basin had the necessary components for a petroleum system (source, migration, reservoir, trap, and seal). They concluded that the basin was thermally mature and there was a high probability of petroleum-producing source rock in the lacustrine successions, especially within the Blomidon and Scots Bay formations. They suggested an abundance of reservoir sandstones within the Wolfville, Blomidon, and Scots Bay formations, with the highest quality reservoirs in the eolian facies. Past exploration activity in the Bay of Fundy involves acquisition of seismic data and the drilling of two deep exploration wells, Chinampas N-37 and Cape Spencer-1. The best reservoir sandstone in the Wolfville Formation is the eolian facies, which is located on the northern side of the Bay of Fundy. The reservoir quality is not as promising for fluvial facies, which is present at Rainy Cove, due to less uniform grain packing and finer-grained interbeds with lower porosity and permeability; however, the sandstones can still be regarded as a possible reservoir component (Wade et al., 1996; Kettanah et al., 2013).

## Chapter 2: Geologic Background

### 2.1 Study Location

Rainy Cove is located approximately 90 kilometres north of Halifax along the south shore of the Minas Basin in the Pembroke area, Nova Scotia, Canada. The beach can be reached by Pembroke Wharf Rd. off of Highway 215, and the study area is a 500 metre walk northwest along the beach from parking site. Satellite images of the location can be seen in Figure 1.1 and Figure 2.1. The area was chosen because of the well preserved erosional surfaces identified in earlier studies (O'Connor, 2016; Kettanah, 2013; Mulcahy, 2006) and erodibility differences observed during previous field trips (Wach, 2016). The studied cliff section is 25 to 30 metres high and approximately 200 metres long. It is composed primarily of Triassic Wolfville Formation deposits, which lie unconformably over steeply dipping Carboniferous metasediments (refer to stratigraphic column in Figure 2.8). The angular unconformity between the two is located on the southern end of the study section. The N-S outcrop section is shown below in Figure 2.1a, and the northern edge of the promontory is shown in Figure 2.1b.

### 2.2 Regional Setting

The Fundy Basin is a tripartite Mesozoic rift basin located on the northwest margin of Nova Scotia containing three linked depocentres: the Fundy, Minas, and Chignecto subbasins (**Error! Reference source not found.**). The subbasins have related stratigraphic successions and structures, but differences in local deformation are controlled by a complex regional fault system (Wade et al., 1996; Olsen and Schlische, 1990). To the north, the subbasins are bounded by NE-trending extensional normal-faults and left-lateral strike-slip faults belonging to the larger Minas Fault Zone (Withjack et al., 1995). The subbasins contain syn-rift sediments deposited in the Late Permian, Triassic, and Jurassic, as well as early Jurassic flood basalts (Sues and Olsen, 2015; Olsen, 1997). Triassic sedimentation is characterized by two separate phases: the lower sand-dominated alluvial-fluvial-eolian deposits, and the upper mud-dominated playa and lacustrine deposits (Leleu and Hartley, 2010). This chapter describes the tectonic controls

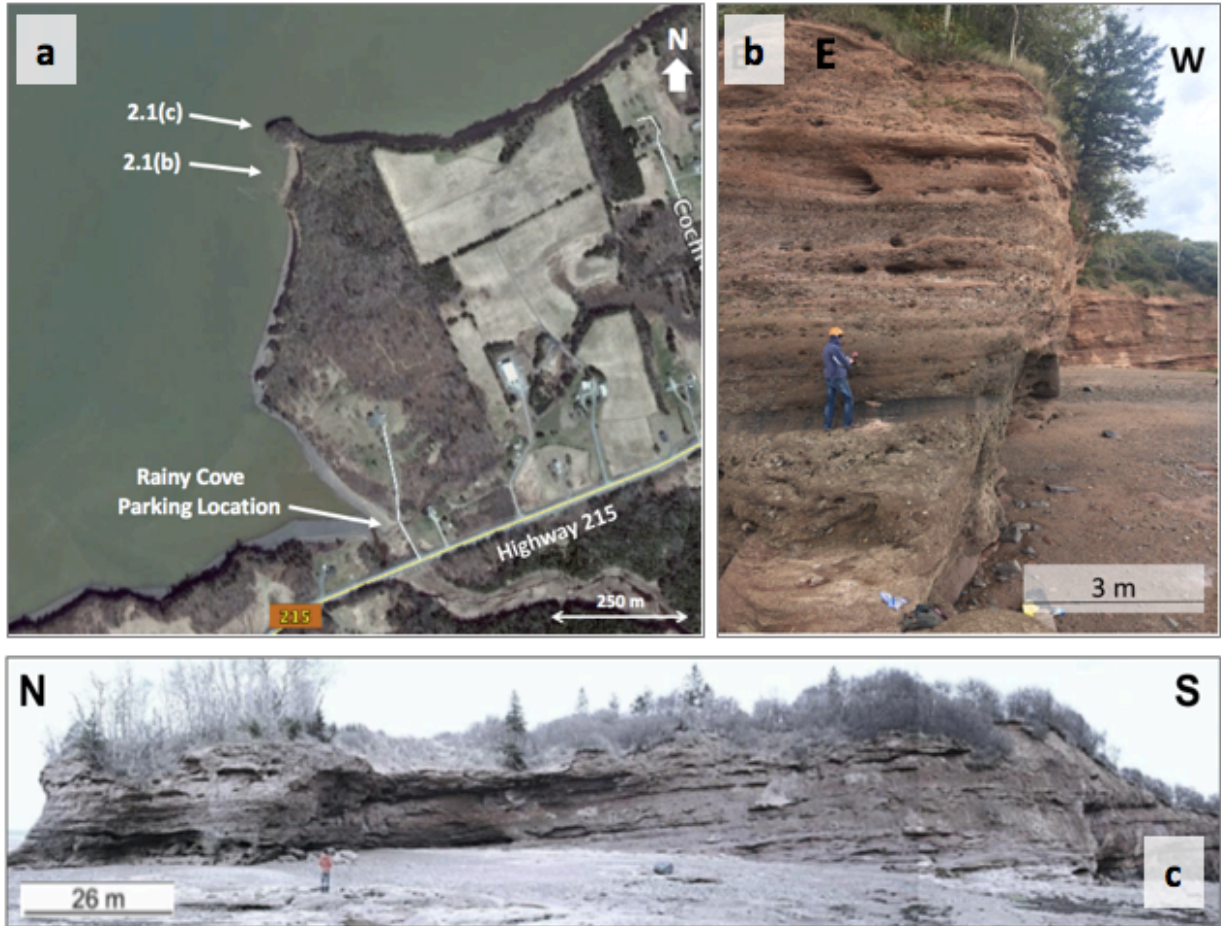


Figure 2.1. (a) Satellite image of Rainy Cove field work location (Google Earth Pro, 2016), (b) N-S outcrop section at Rainy Cove (O'Connor, 2016), and (c) E-W outcrop section of incised channel at Rainy Cove.

on basin formation and the resulting regional stratigraphy as well as geologic characteristics of the fluvial portion of the Triassic Wolfville Formation.

### 2.3 Fundy Basin Tectonic Setting

Geologic evolution of the Fundy Basin and its syn-rift successions were controlled by the formation and breakup of Pangea during the late Paleozoic and early Mesozoic (Olsen, 1997). Formation of the Pangean supercontinent in the late Paleozoic involved collision of the continents Laurentia and Gondwana. The collision closed the Iapetus Ocean and formed the Appalachian Orogeny during the late Carboniferous and early Permian. The Avalon terrane of Laurentia and the Meguma terrane of Gondwana were sutured together to form the modern-



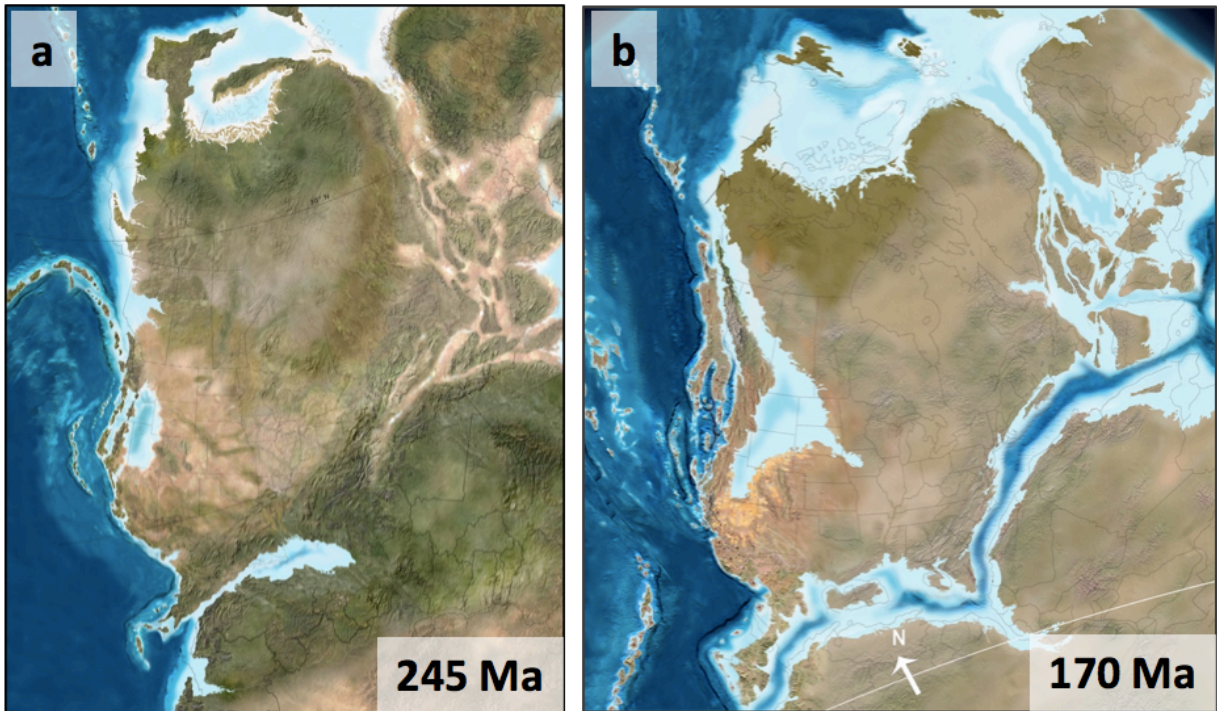


Figure 2.2. Paleogeographic reconstruction of the Atlantic margin in (a) the mid-Triassic and (b) the mid-Jurassic (Blakey, 2016).

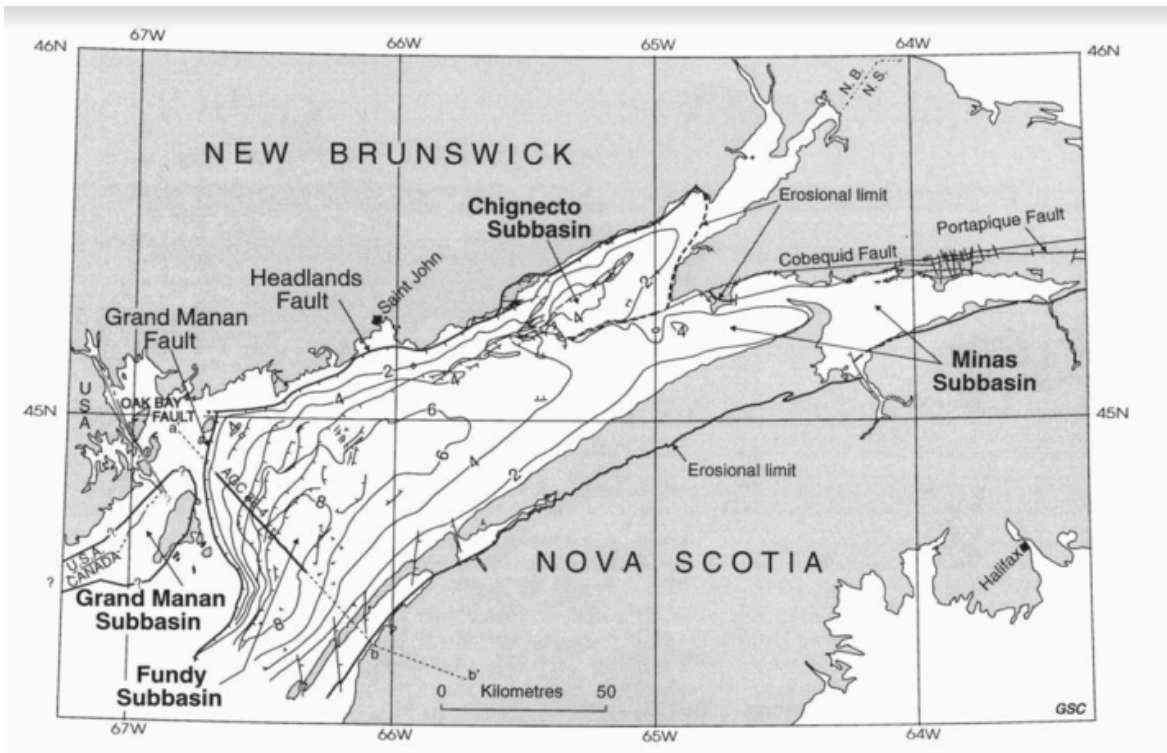


Figure 2.3. Map of the Fundy Basin, made up of the Fundy, Chignecto, and Minas Subbasins (Wade et al., 1996).

day bedrock of Nova Scotia (Keppie, 1982; Murphy et al., 2011). This tectonic compression resulted in cleavage and folding throughout both terranes, including deformation of the Carboniferous-aged Horton Group sediments. The structural complexity and intense folding of the Horton metasediments are exhibited below the angular unconformity at Rainy Cove. The faults associated with this Paleozoic contraction form the majority of the border-fault system that bounds the Fundy Basin. The Minas Fault Zone, also known as the Cobequid/Chedabucto fault zone, is composed of the linked NE and E striking Chignecto, Fundy, and Cobequid/Chedabucto fault systems. It extends along the northern side of the Fundy Basin and Minas Subbasin, separates northern and southern mainland Nova Scotia, and reaches eastward to form the northern bounding fault of the Orpheus Graben (Keppie, 1982; Murphy et al., 2011; Withjack et al. 2009).

The Eastern North American rift system can be divided into three geographic segments: Southern, Central, and Northern (Withjack and Schlische, 2005). The Fundy Basin is located between the Central and Northern sections (Figure 2.4). As Pangea began to break up, crustal rifting occurred along the eastern margin of North America from south to north, creating a series of endorheic basins (discrete basins separated from each other by regional highlands). Rifting was under way in present day Atlantic Canada by the late Triassic (Olsen, 1997) and continued until the mid-Jurassic (Withjack et al., 2009). Extension caused stretching and thinning of the crust as the Laurentian and Gondwanan continents separated and a half graben basin opened along the reactivated boundary between the Meguma and Avalon terranes (Olsen and Schlische, 1990). The syn-rift sediment package of the Fundy Basin increases in thickness toward the border-fault system on its northern side, indicating that syn-depositional faulting took place during rifting (Withjack et al., 2009). Continued extension of the crust caused increased igneous activity and subaerial basaltic flows at the beginning of the Jurassic. This wide scale igneous event formed the Central Atlantic Magmatic Province (CAMP) and marks the tectonic change in the basin from syn-rift to drift. The basin experienced post-rift inversion related to this igneous event that caused significant folding and strike-slip faulting sub-parallel to the border fault zones. This drastically changed the geometry of the basin, which is currently



shorter and shallower than it would have been at the time of deposition for the Wolfville sediments. The basin also experienced post-rift deformation that tilted the eastern side northward, resulting in increased uplift and erosion of the eastern region (Withjack et al., 2009). In the mid to late Jurassic, the rift that opened the Fundy Basin failed and tension shifted southeast of Nova Scotia to the present-day Atlantic Ocean, leaving the Fundy Basin aulacogen as a failed arm of a triple junction (Wade et al., 1996).

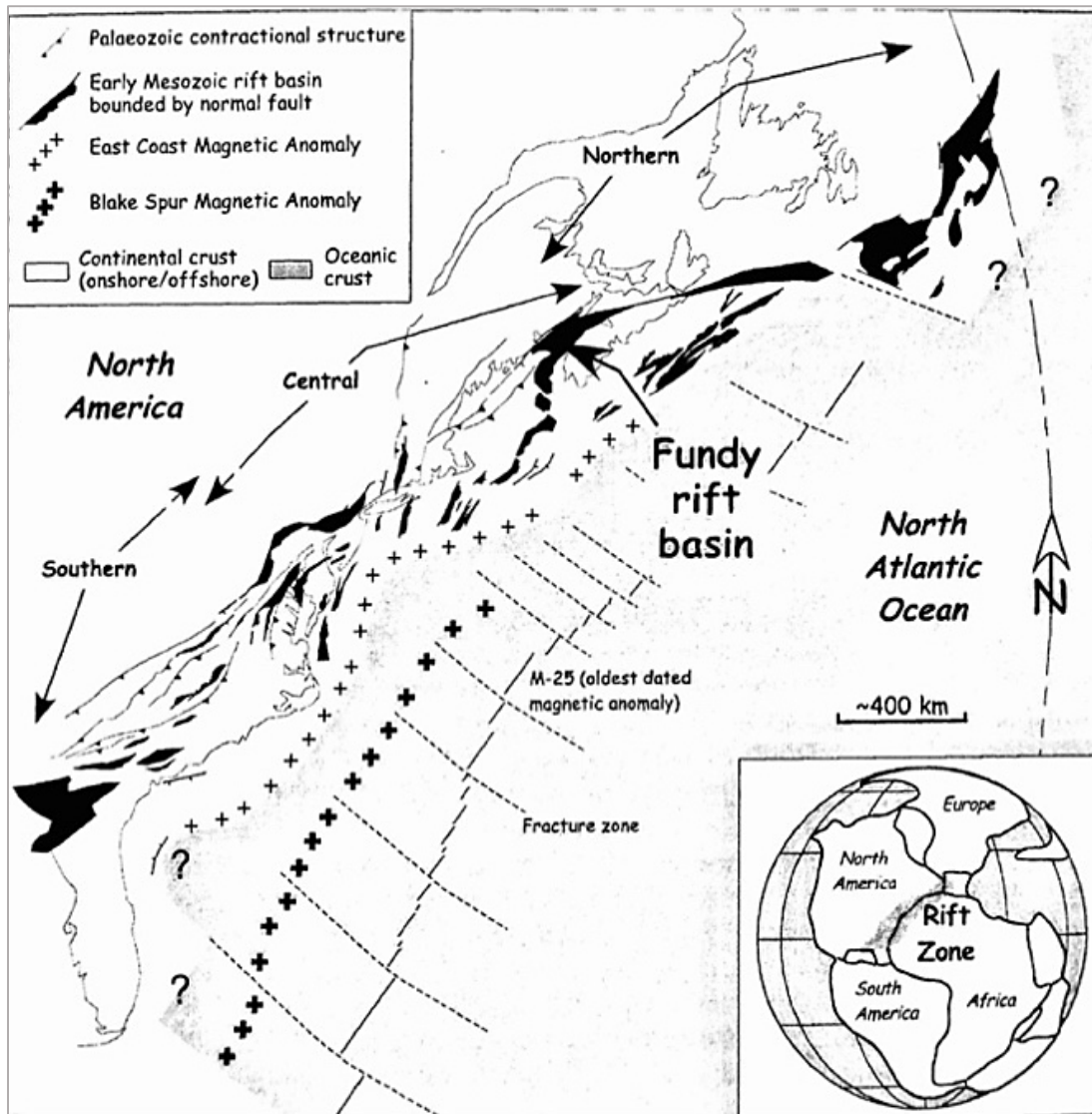


Figure 2.4. Map of the Eastern North American rift system, divided into Southern, Central, and Northern segments (Withjack et al., 2009). The Fundy rift basin is located at the division between the Central and Northern parts.

Thermal subsidence of the Fundy Basin facilitated syn-rift sedimentation by creating accommodation space. The subsidence can be described using the Steer's Head rift basin evolution from Mckenzie (1978). Rapid stretching of continental lithosphere at rifting margins creates upwelling of hot asthenospheric mantle. The thin lithosphere stretches by faulting, increasing heat flux further, then subsides as increased sediment loading thickens and cools the crust (Mckenzie, 1978). In this model, syn-rift sedimentation and stratigraphic onlap can occur in a sedimentary basin by stretching of the lithosphere, without large regional sea level changes (White and McKenzie, 1988). Sedimentary basins that evolve this way have a cross-sectional profile resembling a steer's horns, as seen by the half-basin profile in Figure 2.5.

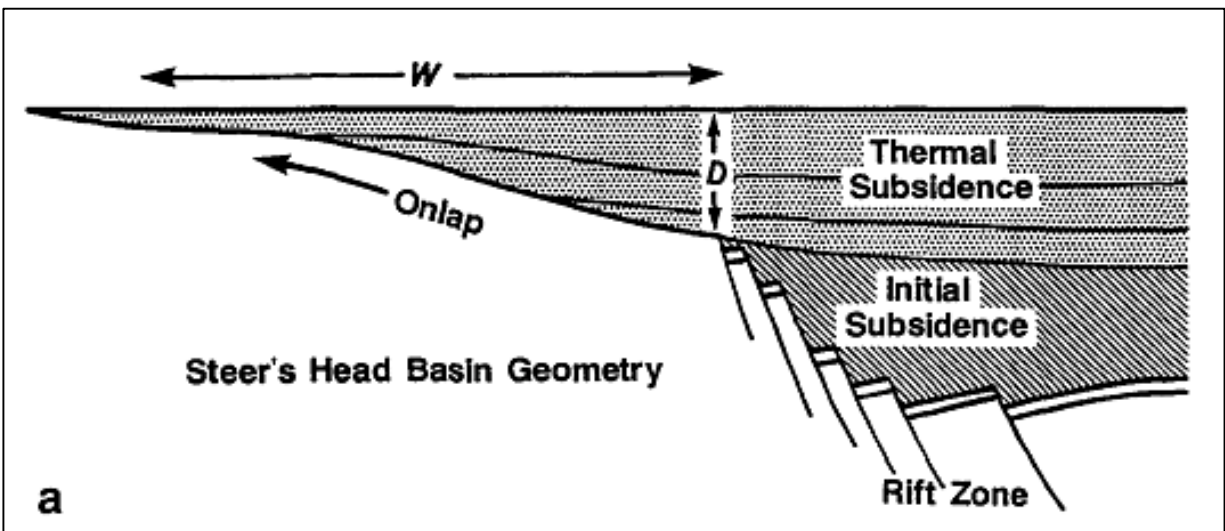


Figure 2.5. Diagram of Steer's Head sedimentary basin geometry (White and Mckenzie, 1988).

## 2.4 Stratigraphy

### 2.4.1 Stratigraphic Descriptions

The lowermost strata observed in the Minas Subbasin are the steeply dipping Carboniferous metasediments of the Horton Group, which are truncated by an angular unconformity surface. Above this unconformity lie the syn-rift deposits of the Wolfville Formation. This section describes the stratigraphy of the Fundy Group, which is part of the Newark Supergroup (Klein, 1962; Willams et al., 1985). Particular attention is given to the

formations observed in the Minas Subbasin and strata at Rainy Cove (refer to Figures 2.7 and 2.8).

The Honeycomb Point Formation is the earliest succession of the Fundy Group. It contains conglomerates and sandstones deposited in alluvial-fan and eolian environments sediments. It dates within the Triassic (Williams et al., 1985) and possibly as early as the Permian (Sues and Olsen, 2015). These successions occur on the northern margin of the Bay of Fundy along the coast of New Brunswick (Sues and Olsen, 2015). They are not present at Rainy Cove. The entire Permian period is missing at the study location where the angular unconformity separates the Carboniferous Horton Group and Triassic Wolfville Formation.

The Wolfville Formation is the lowermost Triassic section present at Rainy Cove. It is a red coloured, coarse to medium grained arenite with pebbly and conglomeratic units near its base that occurs on both the northern and southern margins of the Minas Subbasin (Williams et al., 1985). Clasts are derived from metamorphic and granitic units of the Avalon and Meguma terranes, as well as from proximal Carboniferous metasediments (Williams et al., 1985; Kettanah et al., 2013). The lower Wolfville Formation was deposited during early rifting of the basin in coarse alluvial fans and sand plains (Wade et al., 1996). Alluvial sediments are overlain by the braided channel deposits that are seen at Rainy Cove and elsewhere along the southern Minas Subbasin. The fluvial barforms and incised channels of the braided channel complex create high lateral variability in the formation (Vaughan, 2011; Nickerson, 2010; Mulcahy, 2006). During the Mesozoic, the rifting Laurentian and Gondwanan continents were also drifting northward, causing paleoclimatic change from a hot and humid to hot and arid environment. Accumulation of sediment in more arid climates formed large dune deposits in the upper section of the Wolfville Formation. Outcrops on the northern side of the Minas Subbasin contain such eolian successions (Olsen, 1997). The formation occurs along the extent of the Annapolis Valley on the southern side of the Minas Subbasin and along the north shore on the Cape D'Or Peninsula and between Truro and Economy Mountain, Nova Scotia, and thicknesses range from 60 m to 833 m. The Wolfville Formation has been dated in the Carnian to Norian in the Late Triassic (Williams et al., 1985).

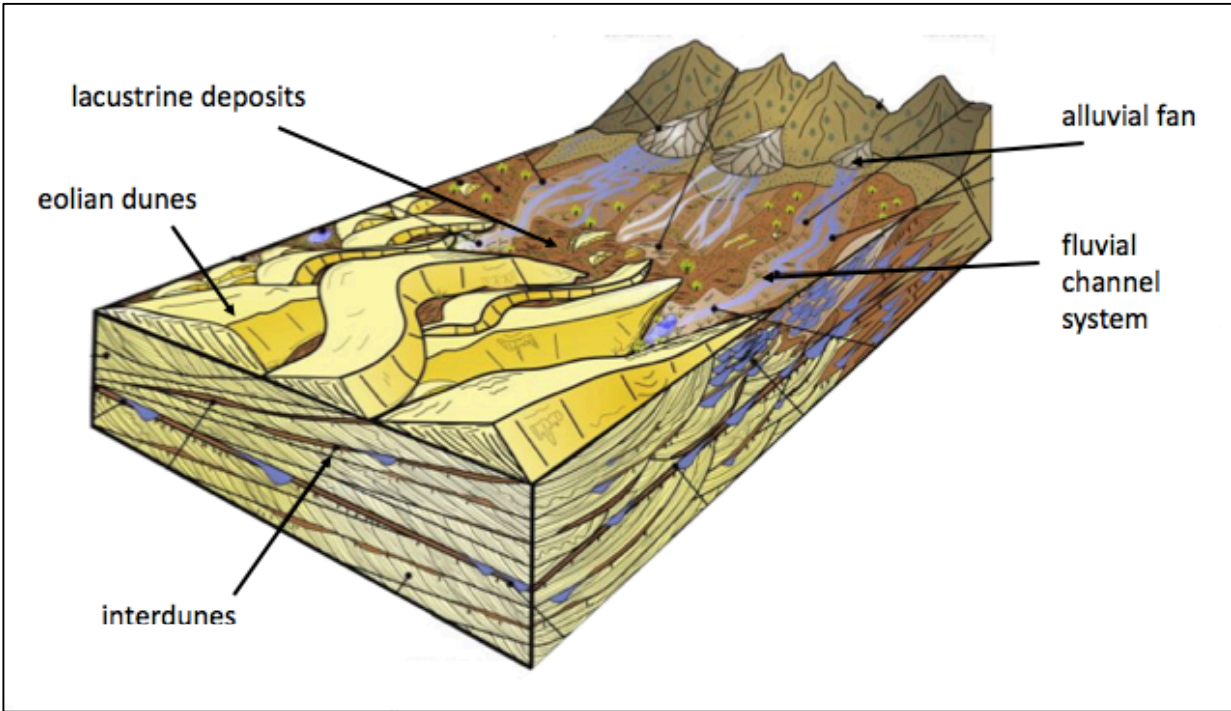


Figure 2.6. Fluvial-eolian system interaction in rift basins (Al-Masrahy and Mountney, 2015). The lower fluvial and upper eolian section of the Wolfville Formation were deposited in similar environments.

The Blomidon Formation conformably overlies the Wolfville Formation and intermittently interfingers with it along the Minas Subbasin (Williams et al., 1985). It is composed of red shales, claystones, and silts deposited in cyclic playa lake and sheetflood deposits from lacustrine systems that filled the basin after the Wolfville fluvial succession. (Williams et al., 1985; Wade et al., 1996). The formation occurs on the southern and northern margins of the Minas Subbasin and ranges from 8 m to 363 m thick. It has been dated in the Rhaetian in the Late Triassic (Williams et al., 1985).

The Blomidon Formation is overlain by the North Mountain Basalt. This subaerial tholeiitic basalt flow is part of the Central Atlantic Magmatic Province (CAMP), a large igneous province formed at the beginning of the Jurassic due to crustal thinning and extension. It underlies the Bay of Fundy and outcrops in the Minas Basin at Cape Split and near Five Islands Provincial Park. The flow contains a lower member up to 200 m thick and an upper member up

to 160 m thick (Williams et al., 1985). It has been dated at  $202 \pm 2$  Ma, placing it at the base of the Lower Jurassic (Hodych and Dunning, 1992).

The Scots Bay Formation is the last of the syn-rift successions in the Fundy Basin and disconformably overlies the North Mountain Basalt. It is made up of fine grained interbedded sandstones, limestones, and chert that were deposited in a lacustrine environment (Williams et al., 1985). The Scots Bay Formation is stratigraphically equivalent to the McCoy Brook Formation, a terrestrial siliciclastic unit that outcrops between Economy and Parrsboro (Williams et al., 1985; Wade et al., 1996).

At Rainy Cove, the Wolfville Formation is the only syn-rift succession present. The Wolfville Formation unconformably overlies the Carboniferous strata, and the fluvial Wolfville successions are unconformably overlain by Quaternary sediments speculated to be glacial in origin. In the Minas Subbasin, the rift succession does not contain sediments younger than early Jurassic Age (Olsen, 1997).

#### 2.4.2 Sequence Stratigraphy

The bounding surfaces in this study can be connected to the sequence stratigraphic history of the Wolfville Formation. The Carboniferous-Triassic Unconformity and the intra-Triassic Unconformity are sequence boundaries. They are erosive and non-depositional surfaces separating genetically related strata within the formation (Boggs, 2012). The smaller erosive and pedogenic surfaces between sediment beds are internal discordances of the formation. These represent smaller scale changes, including resurgences of the fluvial system or small hiatuses in deposition and soil formation during arid climactic periods. The sequence boundaries represent larger gaps of time and are more laterally continuous throughout the rocks than the internal discordances. Due to this more regional influence, the sequence boundaries are expected to have a larger effect on fluid pathways in the formation. However, the internal discordances are present throughout the outcrop and create heterogeneities that may baffle fluid flow within the successions. Both of these possibilities are investigated in this study. The Wolfville Formation sediments were deposited during rifting of the Fundy Basin. The sediment supply entered the basin from the proximal Meguma and Avalon Terranes (Kettanah

et al., 2013). Accommodation space was created by normal faulting in the extensional regime and by thermal subsidence following the Mckenzie model discussed previously (Mckenzie, 1978).

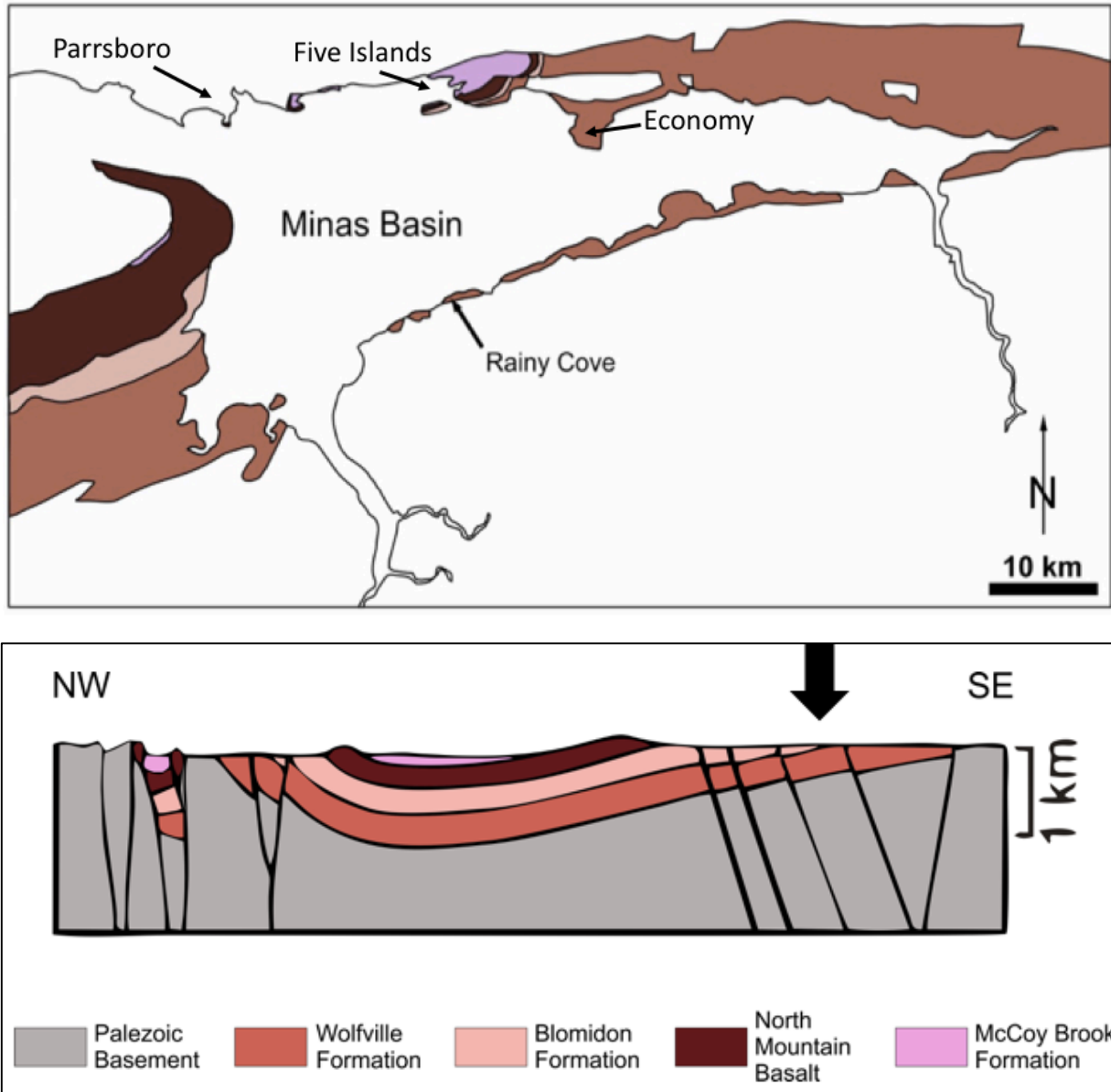


Figure 2.7. Geologic map and cross section of the Fundy Basin stratigraphy (Kettanah et al., 2013; O'Connor, 2016).



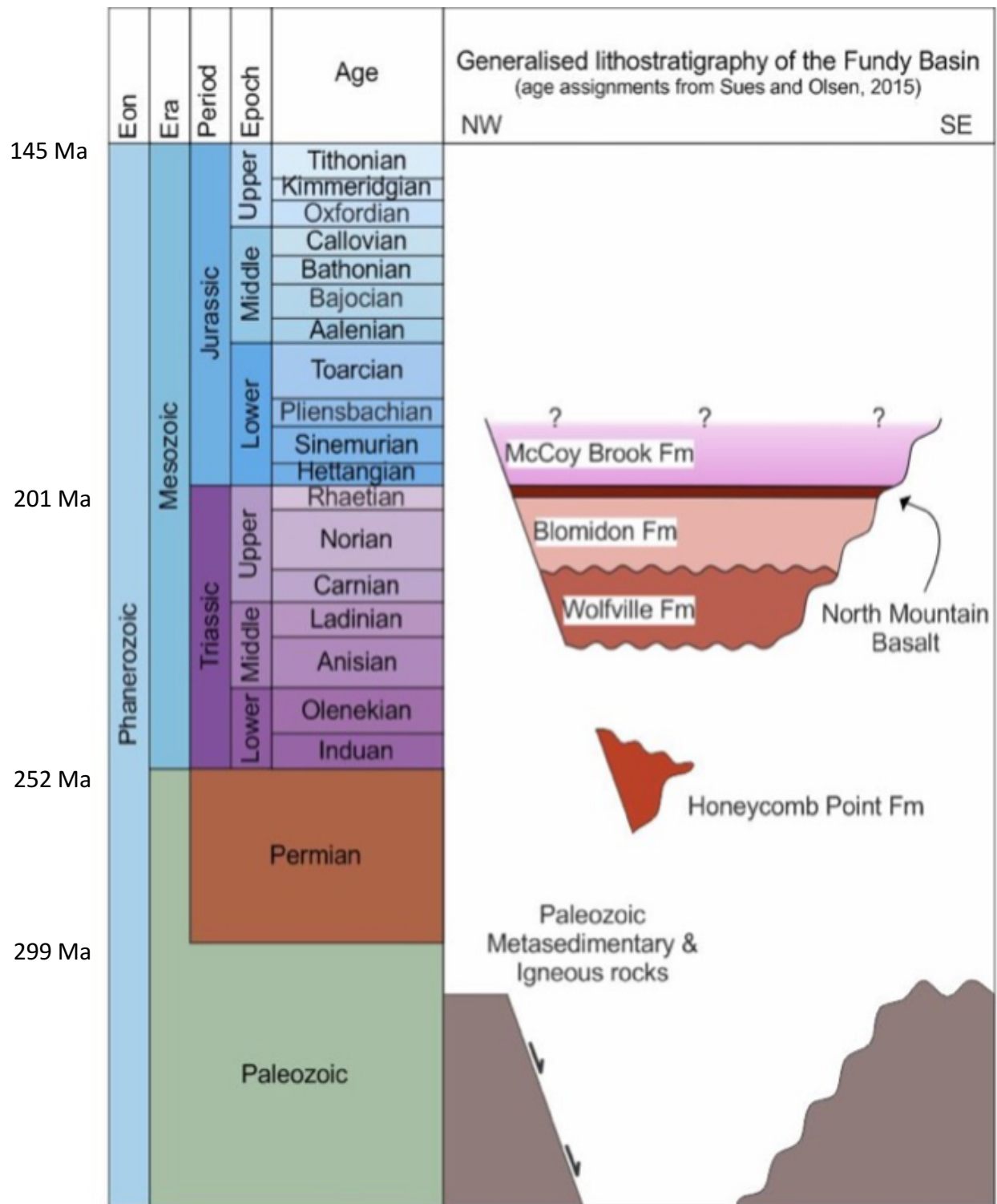


Figure 2.8. Fundy Basin stratigraphic column (O'Connor, 2016, modified from Weston et al., 2012).

## 2.5 Fluvial Channel Deposits

Rivers can travel across long distances and exhibit varying channel morphologies at different points along their path. The commonly recognized channel patterns are straight, anastomosing or braided, and meandering (Figure 2.9) (eg. Reineck and Singh, 1980; Boggs, 2012). These environments can create anastomosing channels, where channels of alluvial plains branch and rejoin, and fluvial braided channel complexes. The majority of the fluvial succession is made up of braided channels, which form when the river begins to deposit barforms. The barforms subdivide the river into multiple channels, and the number of channels changes according to flow energy and water height. Abandoned channels and erosional surfaces are common, and barforms are often not fully preserved. Barform morphology tends to be tabular and asymmetrical, with thicker accumulations on the downstream side where sediment is preferentially deposited by flowing water. Bars actively migrate downstream by slip-face avalanching and erosion of upstream ends, and develop planar cross-bedded structures. The barforms generally comprise coarser material that was too heavy for the flow energy of the river. Coarse, well-sorted material with uniform packing can have high porosity and permeability, which are important reservoir properties. Porosity and permeability may be lower for poorly sorted clast lag sections at the base of channel scours, or in siltier abandoned channel layers (Reineck and Singh, 1980; Nichols, 2009; Boggs, 2012).

Braided channel systems develop commonly in mountain rivers, alluvial fans, and glacial outwash plains. These environments tend to have higher energy, allowing for a large degree of sediment transport and bank erosion. They also exhibit variable flow rates due to intermittent flooding (for example, episodic seasonal melting or monsoonal precipitation). The channel positions shift often by channel avulsion, forming barform complexes that stack in multistoried patterns (Reineck and Singh, 1980; Nichols, 2009; Boggs, 2012). Multistoried fluvial deposits of high porosity and permeability have potential to form stacked high-quality hydrocarbon reservoirs (ex. Atkinson et al., 1990).



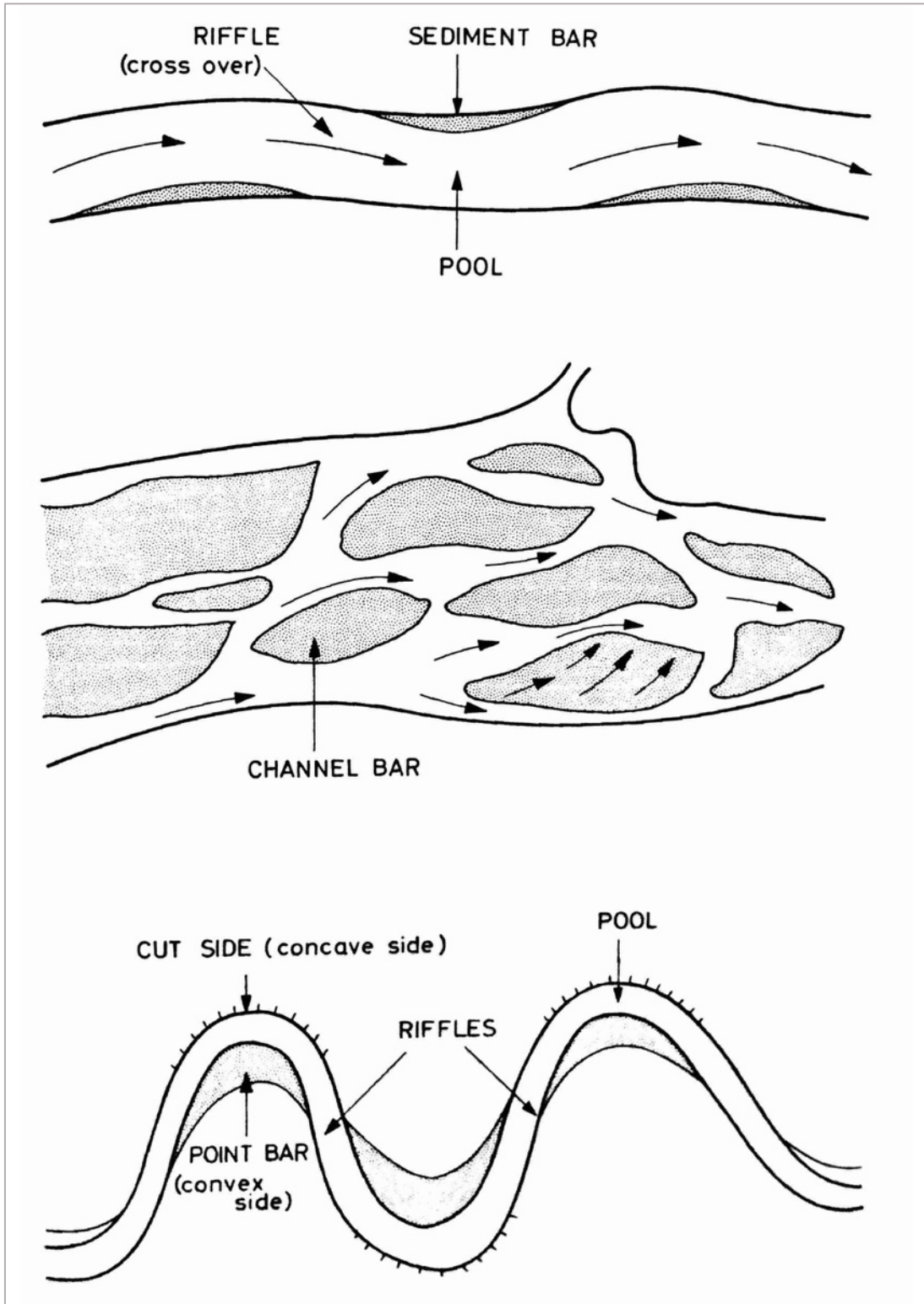


Figure 2.9. Schematic diagram of common fluvial channel morphologies. (Top to bottom) Straight, braided, and meandering channel characteristics (Rieneck and Singh, 1980).

## **2.6 Hierarchy of Sedimentary Structures**

Within the Wolfville Formation, erosional surfaces separate sedimentary packages. The sedimentary packages make up the alluvial and fluvial sandstones described previously. In a 1967 paper, Campbell defined sedimentary packages in terms of lamina, laminasets, beds, and bedsets, which define primary sedimentary structures based on size and the amount of time to deposit the interval (Campbell, 1967). Terminology from Campbell is used in this paper to describe the sedimentary packages in the studied outcrop.

A set is a group of conformable strata that are separated from surrounding sedimentary units by erosional or nondepositional surfaces. The erosional surfaces described in this study bound the different sedimentary units within the formation.

Laminae are the smallest sedimentary unit present in a succession, and generally form thin layers that can be measured in millimetres. Laminae are relatively uniform in composition and texture and do not show internal lamination. Laminasets are groups of conformable laminae that form small-sized beds representing relatively short periods of time. Beds are the larger building blocks of sedimentary rocks. Beds are generally measured on larger scales and require more complex descriptions because their geometry can vary widely by depositional environment and commonly show internal structures. The bounding surfaces of beds (erosional surfaces) are the depositional surfaces for the layer above. They separate varied intervals of time depending on the amount of depositional hiatus or erosion that took place between the layers that they separate (Campbell, 1967).

## **2.7 Sediment Paragenesis**

Paragenetic history describes the chronologic sequence of events during formation of a rock unit from deposition through burial. The sandstones at Rainy Cove have undergone varied post-depositional processes including burial cementation, limited mechanical compaction, partial dissolution of unstable feldspars and cements, and alteration. These diagenetic processes, particularly cementation, exert a strong control on reservoir quality, so it is important to consider paragenetic history of the Wolfville Formation. In a 2013 reservoir quality study of the Wolfville Formation, Kettanah et al. suggested the diagenetic sequence shown in

Figure 2.10. Mechanical compaction occurs throughout burial as increased overburden pressure forces grains closer together and fractures brittle minerals. These effects were observed in subsurface samples from exploration wells, but not in surface samples at Rainy Cove. The effects of chemical compaction include cementation, alteration, replacement, and dissolution of mineral grains. The Wolfville sandstones have been cemented to various degrees by iron coatings, clays, silica, and carbonate, with cement type differing by location. Pore-filling carbonate cement is most prevalent in the sandstones at Rainy Cove. Later diagenesis was relatively mild since feldspar grains, which are generally unstable, are relatively unaltered in the studied samples (Kettanah et al., 2013).

Cementation involves chemical precipitation of minerals from pore fluids into the primary and secondary pore spaces of a rock. In order for precipitation to occur, the pore fluid must be supersaturated with respect to the cement mineral (Flügel, 2010). Cements that fill pore spaces commonly act as lithifying agents for sediments. Sediments with narrow size ranges (well sorted) produce packing orientations with large pore spaces that tend to facilitate cement precipitation (Larsen and Chilingar, 1979). Cement crystals are commonly clear and clean with well-defined boundaries and sharp grain contacts, often forming triple junctions with 180 degree angles. Cement crystals do not cut across framework grains. Carbonate cements can form in environments ranging from the surface and seafloor to deep burial zones in the subsurface.  $\text{CaCO}_3$  is commonly sourced from the sediment itself or from sea water (Flügel, 2010).

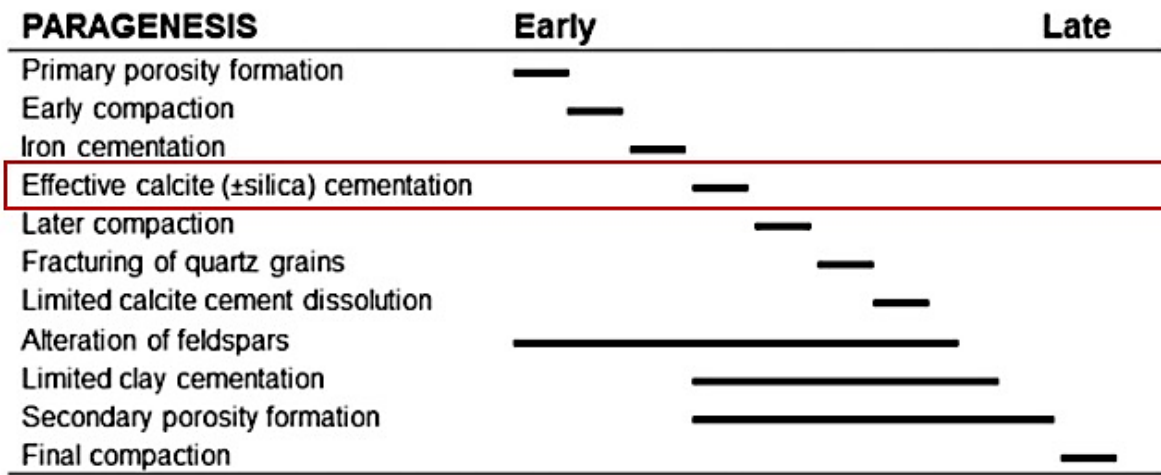


Figure 2.10. Suggested paragenesis of diagenetic events in the Wolfville Formation at Rainy Cove, Nova Scotia (Kettanah et al., 2013) with box indicating cementation event studied in this project.

## Chapter 3: Methods

### 3.1 Sample Collection

Sixteen samples were collected from the outcrop at Rainy Cove in September of 2016. Sample locations were selected above and below identified erosional surfaces. Samples were taken from the outcrop using a chisel and hammer (Figure 3.2), labeled with two arrows, one oriented towards the north and one oriented toward the top of the sample, and placed in plastic bags labeled with sample name. Exact sample locations were recorded on outcrop photos (Figures 3.1 to 3.3). The samples were then brought back to Dalhousie University for thin section preparation.

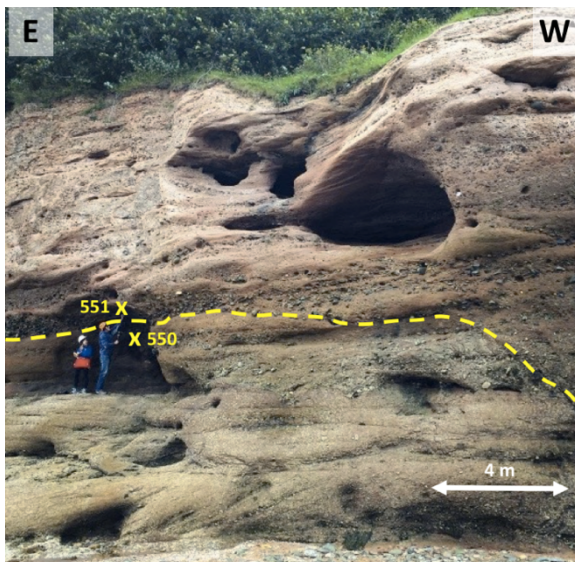


Figure 3.1. Field work in Fall 2016. Intra-Triassic unconformity marked in yellow and sample locations on northern end of outcrop section.

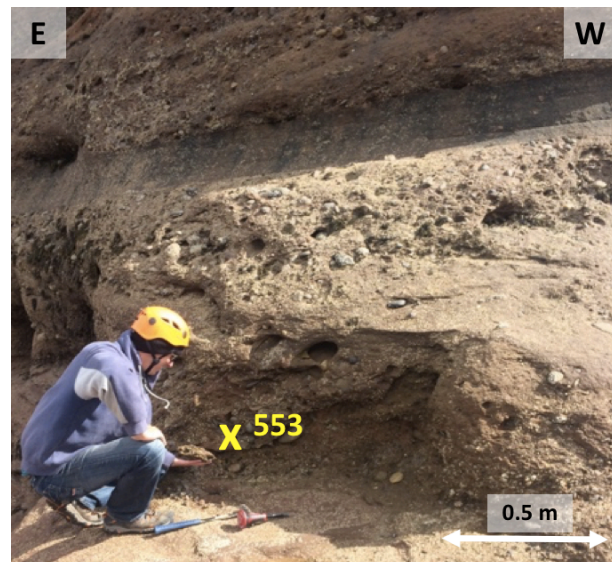


Figure 3.2. Sample collection with chisel and hammer. Location of sample 553 at base of intra-Triassic unconformity on northern end of outcrop.

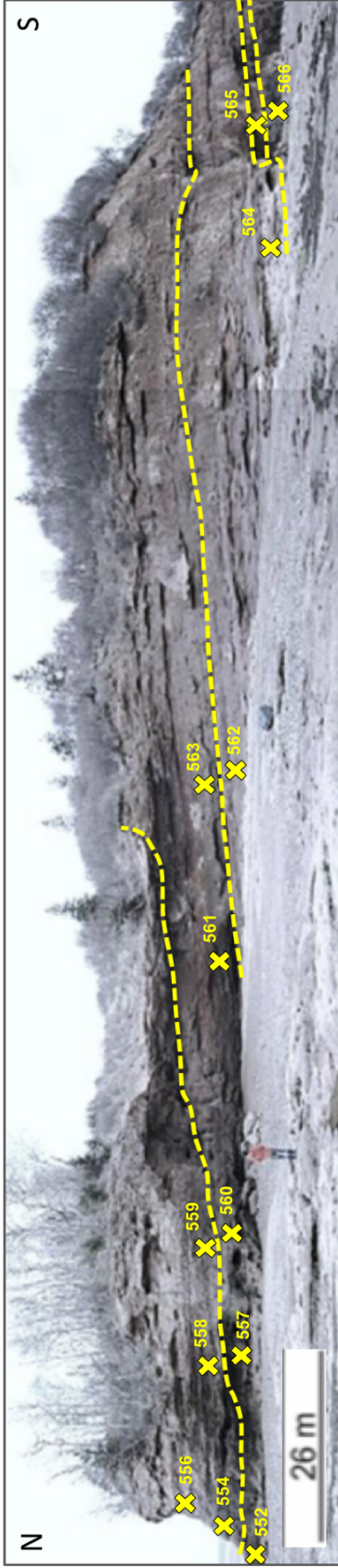


Figure 3.3. Rainy Cove outcrop with major bounding surfaces and sample locations, excluding samples 550, 551, and 553, which are located around the northern end of the outcrop (photo from O'Connor, 2016).



### 3.2 Measured Section Logs

Stratigraphic sections were logged across the main erosional surfaces in the Wolfville Formation at Rainy Cove. There are three measured sections: the Carboniferous-Triassic unconformity (Section 1), alluvial and fluvial erosional surfaces (Section 2), and the intra-Triassic unconformity (Section 3). The locations of these sections are shown in Figure 3.4. Notes were taken describing grain size, lithofacies, and physical sedimentary structures. These observations were used to classify the rocks according to lithofacies and facies associations. The sections describe at least one metre of outcrop on either side of the erosional surfaces, with the exception of the Carboniferous-Triassic unconformity where only 0.2m of the Carboniferous metasedimentary rocks were logged. Grain size descriptions were made using a hand lens and grain scale chart (Figure 3.5). The sizes correspond to the Wentworth size classes (Figure 3.6).



Figure 3.5. Ruler held next to outcrop for measured section work, Fall 2016.

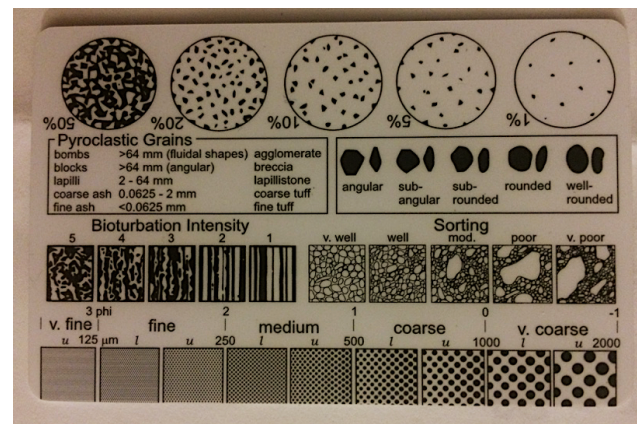


Figure 3.4. Example of a grain card used to estimate grain size, shape, and sorting in the field.

	US Standard sieve mesh	Millimeters	Phi ( $\phi$ ) units	Wentworth size class		
GRAVEL		4096	-12	Boulder		
		1024	-10			
		256	256	-8	Cobble	
		64	64	-6		
		16		-4	Pebble	
	5	4	4	-2		
	6	3.36		-1.75	Granule	
	7	2.83		-1.5		
	8	2.38		-1.25		
	10	2.00	2	-1.0		
SAND	12	1.68		-0.75	Very coarse sand	
	14	1.41		-0.5		
	16	1.19		-0.25		
	18	1.00	1	0.0		
	20	0.84		0.25	Coarse sand	
	25	0.71		0.5		
	30	0.59		0.75		
	35	0.50	1/2	1.0		
	40	0.42		1.25	Medium sand	
	45	0.35		1.5		
	50	0.30		1.75		
	60	0.25	1/4	2.0		
	70	0.210		2.25	Fine sand	
	80	0.177		2.5		
	100	0.149		2.75		
	120	0.125	1/6	3.0		
	140	0.105		3.25	Very fine sand	
	170	0.088		3.5		
	200	0.074		3.75		
	230	0.0625	1/16	4.0		
MUD	SILT	270	0.053		4.25	Coarse silt
		325	0.044		4.5	
			0.037		4.75	
			0.031	1/32	5.0	Medium silt
			0.0156	1/64	6.0	
	CLAY		0.0078	1/128	7.0	Fine silt
			0.0039	1/256	8.0	Very fine silt
			0.0020		9.0	Clay
			0.00098		10.0	
			0.00049		11.0	
	0.00024		12.0			
	0.00012		13.0			
	0.00006		14.0			

Figure 3.6. Wentworth grain-size scale chart for sediments (Boggs, 2012).



### 3.3 Gamma Ray Spectrometer Measurements

Spectrometer measurements were taken at outcrop using the GEORADIS GT-40 Multipurpose Gamma Ray Spectrometer, Revision 1.1 (Figure 3.7). This is a handheld instrument that can survey the amount of radioactive content in the sample and quantitatively measure the uranium, potassium, and thorium content. Gamma rays emitted from radioactive elements in minerals are detected by a sodium iodide crystal within the instrument, which emits electrical pulses. The number of pulses is determined by the strength of the radiation. Rocks with a greater amount of radioactive content cause a greater number of pulses to be emitted (O'Reilly, 1982).

Scintillometer measurements were taken following these steps:

1. *The device was turned on and put it into survey mode, ensuring that the lead collimator has been placed in the device.*
2. *The device was held to the outcrop surface, ensuring contact between the rubber boot of the instrument and the rock face.*
3. *The instrument reports total radioactivity count as the number of recorded gamma incidents within the last second (cps).*

Spectrometer measurements were taken following these steps:

1. *The device was turned on and put it into ASSAY mode.*
2. *The device was held to the outcrop surface, ensuring contact between the rubber boot of the instrument and the rock face.*
3. *The instrument reports radioactivity of potassium (ppm), uranium (ppm), and thorium (%) as well as the dose and dose rate in nSv per hour. The instrument was held at the rock face until the dose rate was reported. Measurements were taken at each bed across the erosional surfaces at the measured section locations.*

The gamma counts were recorded over five to ten seconds at 20 cm intervals across the erosional surfaces at the measured section locations, and then averaged to obtain the reported value. The intention of taking gamma readings at 20 cm intervals was to provide a detailed lithologic log similar to a gamma wireline log, but the instrument measures radioactivity with a

sensitivity volume of an approximately  $1 \text{ m}^3$ . A lead collimator was inserted into the instrument to reduce the range of sensitivity by shielding the sodium iodide crystal and allowing only a narrow beam of interaction between the instrument and radioactive particles emitted by the sample. However, there may still have been some interference preventing accurate detection of gamma changes at each 20 cm increment, so measurements provide only a general trend of radioactivity changes.



Figure 3.7. GEORADiS GT-40 Multipurpose Gamma Ray Spectrometer.

### 3.4 Hand Held Permeameter Measurements

Permeability measurements were taken on hand samples collected from the field using the TinyPerm II instrument from New England Research (Figure 3.8). The unit works by measuring rock matrix permeability by means of drawing air from a sample (rock in this study) into the vacuum chamber of the unit. The unit monitors the volume of the transient vacuum

pulse that is created as air moves from the sample and into the Tinyperm II unit. Measurements reported by the instrument are then referenced to the calibration curve (Figure 3.9) to obtain an absolute permeability value for the rock. Exact values from the calibration curve are included in table format in Appendix B.

Permeameter measurements were taken following these steps:

1. *The TinyPerm II was turned on*
2. *The plunger was pulled back until the screen read "Push + Hold" and reported a number of 0 (no vacuum)*
3. *The rubber nozzle, with edges covered by plasticine for improved seal, was firmly pressed against a relatively flat and uniform part of the rock surface*
4. *The plunger was depressed completely and held until the screen measurement status bar indicated the measurement is complete*
5. *Results were recorded from the screen and the plunger was pulled out*
6. *Steps 2-5 were repeated two more times to obtain an average reading for the sample*
7. *The average reading was referenced to the permeability calibration chart to get the measured permeability value for the sample*

Permeability data was not collected in the field due to wet weather conditions. Measurements were completed in the lab on the samples that were large enough to have a sufficient seal between the TinyPerm II nozzle and the rock surface



Figure 3.8. TinyPerm II handheld permeameter and data reporting screen from New England Research.

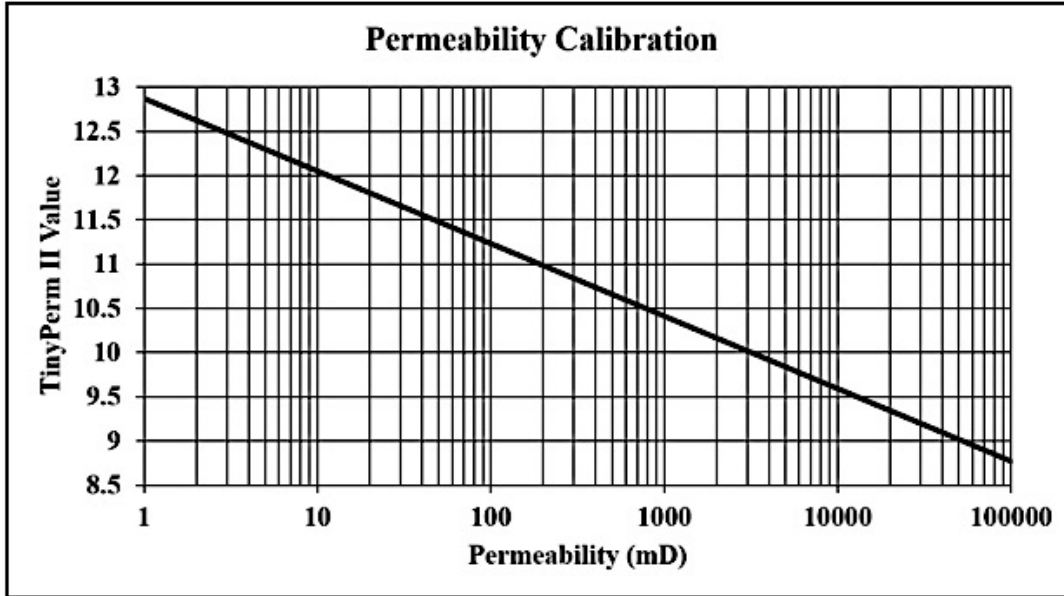


Figure 3.9. New England Research permeability calibration chart used to correlate TinyPerm II values to permeability values.

### 3.5 Thin Section Microscopy

Sixteen thin sections were prepared from the collected samples. Five of the samples were made into standard thin sections and 11 were made into polished sections (as required for later analysis using cathodoluminescence microscopy). All thin sections were studied using polarizing and reflected light microscopy. This work was completed in the Basin and Reservoir laboratory in the Earth Sciences Department at Dalhousie University using an Olympus BX51 polarizing microscope with attached Olympus DP71 digital camera (Figure 3.10a) and at the University of Calgary Department of Geoscience using a Nikon Eclipse 50iPOL polarizing microscope with attached Motican 2500 camera (Figure 3.10b). Sample analysis focused on description of mineral assemblages, grain size, cement composition and texture, mineral alteration, and porosity.



Figure 3.10. (left) Dalhousie University Basin and Reservoir Lab Olympus BX51 microscope and (right) University of Calgary Nikon 50iPOL microscope.

Grain size measurements were taken for 100 random grains per sample. To ensure measurement precision, thin section images taken using the Olympus camera with calibrated scale bars were uploaded onto a computer and grains were measured using ImageJ software.

Measurements were taken along the long axis of the framework grains. Since measurements were done on thin sections rather than on loose sediments, the values have associated uncertainty due to the effect of apparent dimensions as thin sections may not cut grains along the exact centre, so the length viewed in section depends on which part of the grain is passed through by the plane. As a result, the measured grain lengths may be lower than the true values.

### **3.6 Cathodoluminescence**

Cathodoluminescence (CL) microscopy was used in this study to investigate composition of carbonate cements and to look for zoning features to indicate separate phases of diagenesis. CL emissions are useful to investigate trace element composition of minerals and to see mineralogical and textural features that are not visible using light polarizing microscopy.

When a material is bombarded with a high energy electron beam, produced by a cathode, it will emit characteristic luminescence. This is called cathodoluminescence and can be used to study minerals in polished thin sections. The bombardment of energy excites electrons within the valence bands of atoms in the mineral's crystal structure. The excited electrons are promoted to higher (outer) bands. As the electrons fall back to the ground-state valence band, they may become temporarily trapped in the crystal's structural defects or impurities. When the electrons leave the traps, they release energy in the form of photons (i.e. light). If the energy is in the correct wavelength, the sample will luminesce. CL includes primarily the visible light spectrum (400-700nm) with some infrared or ultraviolet portions. Luminescence due to structural impurities is called extrinsic luminescence. Certain trace elements may promote CL and are called activators or sensitizers. Others can inhibit CL and are called quenchers (Henry, 2016).

Cathodoluminescence work for this study was completed using the Reliotron Cold-Cathode CL system of the Acadia Centre for Microstructural Analysis (ACMA) at the Department of Earth & Environmental Science, Acadia University, Wolfville, Nova Scotia (Figure 3.11). The CL system is attached directly to a microscope with a camera attachment. Polished samples are used because the electron beam must be able to react with trace elements unimpeded by a



glass cover slip, found on most common thin sections. Samples were placed in the vacuum tray of the CL system, the tray was closed, and the vacuum pump turned on. Once a vacuum was attained, the cathode was turned on and the sample bombarded with the electron beam. Photos were taken using the camera attachment.

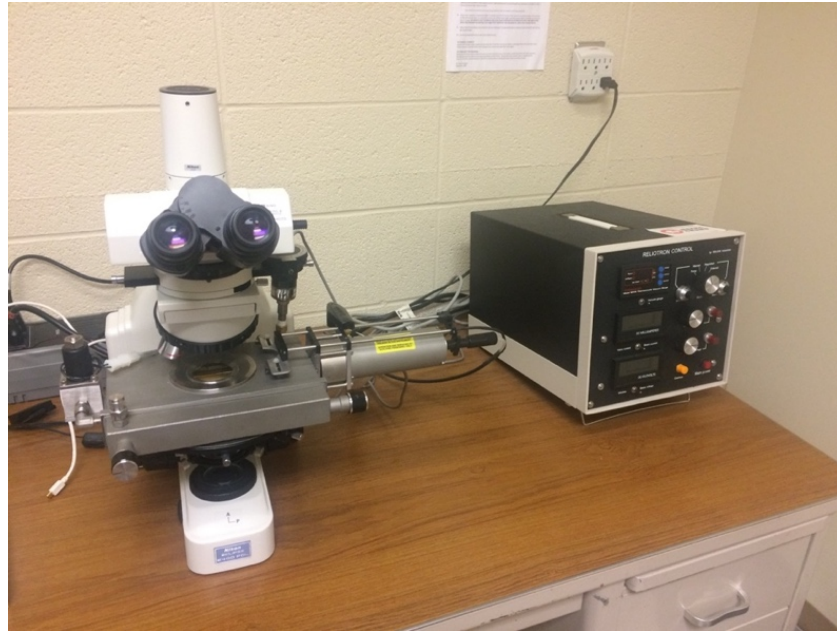


Figure 3.11. Acadia University Reliotron cold-cathode CL system.

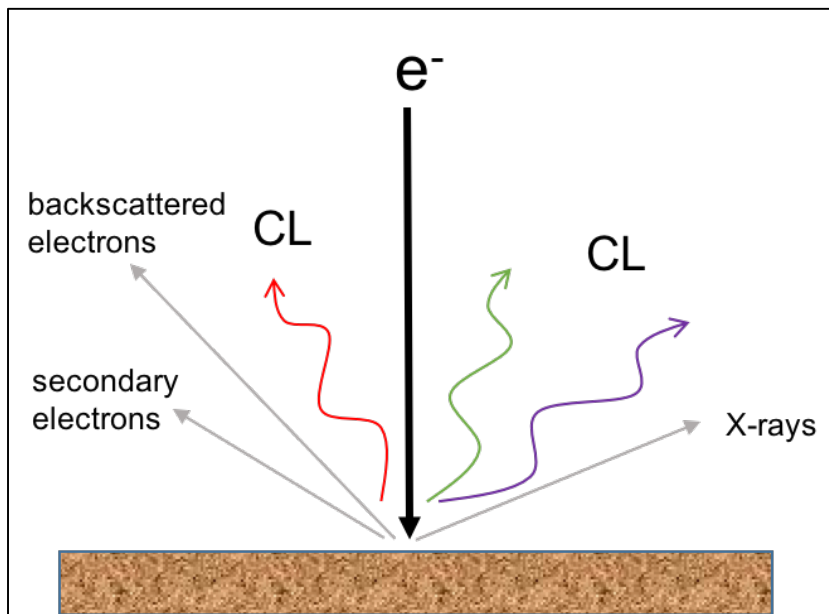


Figure 3.12. Simplified diagram of cathodoluminescence and other released energy in response to electron bombardment.

## Chapter 4: Results

### 4.1 Lithofacies descriptions

The term “facies” originated from Gressly, 1838, but its use from here within is based on a refinement from Reading (1996). Rock units can be grouped into facies according to shared characteristics that reflect a certain depositional process or environment. The term lithofacies is used when groupings emphasize shared or similar physical and chemical structures is used for grouping of similar rock units. Interpretations of depositional environment allow grouping of environmentally related lithofacies by facies association, which provides more insight into the depositional history of an outcrop containing genetically related strata (Reading, 1996). Based on field observations, six lithofacies have been identified in bedsets that are separated by the studied erosional surfaces in the Wolfville Formation at Rainy Cove (Table 4.1). The facies descriptions and interpretations are supported by similar observations in regional studies by Nickerson (2010) and O’Connor (2016).

#### *Lithofacies 1 (F1) – Matrix-supported clastic breccia*

*Description:* This lithofacies comprises moderately sorted metasedimentary clasts in a sand matrix. Clasts are dominantly metasilstone fragments that appear to be sourced from the underlying Horton Group rocks. Clast sizes range from 1-40 mm and tend to be subangular to angular in shape with low sphericity. Clasts make up 10-15% of the rock volume. The matrix is a dark red, fine-grained sandstone of which appears well cemented. Grey-coloured redox mottling is apparent throughout the unit. There are no identified biogenic structures. This facies is approximately 0.5 m in thickness and is found at the base of the Wolfville Formation.

*Interpretation:* A massive bed containing brecciated clasts suggests deposition by alluvial debris flows. The dominant metasedimentary angular clasts indicate a proximal or intrabasinal source (likely the Carboniferous Horton Group) and a relatively short transport distance. The red colour and redox mottling indicate deposition in an arid environment with periodic subaerial exposure and potential vegetation or post-depositional ground water infiltration.



### *Lithofacies 2 (F2) – Clast to matrix-supported conglomerate*

*Description:* This lithofacies forms faintly trough cross-stratified units of poorly sorted conglomerate. Clasts are subrounded and range from pebble to cobble size, making up 30-40% of the rock. Clast compositions include a variety of lithologies including slates, granitic fragments, and quartzites. Beds often show clast imbrication, especially in the clast-supported sections. The matrix is composed of red grains with average grain size of medium-upper to coarse-lower sand and is well cemented. Beds typically fine upwards, transitioning from clast-supported to matrix-supported conglomerate. There are no identified biogenic structures.

*Interpretation:* This lithofacies was deposited as channel infill and bar deposits in a fluvial channel system. The clast-supported conglomerate at the base of the units represents the bedload transport of the river, and trough cross-stratification forms by barform migration with coarser sediment in deeper portions of the river flow (Rieneck and Singh, 1980). The lithofacies forms interpreted barform structures on the beach and beds in outcrop ranging in thickness from 0.2 m to upwards of 2.0 m due to frequent erosional breaks. Clast imbrication results from the unidirectional fluvial flow regime.

### *Lithofacies 3 (F3) – Pebbly to clean sandstone*

*Description:* This lithofacies forms sandstone units with common (15-20%) subrounded to rounded pebble-sized clasts of varying lithologies including slates, granitic fragments, and quartzites. The matrix is a red sandstone with average medium-lower grain size and is well cemented. Some sections fine upward and show parallel lamination near the top of beds. Pebbles tend to be common along the base of the units and become rare higher in the section. This lithofacies forms beds 0.2 m to 1.0 m thick with sharp basal surfaces. There are no identified biogenic structures.

*Interpretation:* This lithofacies formed from bedload and suspended load deposits within the braided channel system, where flow energy was too weak to transport clasts larger than pebble-size. The sand-size grains are interpreted to have been deposited in fluvial barforms under fluctuating flow energies (Rieneck and Singh, 1980).

#### *Lithofacies 4 (F4) – Silty sandstone*

*Description:* This lithofacies forms sandstone units with grain sizes ranging from silt to medium-lower sand, with an average grain size of fine-upper sand. The sandstone beds are 0.5 m or less and contain a small number of pebble size rounded clasts and rare 10-20 cm thick scoured sections filled with coarser grains and pebble lag (lithofacies 2 and 3). Some units also show faint parallel laminae. There are no identified biogenic structures.

*Interpretation:* This lithofacies represents the deposition of sediment from suspension and bedload transport in a fluvial channel system during periods of lower energy flow (Rieneck and Singh, 1980). Deposition is punctuated by higher energy periods eroding the small scoured sections into the underlying beds.

#### *Lithofacies 5 (F5) – Clay*

*Description:* This lithofacies is a structureless clay containing rare subrounded pebble clasts of varied metasedimentary lithology. The clay bed drapes over the underlying silty layer (lithofacies 4) and is overlain by an erosive conglomeratic bed (lithofacies 1). There are no identified biogenic structures. This lithofacies was recorded only in one location, where it forms a thin red clay bed varying in thickness from 4 to 8 cm.

*Interpretation:* Fine clay sized grains are deposited by suspension settling in quiet waters. This bed likely formed in an abandoned portion of the fluvial channel system where energy conditions were low for a long enough period to allow settling.

### *Lithofacies 6 (F6) – Paleosol*

*Description:* This lithofacies comprises massive 0.5 to 1.0 m beds of silty to fine grained red sandstone with common grey redox patches. The beds are sharp-based and capped by erosional surfaces. The beds may be capped by carbonate nodules that increase in frequency upward until they coalesce to form a thin caliche horizon approximately 0.05 m thick. There are no identified biogenic structures.

*Interpretation:* This is a paleosol layer where soil formed during periods of subaerial exposure. The grey redox mottling may indicate plant rooting. The caliche deposit formed by precipitation of carbonate from supersaturated groundwater in the sediment (Leeder, 1975). The caliche horizon is presently at the top of the bed, but would have precipitated below the surface of the soil. This indicates a semi-arid climate with alternating rainy and dry seasons. During dry seasons, groundwater is driven out of the sediment, promoting calcium carbonate precipitation.


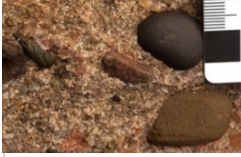

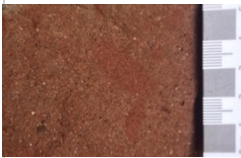


Facies	Lithology	Description	Interpretation	Facies Association	Field Photo
F1	Matrix-supported breccia	Chaotic beds of poorly sorted 1-40 mm angular metasedimentary clasts in red sand matrix	Viscous debris flow deposits	Alluvial fan	
F2	Clast to matrix supported conglomerate	Trough cross-stratified, poorly sorted beds with subrounded, pebble to cobble sized clasts of varied lithology in red sandstone matrix	Channel infill and barform bedload deposits of braided channel system	Fluvial	
F3	Pebbly to clean sandstone	Planar cross-stratified medium to coarse grained sandstone with common subrounded pebble clasts	Bedload and suspended load deposits in fluvial braided channel system	Fluvial	
F4	Silty sandstone	Silt to medium-lower sand size red sandstone with occasional subrounded pebble clasts and rare 10-20cm scale scoured channel sections	Low to intermittent energy suspension load deposits in fluvial braided channel system	Fluvial	
F5	Clay surface	Thin red bed of massive clay with very rare subrounded pebble clasts	Abandoned channel or low energy deposits in fluvial braided channel system	Fluvial	
F6	Carbonate noduled paleosol	Massive beds of silt to fine sand size red and grey mottled unit, containing thin horizons of carbonate nodules	Mature paleosol	Fluvial	

Table 4.1. Descriptions, associations, and photographs of identified lithofacies in the Wolfville Formation at Rainy Cove.

## 4.2 Measured Sections

Measured sections were logged across the main erosional surfaces in the Wolfville Formation at Rainy Cove (Figure 4.1). The three measured sections are: the Carboniferous-Triassic unconformity (Section 1), the fluvial erosional surfaces (Section 2), and the intra-Triassic unconformity (Section 3). The locations of each of the three measured sections are shown below in Figure 4.1 and the corresponding logged sections with labelled lithofacies are shown in Figures 4.2-4.4.

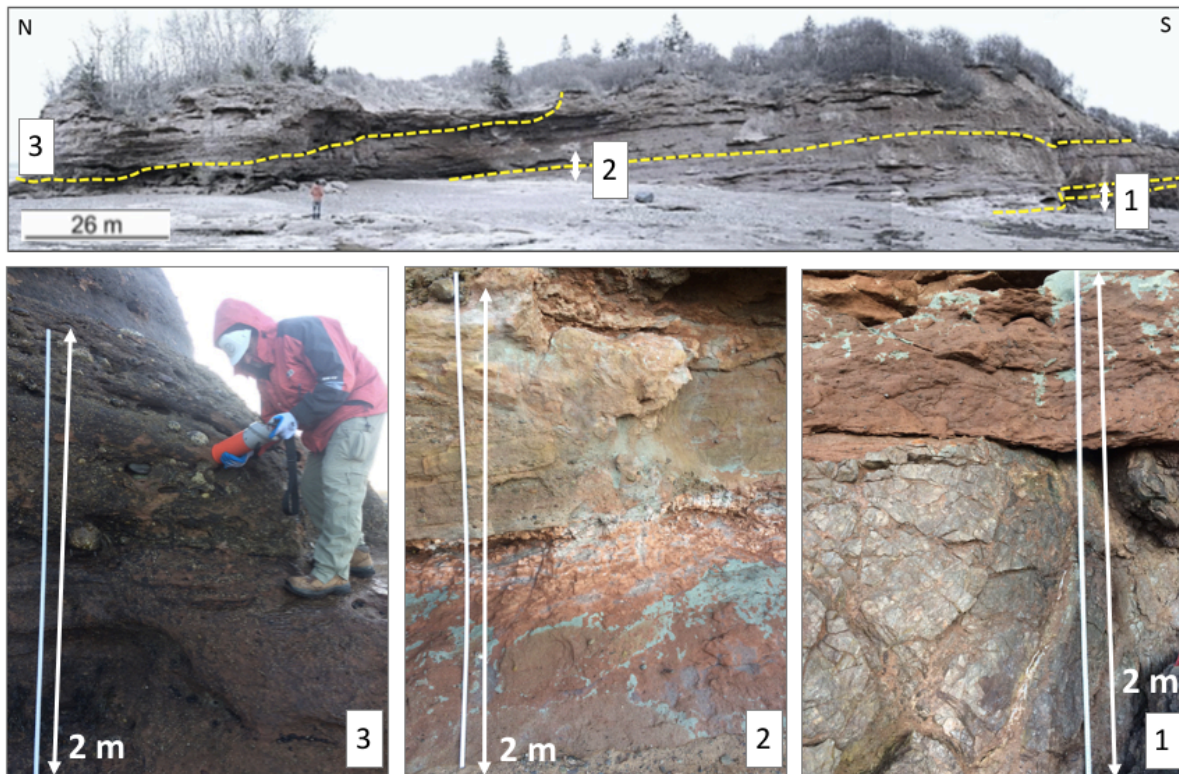


Figure 4.1. Rainy Cove outcrop and locations of the three measured sections at (1) the Carboniferous-Triassic Unconformity, (2) the fluvial contacts, and (3) the intra-Triassic Unconformity.

### *Section 1: Carboniferous-Triassic Unconformity*

Section 1 depicts 1.4 m of Triassic sediments overlying the steeply dipping Carboniferous metasediments (Figure 4.2). Near the top of the Carboniferous section, small fractures have opened along the tilted bedding planes of the metasediments. Triassic sandstones have filled in these openings (Figure 4.2). Directly above the angular unconformity

lies a 0.9 m layer of brecciated sandstone (F1) made up of fine grained sand with angular metasedimentary clasts. Evident throughout this unit are 10 to 15 cm scale grey redbox patches. Overlying the breccia is a sharp contact underlying a pebbly sandstone bed (F3) containing several 10 cm high scours with clast lags.

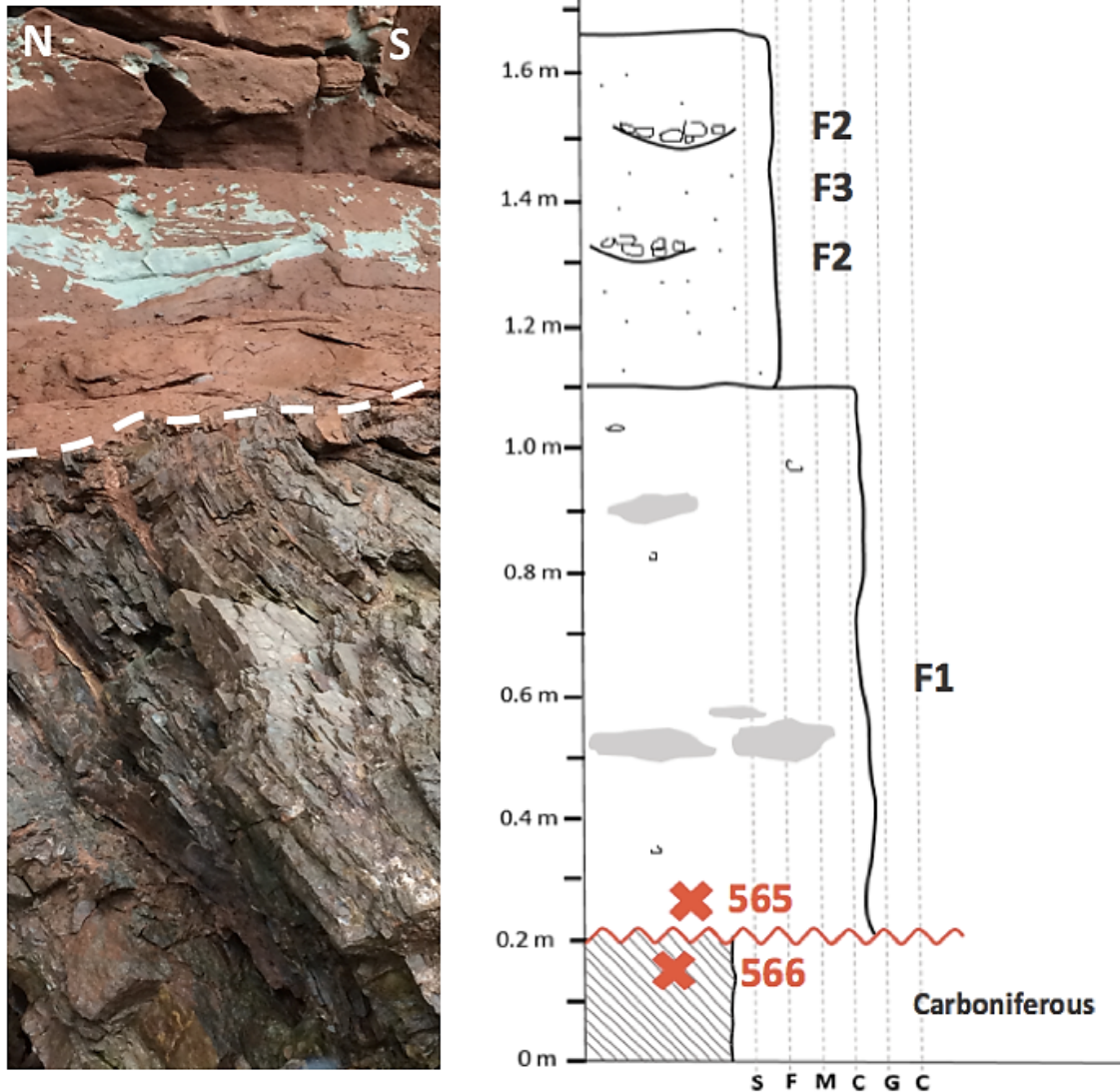


Figure 4.2. Measured section of the Carboniferous-Triassic Unconformity beside an outcrop photo. Sample locations are marked with an x and the lithofacies are labelled beside the section. The angular unconformity surface is marked by a red line.

## *Section 2: Fluvial Contacts*

Section 2 shows erosional boundaries within the alluvial and fluvial sections of the Triassic sediments (Figure 4.3). The Carboniferous-Triassic unconformity is not present at this location. The first unit is a 0.5 m sand bed (F3) made up of fine grained sand with occasional pebble clasts. At the top of this section is a paleosol horizon (F6) with 5 to 10 cm thick white carbonate nodules. Directly overlying the caliche horizon is a sharp based conglomeratic sandstone (F2). This contact is interpreted to represent a short hiatus in time where the paleosol was eroded to the depth of the caliche. The paleosol horizon would have formed on a well-drained alluvial plain with arid conditions allowing carbonate precipitation from pore waters (Leeder, 1975). This paleosol was then eroded down to the carbonate-rich caliche layer prior to or during the resurgence of the fluvial system. The conglomeratic bed transitions upward to a pebble sandstone bed (F3) that is fine to medium grained and contains grey redox patches. It has a conglomeratic base that transitions upward to occasional pebble and cobble-sized rounded metasedimentary clasts. The layer is faintly planar cross-stratified. The next unit is a sharp-based layer of pale red silty sandstone (F4) with grey redox patches and few clasts. Over this layer is a thin bed of massive clay (F5). At the top of the section is an erosional scour-base fluvial section with a poorly sorted lag of subrounded cobbles 2-10 cm in size.



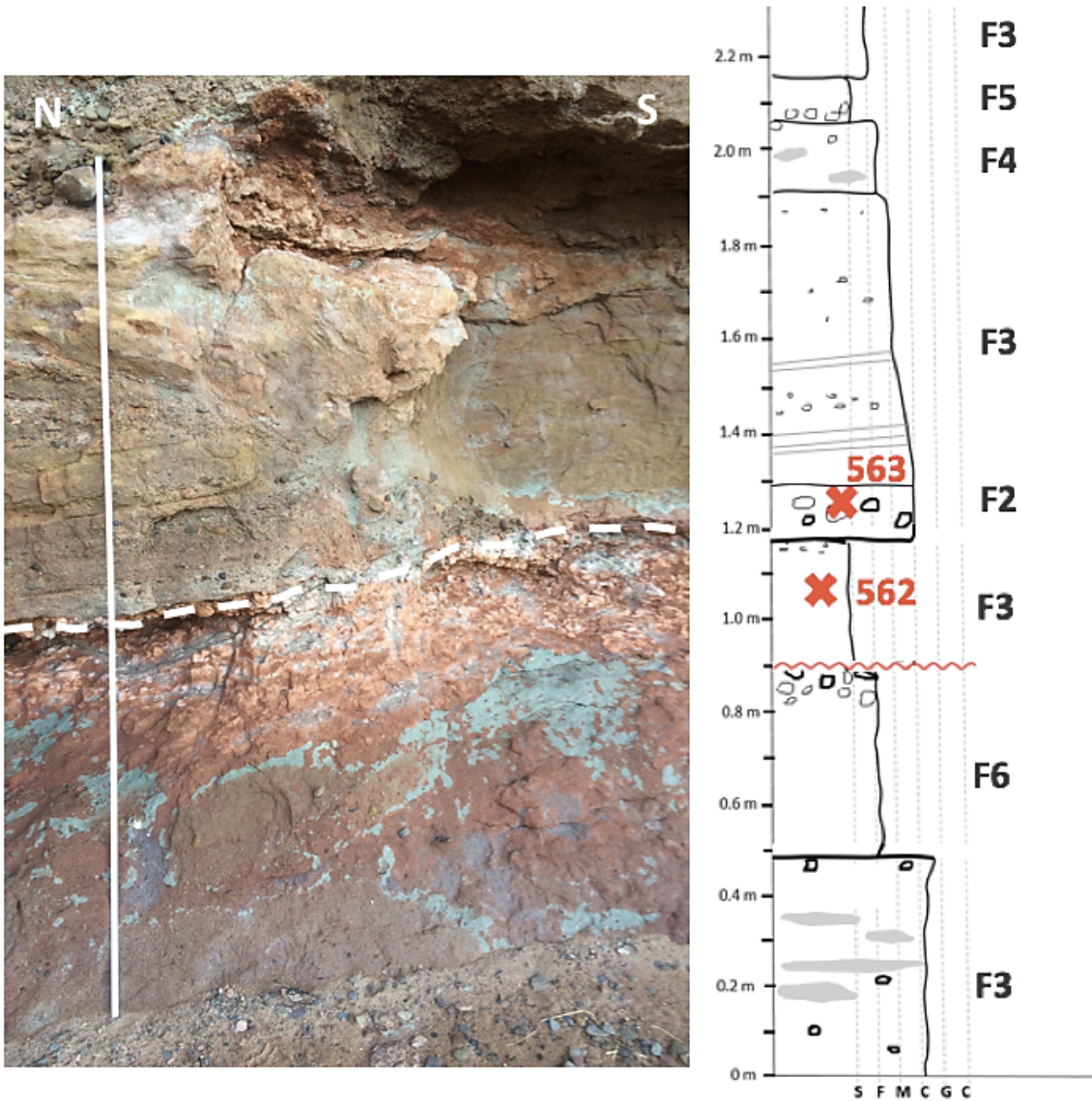


Figure 4.3. Measured section of erosional surfaces in the Triassic fluvial section beside an outcrop photo. Sample locations are marked with an x and lithofacies are labelled beside the section. The red line marks and unconformity surface representing a significant time interval.



### *Section 3: Intra-Triassic Unconformity*

Section 3 was measured on either side of the intra-Triassic unconformity near the promontory point (Figure 4.4). The bed below the unconformity is medium-grained planar laminated to featureless sand that fines upward before encountering the erosive intra-Triassic unconformity. There are some subrounded metasedimentary pebble clasts that increase in concentration toward the contact. This bed is part of a large fluvial barform that is preserved within the mid-intertidal zone on the beach and displays planar cross-stratification showing northward paleoflow. At the angular unconformity, the erosional scour base of the incision channel is marked by large subrounded metasedimentary clasts 10 to 15 cm long. These clasts show imbrication and alignment of their long axes subparallel to the channel base. The rest of the fluvial section contains alternating pebbly sandstone and conglomeratic lithofacies (F3 and F2, respectively).

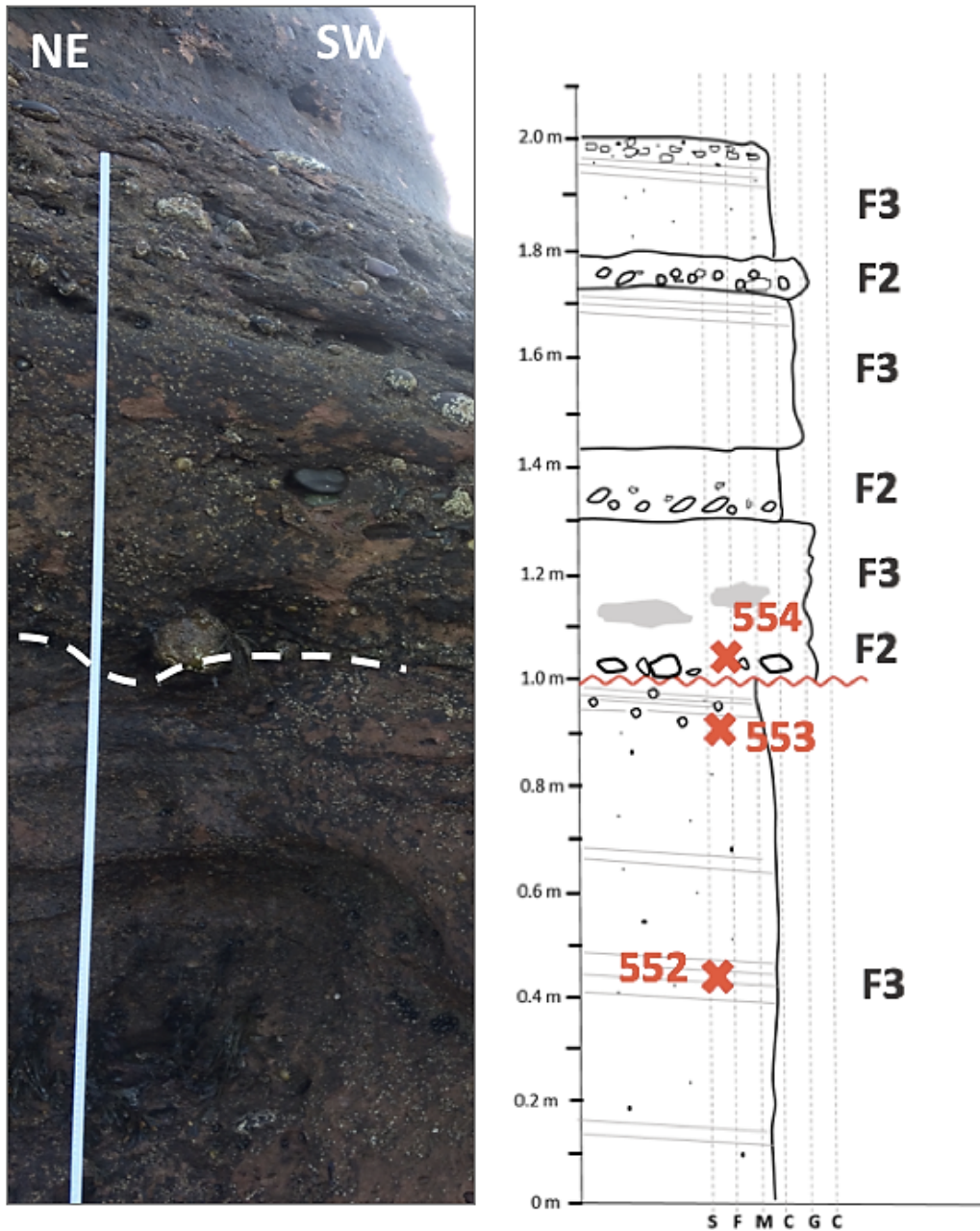


Figure 4.4. Measured section of the Intra-Triassic Unconformity (ITU) beside an outcrop photo. Sample locations are marked with an x and lithofacies are labelled beside the section. The red line marks the ITU surface.

### 4.3 Gamma Scintillometer Readings

Gamma ray scintillometer counts taken along each of the measured sections have been plotted against section height (Figures 4.5, 4.6, 4.7). The main erosional surfaces for each section are marked with a dotted line. Higher gamma ray counts indicate higher quantities of radioactive elements Potassium, Uranium, and Thorium. Rocks with higher shale content or organic matter tend to have higher radioactive element content (Nichols, 2009).

#### Section 1: Carboniferous-Triassic Unconformity

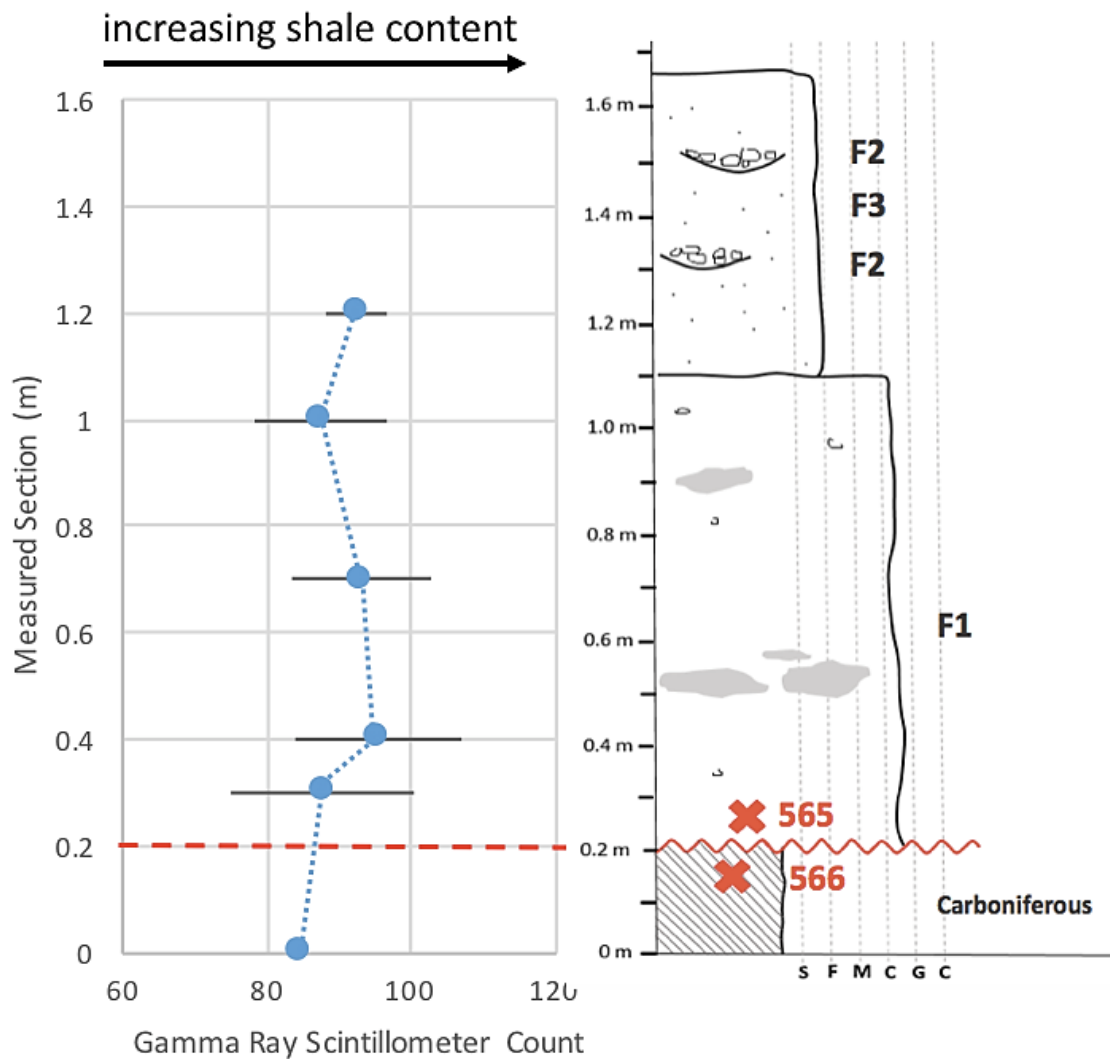


Figure 4.5. Gamma ray scintillometer counts plotted against metres measured for Section 1 (Carboniferous-Triassic Unconformity).

Section 2: Fluvial Contacts

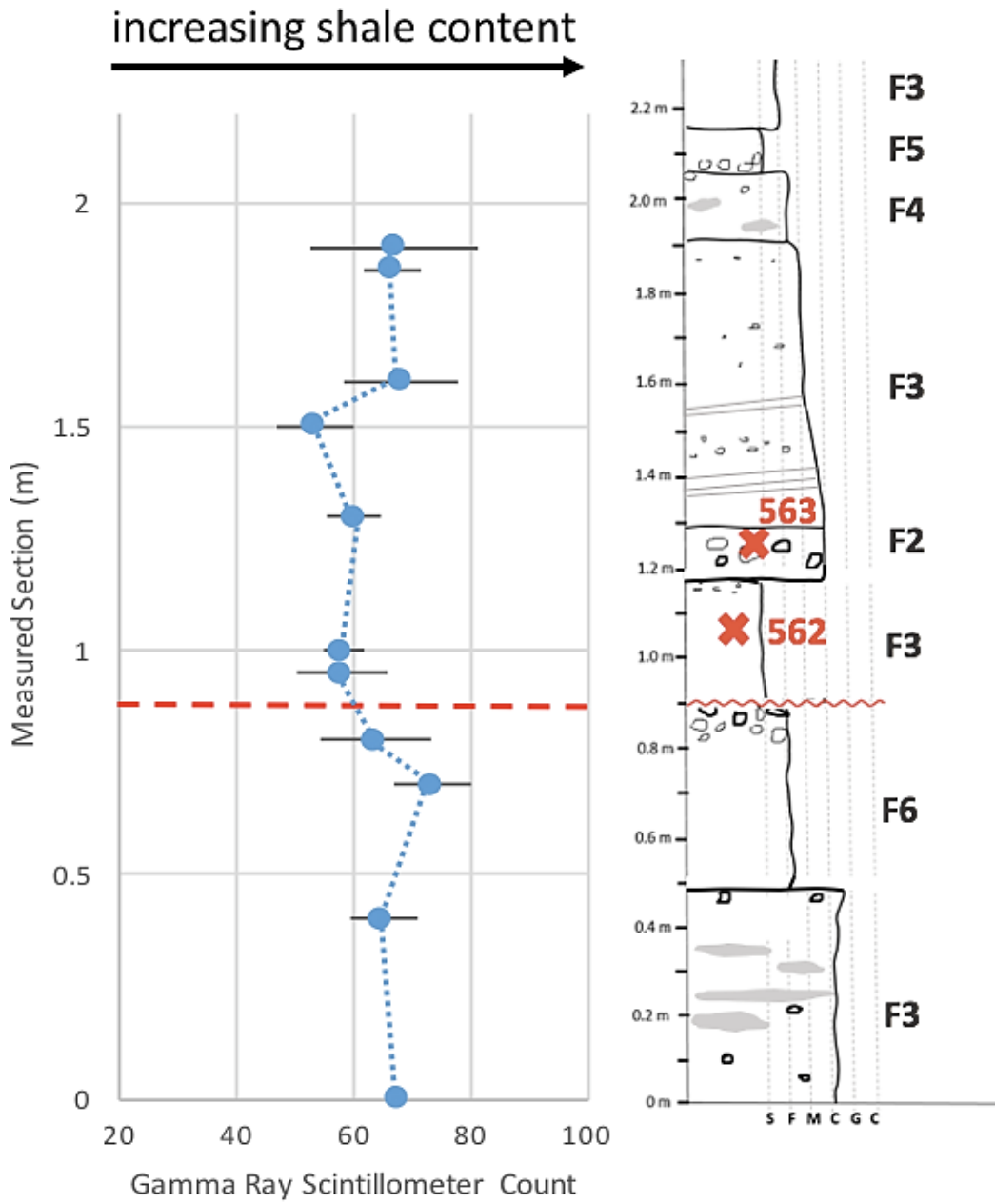


Figure 4.6. Gamma ray scintillometer counts plotted against metres measured for Section 2 (Fluvial Contacts).

Section 3: Intra-Triassic Unconformity

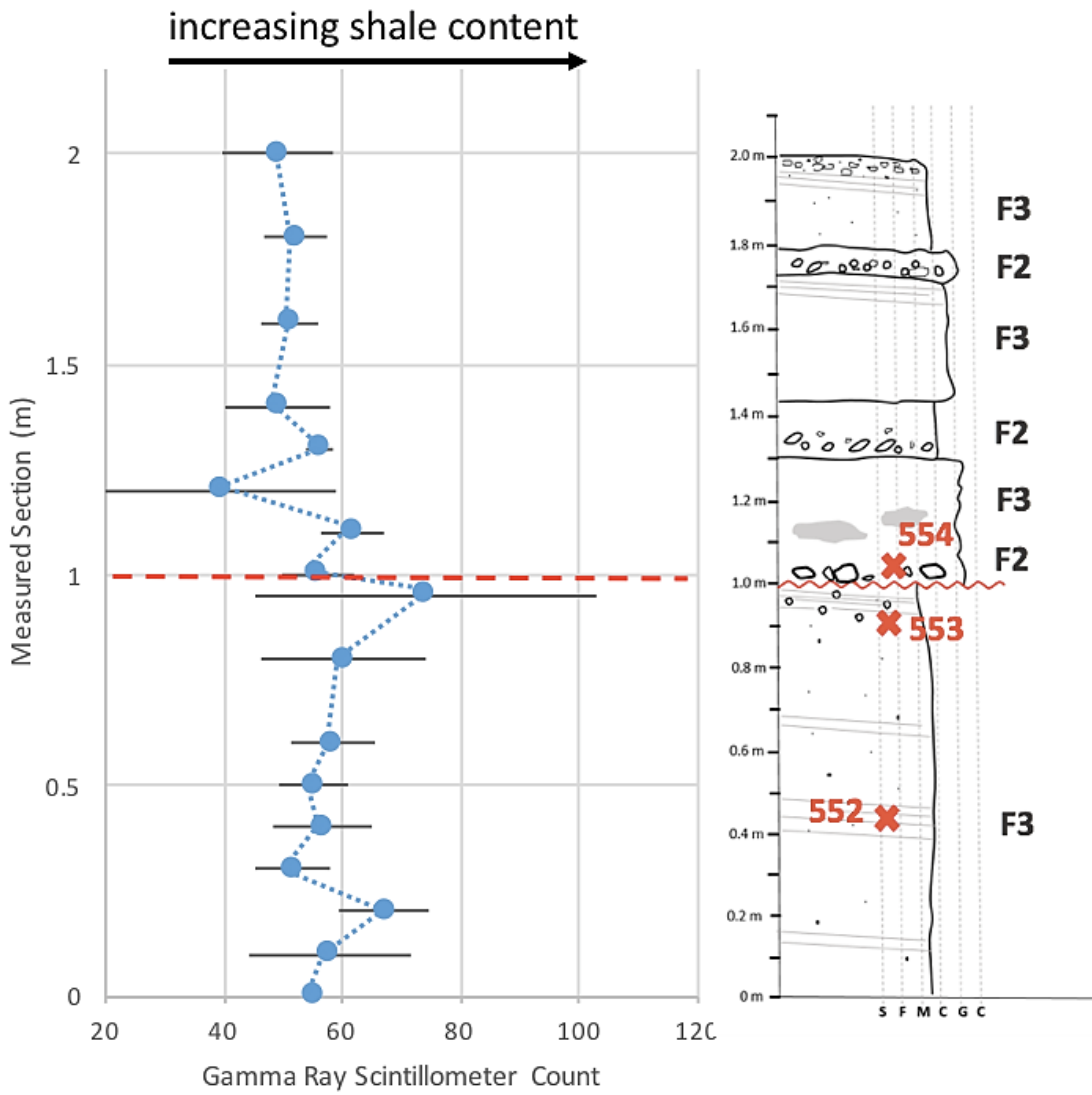


Figure 4.7. Gamma ray scintillometer counts plotted against metres measured for section 3 (Intra-Triassic Unconformity).

#### 4.4 Permeability

Results from the permeability data are reported below in Table 4.2. The table presents the average TinyPerm value from three readings and the permeability value that was calculated for each sample using the chart in Figure 3.8. Seven of the sixteen hand samples were of sufficient size to take permeability readings. The permeability averages range from 32.78 to 276.53 mD.

Sample No.	Avg Permeameter Reading	Permeability (mD)
GW553-2016	11.28	87.52
GW554-2016	11.63	32.78
GW559-2016	11.59	36.67
GW560-2016	11.14	129.64
GW561-2016	10.87	276.53
GW562-2016	11.00	192.01
GW563-2016	11.21	106.52

Table 4.2. TinyPerm II readings and calculated permeability values for collected hand samples. Reported readings are an average of three readings taken per sample.

#### 4.5 Grain Size Measurements

Average grain sizes and standard deviations, in millimetres and in the phi scale, are reported in Table 4.3. Frequencies of grain size in phi scale (Boggs, 2012) are plotted below in histograms for each sample (Figure 4.8).

Sample	Average Grain Size (mm)	Standard Deviation (mm)	Average Grain Size (phi)	Standard Deviation (phi)
GW550-2016	0.44	0.24	1.33	0.64
GW551-2016	0.91	0.55	0.52	0.78
GW552-2016	0.61	0.70	1.13	0.94
GW553-2016	0.38	0.36	1.71	0.87
GW554-2016	1.13	1.03	0.19	0.95
GW556-2016	1.42	1.36	-0.16	0.93
GW557-2016	0.65	0.48	0.82	0.70
GW558-2016	0.82	0.55	0.54	0.83
GW559-2016	16.91	112.69	0.04	1.67
GW560-2016	3.72	26.71	0.23	1.27
GW561-2016	0.37	0.15	1.51	0.52
GW562-2016	0.19	0.21	2.82	1.11
GW563-2016	1.12	1.13	0.30	1.10
GW564-2016	0.82	0.55	0.52	0.78
GW565-2016	0.24	0.34	2.84	1.33

Table 4.3. Grain size measurements. Average grain size and standard deviation in millimetres and in the phi scale ( $-\log_2$  of size in mm) readings. Grain size decreases with increasing phi value.

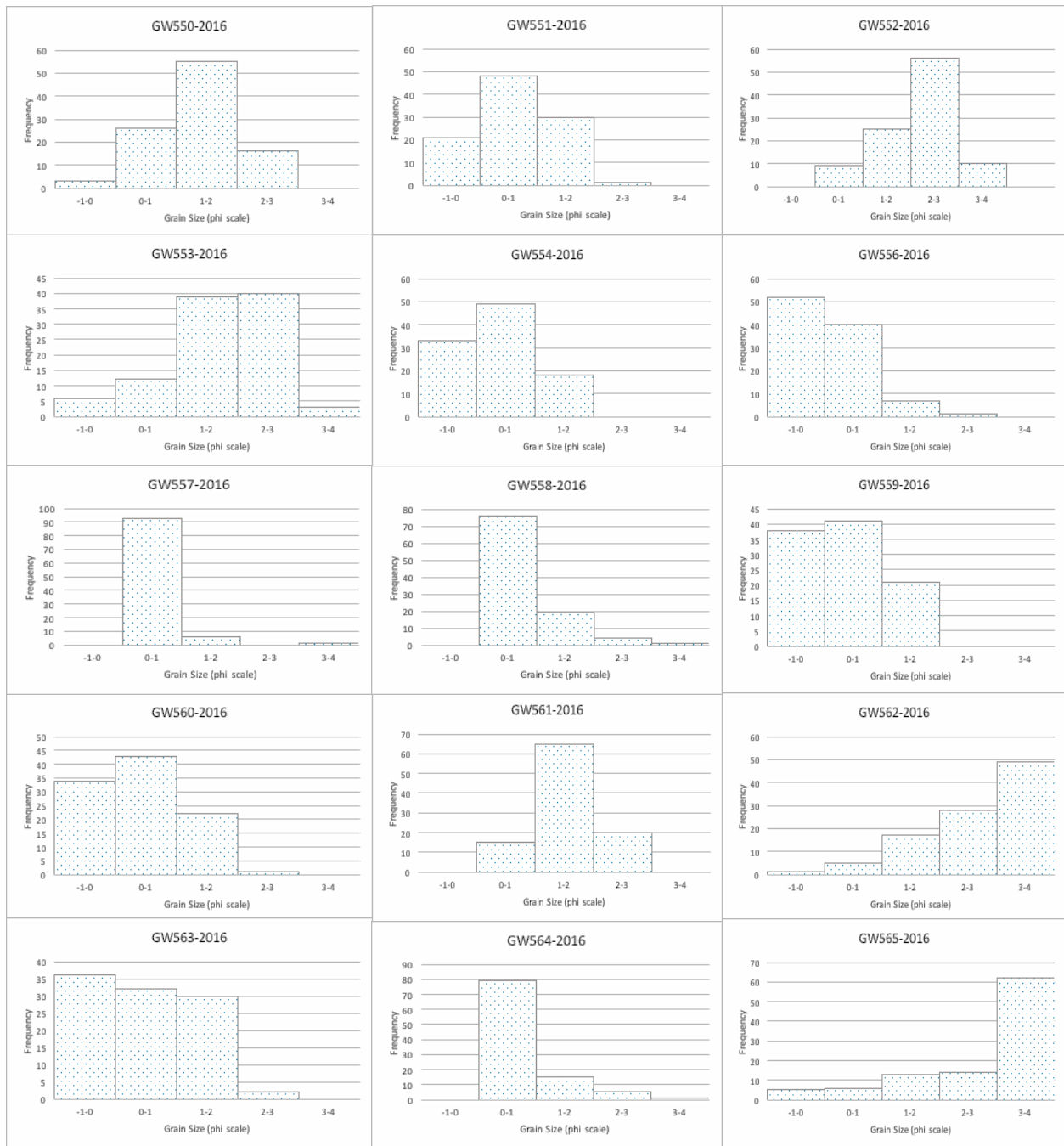


Figure 4.8. Histogram plots for frequency of grain sizes in phi scale for each of the Triassic sediment samples.



## 4.6 Cement Textures

Textural cement analysis of the 15 samples was completed using light polarizing microscopy. Detailed petrographic descriptions were not the focus of the work, as the rocks have been previously described (Kettanah et al., 2013; O'Connor, 2016). This section presents an overview of the petrography of the samples and the diagenetic textures observed, as well as the carbonate cement textures present.

The samples are composed dominantly of quartz grains, lithic clasts, feldspars, opaque minerals, sheet silicates, and rare accessory minerals garnet and tourmaline. Grain shapes are subangular to subrounded. Many samples show brown mineralization around the framework grains, likely from clays or from iron oxidation, and many of the feldspar grains have been altered or show partial dissolution. Samples also have rare smashed quartz grains, where secondary porosity has opened along microfractures. Cements in the pore space are not seen in the microfractures. Grain packing is loose with framework grains either not in contact or with limited tangential contact. All samples are well-cemented with carbonate. Other cements present include homogenous cement rims around the outside of framework grains, commonly the lithic fragments, which appear to be silica. Typical petrographic features in these sediments are shown in Figures 4.9 and 4.10.

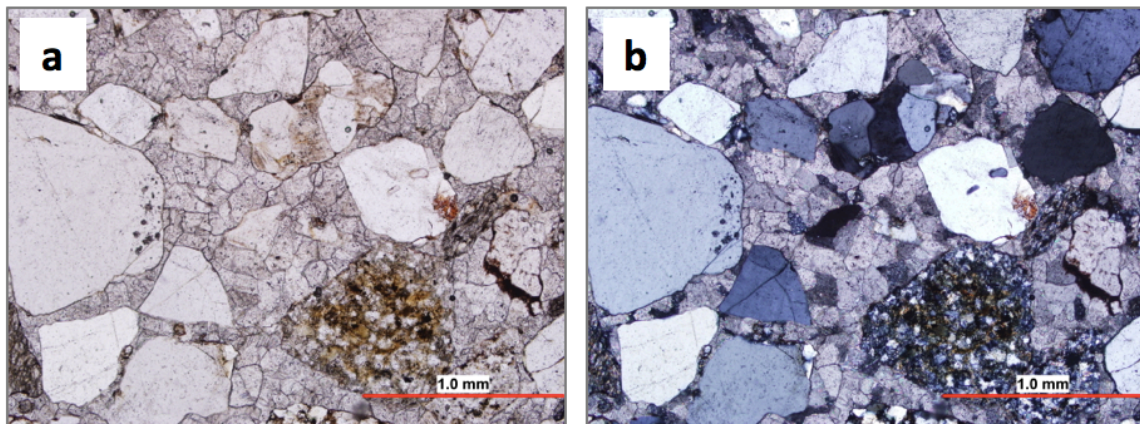


Figure 4.9. Photomicrograph in (a) plane-polarizing light and (b) cross-polarizing light showing the typical petrography of the Rainy Cove Triassic sediments. Framework grains are composed primarily of quartz, lithic fragments, and feldspars, and are well cemented with carbonate.

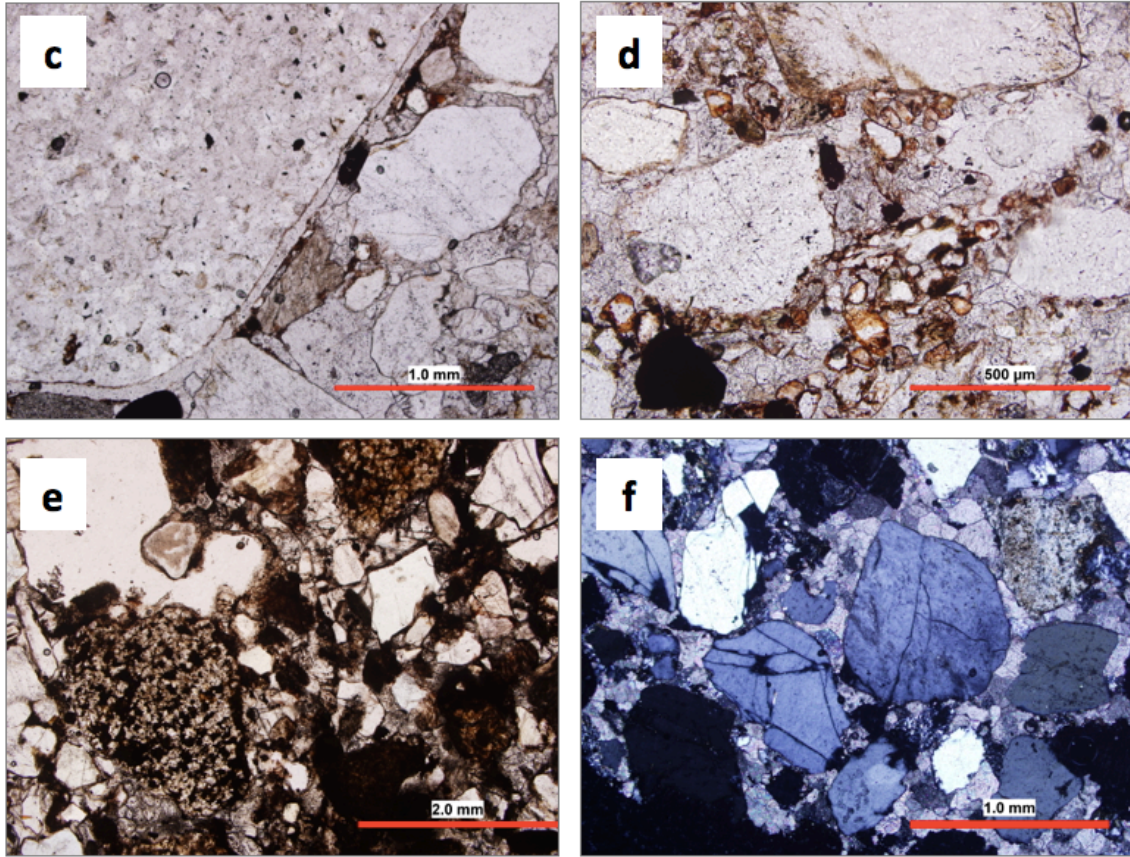


Figure 4.10. Photomicrographs showing some textural features of the Rainy Cove Triassic sediments. (c) Lithic fragment with rim of quartz, (d) feldspar grain with altered edge, (e) framework grains with brown clays around rims, and (f) smashed quartz grain with secondary porosity in the microfractures.

Carbonate cements are sparry and pore filling in all of the Triassic sediment samples. The carbonate crystals tend to be blocky, with sharp grain contacts and irregular grain edges. Grains have approximately equigranular size from the pore rim to the centre of the pore space. The grain size of the sparry carbonate crystals varies slightly between samples; some samples have a blocky mosaic where crystals appear relatively large within the pore space while others have a more granular mosaic with relatively smaller cement crystals. In the finer grained facies, pore space by missing grains is filled by a single continuous carbonate crystal. The other variation on the sparry texture is the presence of dogtooth cements. The dogtooth texture consists of bladed prismatic crystals that radiate outward from the edges of clasts before transitioning to a blocky sparite in the centre of the pore space. Simple drawings of these textures are shown in Figure 4.11, and photographs from the samples are shown in Figures 4.12 and 4.13.

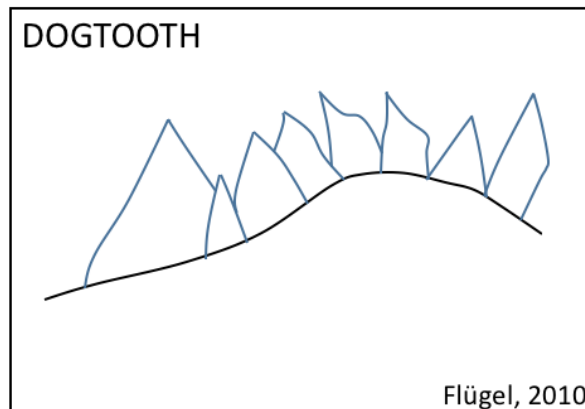
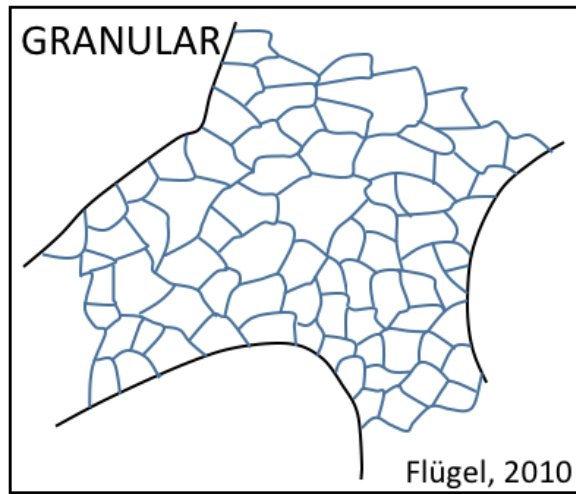
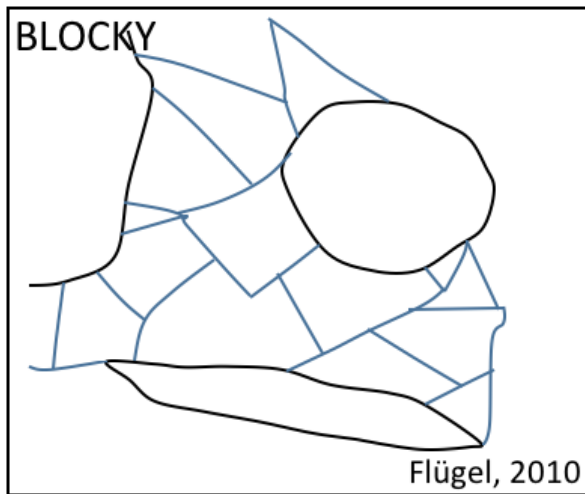


Figure 4.11. Simple drawings of blocky, granular, and dog tooth carbonate cement mosaics (Flügel, 2010).



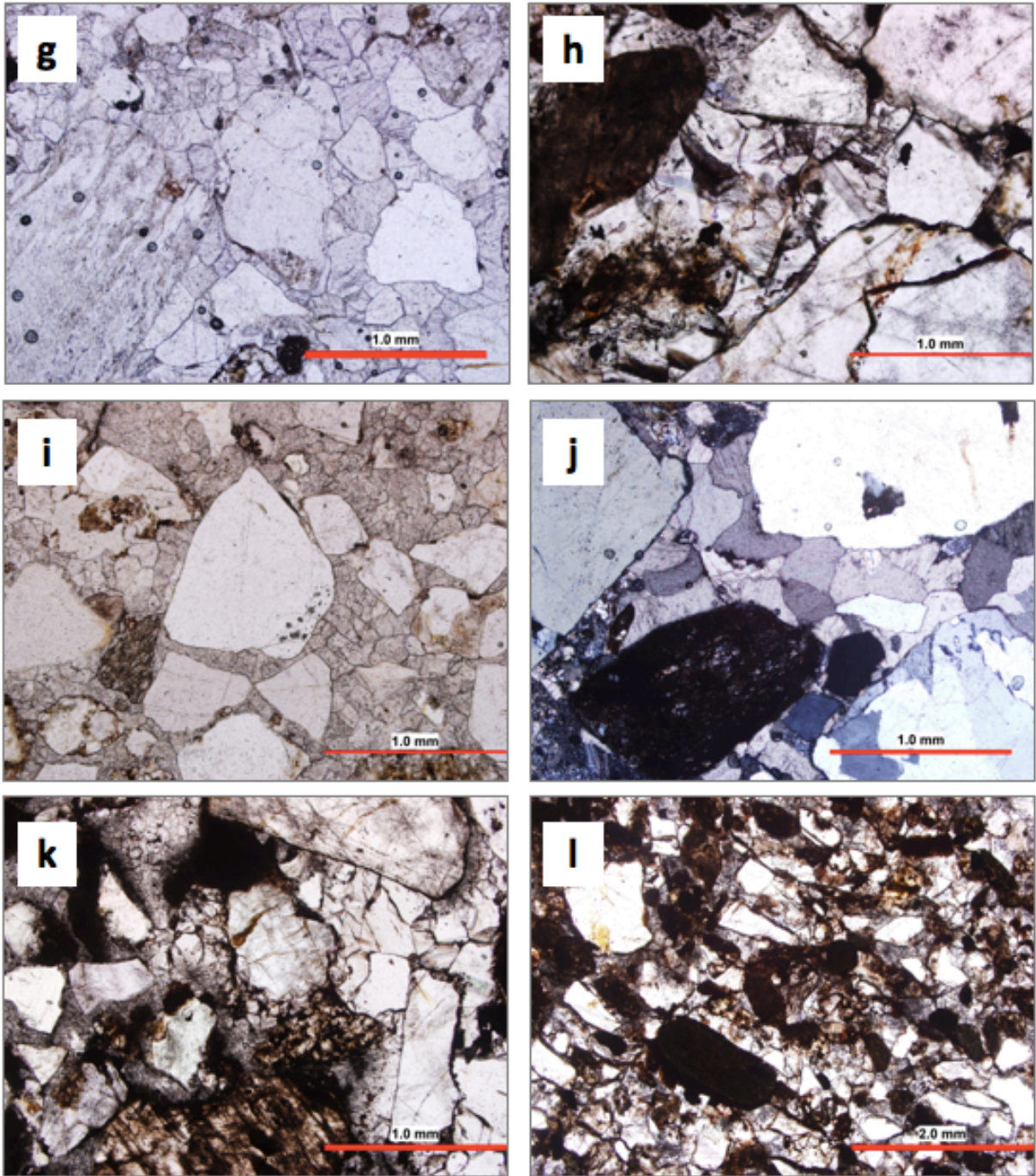


Figure 4.12. Photomicrographs showing sparry cement textures: (g, h, i, j) blocky mosaic, and (k, l) granular mosaic.

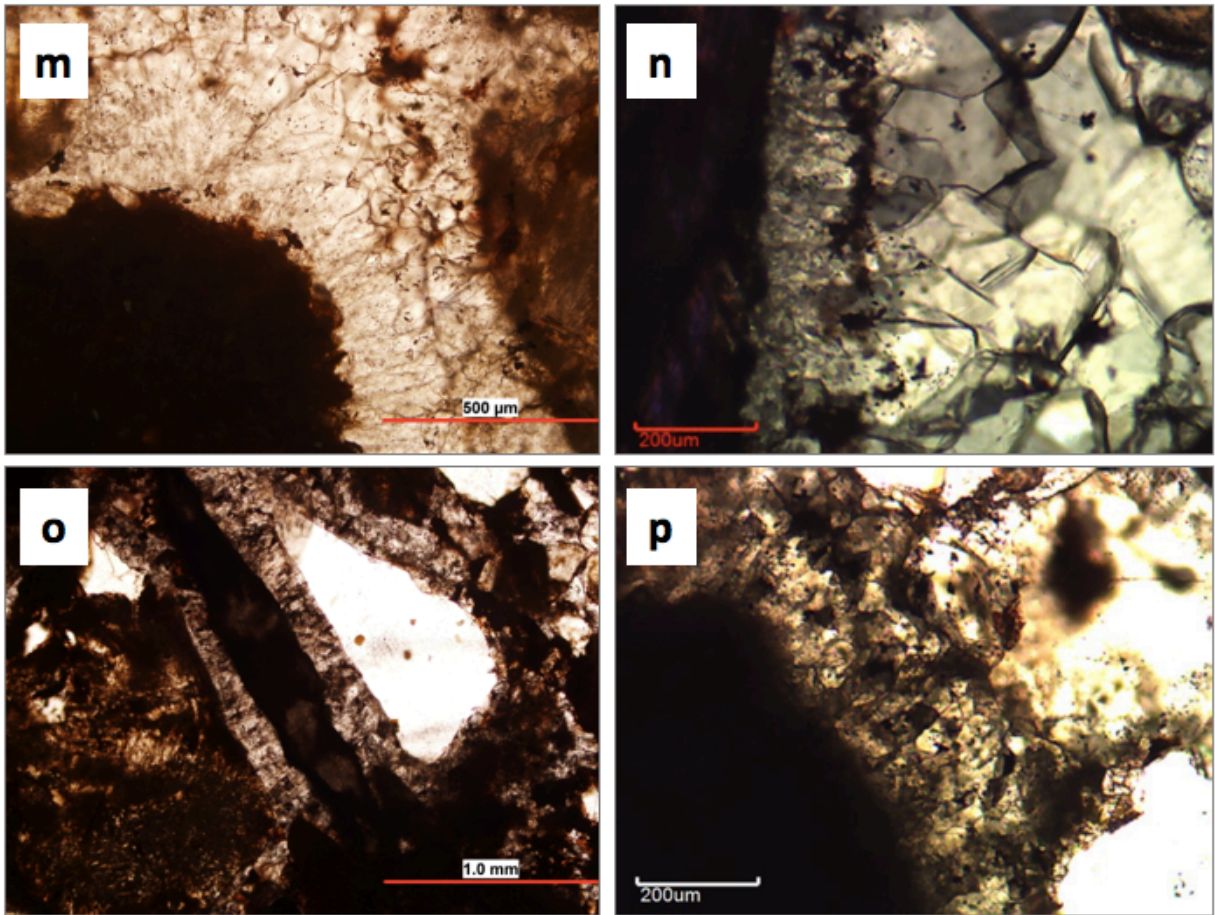


Figure 4.13. Photomicrographs showing dogtooth cement textures in the carbonate cements. Prismatic cement crystals radiate outward from the edges of framework grains and transition to sparry textures toward the centre of the pore space.



Table 4.4 sorts samples by the identified lithofacies and lists the observed cement textures and measured average grain sizes and permeability values. The cement textures do not appear to be grouped by any single facies or interpreted depositional environment.

		Cement Texture			Facies
		blocky	granular	dogtooth	
Sample Number	GW565-2016	✓			F1
	GW551-2016	✓			F2
	GW553-2016		✓		
	GW554-2016	✓	✓	✓	
	GW558-2016		✓	✓	
	GW563-2016	✓		✓	
	GW552-2016	✓			F3
	GW556-2016	✓			
	GW557-2016	✓		✓	
	GW559-2016		✓		
	GW560-2016		✓		
	GW562-2016	✓	✓		F4
	GW550-2016	✓			
	GW561-2016	✓			
	GW564-2016	✓			

Table 4.4. Summary of results connecting cement textures to lithofacies and lithofacies associations.

#### 4.7 Cathodoluminescence Photomicrographs

Cathodoluminescence photos were taken for four collected samples: GW552, GW554, GW557, and GW562. The features of interest in the cathodoluminescence photos are the luminescence colour, the brightness of luminescence, and variations in brightness. These features result from the chemical composition of the cements and change according to changes in composition of the pore fluids during cementation. Representative photos are shown in Figure 4.14.

The carbonate cements in these samples exhibit dull cathodoluminescence, with some bright orange luminescence around the rims of both framework and cement grains. Orange luminescence is common for carbonate cements. Much of the pore space appears black in samples, even where carbonate cements are present, cathodoluminescence of the cements is localized around grain rims or in isolated patches. Most grain rims luminesce a bright orange and the grain interiors are dark or black. The rims are generally faint around the carbonate crystals, and brighter around the framework grains. There are some single crystals that are very brightly luminescent compared to the surrounding cements, but they do not appear in groups of bright crystals or in specific patterns. Some carbonate crystals show evidence of zoning, where there are two or three layers of varying brightness within individual crystals. Occasional zoned grains were observed in each of the samples.

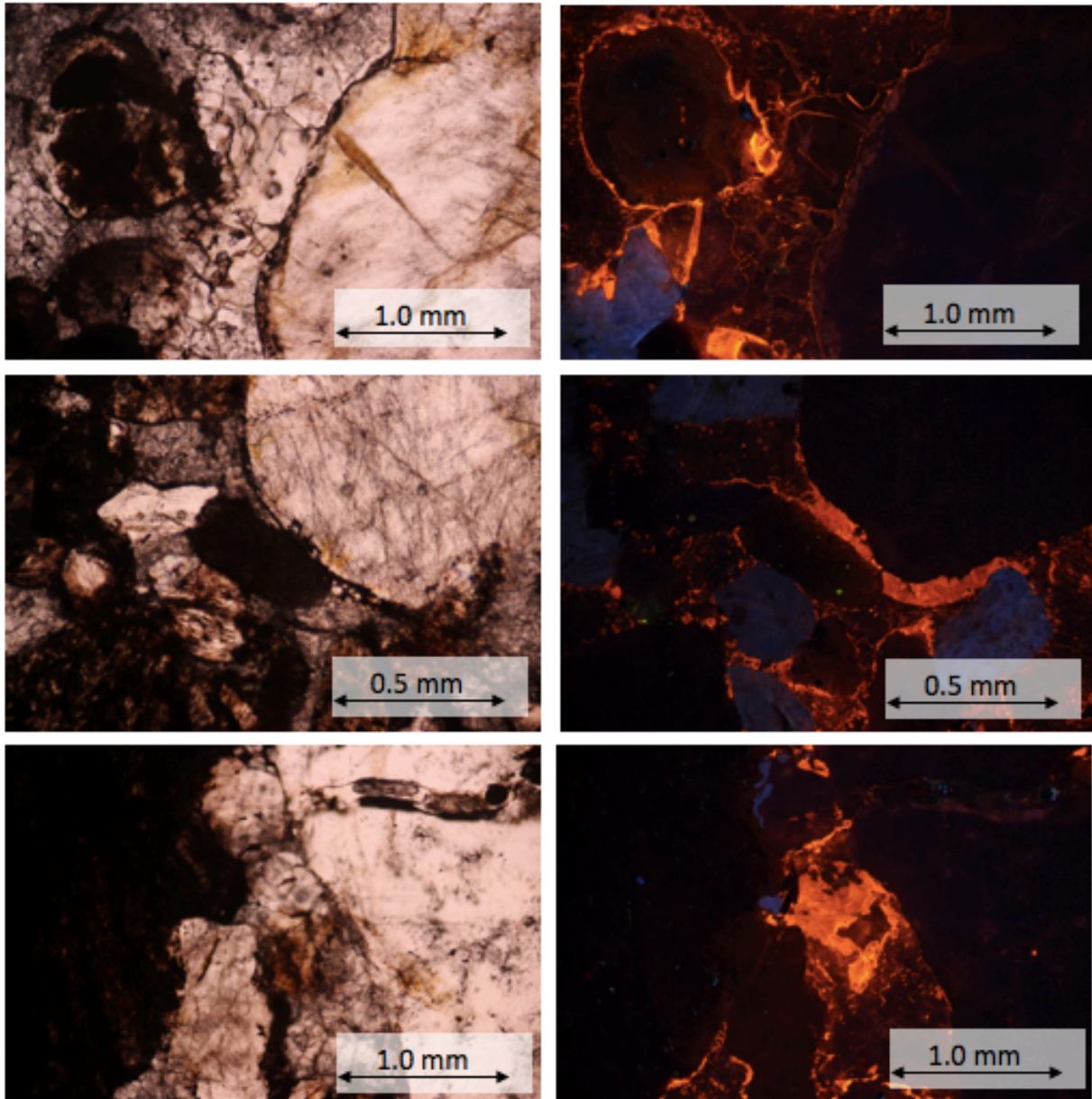


Figure 4.14. Photomicrographs under plane-polarized light (left) and corresponding sections under cathodoluminescence (right). The bright orange luminescence is from carbonate cements. Cements are brightest around grain edges and show limited crystal zoning.



## Chapter 5: Discussion

### 5.1 Lithologic Characteristics

The identified lithofacies in the Wolfville successions at Rainy Cove are interpreted to have been deposited in an active alluvial-fluvial depositional environment. The lowermost lithofacies, F1, represents early syn-rift deposition of proximal sediments in alluvial debris flows. It transitions up-section into fluvial lithofacies (F2, F3, F4, F5) representing a deposition in a fluvial setting. Presence of paleosol beds (F6) indicates periods of increased aridity and subaerial exposure of the sediment, along with percolation of supersaturated fluids and carbonate nodule cementation. Grain size measurements show that sediments commonly exhibit poor to moderate sorting. The lithofacies packages are separated by erosional surfaces. The major lithologic changes within the Triassic successions are between the alluvial and fluvial packages, between the paleosol and fluvial beds, and across the intra-Triassic unconformity. Grain sizes are larger directly above the erosional surfaces, which are produced by scouring and incision by fluvial channels. Channel bases tend to contain coarser material and then fine upward within fluvial beds, suggesting higher energy deposition at erosive bases and waning energy upwards.

Gamma ray spectrometry measurements showed little variation across the erosional surfaces (Figures 4.5 to 4.7). There was only a slight increase in gamma count across the Carboniferous-Triassic Unconformity, which was unexpected between the Carboniferous slates and the Triassic breccias. At the unconformity, the Triassic sediments fill in cracks at the top of the tilted Carboniferous beds, so the gamma measurements were interpreted to reflect measurement error due to contamination of the Carboniferous measurements with infiltration of Triassic sediments on the scale of the measurement intervals. It is also possible that the Triassic breccias overlying the Carboniferous have been contaminated by water percolation along the contact surface, which could transport radioactive elements between the Carboniferous and the lower Triassic sediments. The largest spectrometry change occurred at the intra-Triassic unconformity, where gamma count decreased sharply across the contact surface. The conglomeratic facies at the base of the incision channel had lower radioactive content than the barform sediments below. This could be due to a number of reasons including

higher amounts of fine sediment in the barforms, percolating groundwater in the lower successions, or small changes in sediment source and clast composition. The main lithologic change between the pebbly sandstone lithofacies (F3) at the top of the barform and the conglomeratic lithofacies (F2) at the base of the overlying incision channel is the grain size, which likely accounts for the change in gamma count.

Measured permeability data ranges from 32.78 mD to 276.53 mD. These values are considered to be relatively low and are most likely low due to pervasive carbonate cements that fill pore throats and prevent connectivity of any uncemented pore space. The lowest permeability value was recorded in the pebbly sandstone (F2) lithofacies and the highest in the silty sand (F4) lithofacies. The siltier sands with smaller grain size also displayed the best sorting (Figure 4.8). The best porosities and permeabilities are expected in well sorted sandstones because packing orientations have large interconnected pore throats (Boggs, 2012). Poorer sorting reduces porosity because smaller grains fill the pore spaces between larger grains. Grain size ranges were much higher for samples from the conglomeratic and pebbly sandstone lithofacies (F3 and F2) so the lower permeability values are consistent with expectations.

## **5.2 Carbonate Cementation**

### **5.2.1 Cementation Environment**

The main cement textures observed using microscopy are carbonate mosaics, with both blocky and granular variations. Four samples also show dogtooth textures. The observed cement textures likely indicate early meteoric cementation and later cementation in a burial environment. A schematic diagram of carbonate diagenetic environments, including the burial zone, is provided in Figure 5.1. The freshwater meteoric environment contains fluids of shallow groundwater systems that interact with surface water. In a burial diagenetic environment, the pore water has undergone interactions with the subsurface rocks and other fluids at subsurface conditions of higher temperature and pressure. This causes chemical modification of the pore fluids, resulting in different cement textures and geochemical signatures (James and Jones, 2016).

Blocky and granular carbonate mosaics are common to burial and meteoric cementation environments. They can also precipitate from recrystallization of previous cements. Dogtooth cements are common to shallow-burial or meteoric environments (Flügel, 2010). The three observed textures in the Wolfville successions could therefore occur in the meteoric and burial cementation environments. This is supported by the nature of the cement crystals. The cements are fairly clear and inclusion-free, which is common to burial and meteoric cements where pore waters have low ionic strength and are less microbially influenced compared to marine environments. The cements also fill the pore space completely as isopachous cements, which indicates that the pore space was filled with fluid prior to cementation (James and Jones, 2016). The crystal habit and clear nature of the cements is characteristic of diagenetic low-magnesium calcite (<4 mole %  $\text{MgCO}_3$ ). This is the most thermodynamically stable carbonate phase in non-marine pore water, so it commonly forms meteoric and burial cements (Flügel, 2010; Pufahl, personal communication, 2017).

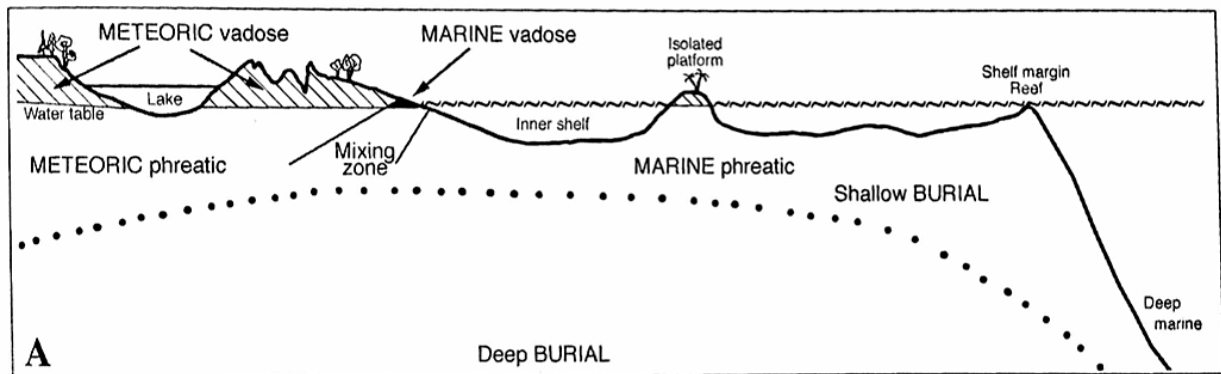


Figure 5.1. Schematic diagram of the carbonate diagenetic environments (Flügel, 2010).

Bright cathodoluminescence in carbonate minerals is most commonly due to excitation of reduced manganese ( $\text{Mn}^{2+}$ ) in the carbonate crystal structure. However, cathodoluminescence is inhibited by the presence of  $\text{Fe}^{2+}$ , which acts as a “quencher” element. Since these two elements act in opposition to produce the cathodoluminescence response, the iron to manganese ratio generally determines the brightness of cathodoluminescence (McIlreath and Morrow, 1990). Two cathodoluminescence microfacies are observed in the Rainy Cove samples: dull cements and brightly zoned cements. These are interpreted to be

from burial and meteoric cementation environments, respectively. Burial cements commonly have dull cathodoluminescence because of their higher  $\text{Fe}^{2+}$  content relative to  $\text{Mn}^{2+}$ . This occurs because the cements are generally precipitated out of reducing pore fluids in the subsurface (James and Jones, 2016). The cements in the samples showed dim luminescence overall, indicating a higher iron to manganese ratio. Most crystals were not strongly zoned, which is due to lack of chemical fluctuation in the pore fluids. In a burial environment, chemical composition of subsurface brines does not vary as much as in the near surface, so the zoning is not bright or pervasive (McIlreath and Morrow, 1990). Circulation of the brines through buried sediments replenishes pore fluids to maintain relatively consistent chemical signatures throughout cementation. However, the samples do show some grains with zoning and bright luminescence. These bright and zoned grains indicate slightly lower iron to manganese ratio and greater compositional variation than surrounding crystals. The meteoric phreatic zone lies in the shallow subsurface below the level of the water table, where water fills available pore space. In this environment, groundwater tends to flow toward local water base levels (in this case, water would flow basinward) and movement of water is locally active (James and Jones, 2016). This can produce chemical variation and crystal zoning if sediments are flushed with groundwater different chemical signatures. The cathodoluminescent variance may also be affected by accessory minerals in the rock causing chemical variation in the local pore water. Zoning may also occur where pore water is static and there is progressive change of chemical composition with continued cement precipitation. This is not observed in these samples as there is oscillatory rather than progressive zoning. Cementation in a marine environment is unlikely for these sediments, which were deposited and buried in continental rather than marine environments (Williams et al., 1985). The Wolfville sediments likely experienced two phases of cementation in their paragenetic history: zoned and brightly cathodoluminescent cement crystals in the meteoric and shallow burial environments, followed by blocky and granular mosaics with dull cathodoluminescence in the deeper burial environment. The early phase was likely quite limited, while the majority of cementation occurred during deeper burial.

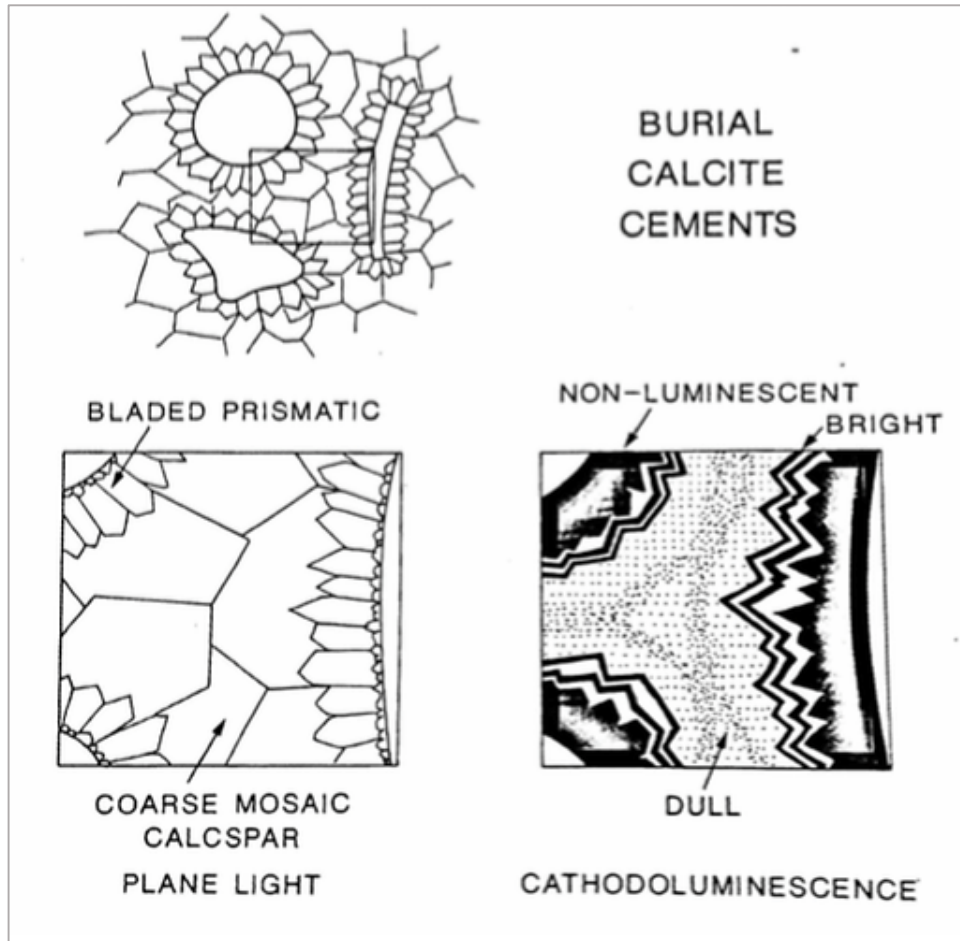


Figure 5.2. Characteristics of typical burial calcite cements, including blocky mosaics and dull cathodoluminescence (McIlreath and Morrow, 1990).

### 5.2.2 Impact of Cementation on Erosion

There is little variation in cement texture between different lithologies (Table 4.4). Although small variations in cement crystal size can be seen between the samples, the cements have similar overall characteristics and the observed cement textures are not limited to any single lithofacies. Had there been large differences in cement textures across lithofacies, this could indicate changes in cementation environment. If all cementation had occurred in shallow environments, it could be possible to have different cementation phases separated by the erosional boundaries. However, there is little textural variation and the entire outcrop section was likely cemented within the same relative time frame. Since the majority of cementation is interpreted to be from a burial environment, then all of lithofacies and erosional surfaces would have formed prior to the carbonate cementation. Despite small variations, there is no indication that changes in cement textures could account for different erodibility across the outcrop. All lithofacies are well cemented and all of the carbonate textures are a variation of a sparry mosaic and should not behave differently under erosive forces. The differences in erodibility causing preferential preservation of the barforms on the beach and the intra-Triassic channel promontory must be attributed to another geologic factor such as the grain sizes or sedimentary structural controls. The differences in cement crystal sizes can be attributed largely to precipitation rate (James and Jones, 2016). Grain size differences between lithofacies could also exert control on the available space for cementation (permeability) and the resulting cement distribution as well as cement crystal size.

### 5.3 Fluid Flow Implications

Fluid flow through rocks is controlled dominantly by porosity (the amount of void space in the rock) and permeability (the interconnectedness of the void space) (Ohen and Kersey, 1992). The nature of the pore space today determines the reservoir and aquifer quality of the rock, while the nature of the pore space in the past determines diagenetic patterns. Thin section analysis shows that the carbonate cements completely fill a significant amount of pore space in the Wolfville Formation at Rainy Cove. Prior to cementation, the porosity and permeability of this formation was likely quite high, which allowed the circulation of the fluid

that precipitated those cements. The best porosities and permeabilities are expected in well sorted sandstones because packing orientations have large interconnected pore throats. Poorer sorting reduces porosity because smaller grains fill the pore spaces between larger grains. The fluvial barforms and channel sands displayed moderate to poor sorting and lower permeability than silty sands. Permeability would be reduced through the more conglomeratic layers by poorer sorting, which tend to occur directly above erosional surfaces. However, the fact that the carbonate cements are prevalent and fill pore space throughout the Rainy Cove section indicates that original porosity and permeability was still of high enough quality to allow fluid percolation and cementation to occur. The matrix-supported conglomeratic facies still have sand-sized grains forming the matrix rather than finer silt or clay sized particles. Packing orientation for matrix sand grains between clasts did not reduce the pore space enough to prevent cementation.

In addition to cementation, the greatest impedance to fluid flow in these successions occurs from the vertical and lateral heterogeneity created by internal discordances. Baffles to fluid flow are created by areas or layers of lower porosity and permeability. Poorly sorted debris flow deposits and conglomeratic lithofacies sitting above erosional boundaries could create such baffles, limiting fluid flow. The silty sand and clay layer lithofacies (F4 and F5) present near the alluvial and fluvial contacts could also prevent fluid migration. Since these layers tend to be beds with trough or planar cross-stratification, the barriers would prevent vertical flow and may encourage horizontal flow along permeable layers separated by the laterally continuous sequence boundaries at the Carboniferous-Triassic and Intra-Triassic unconformities. This is likely controlled by breaks in cementation that may have opened along the unconformities, but could also occur along sequence boundaries of non-cemented fluvial systems where uniform lithofacies are eroded by poorly sorted channel deposits. High permeability pathways can act as “thief zones” that allow preferential flow and cause fluids to bypass the formation rather than accumulate in the rocks (Atkinson et al., 1990).



#### **5.4 Reservoir Quality Implications**

As stated previously, porosity and permeability measurements indicate poor reservoir quality in the sediments at Rainy Cove most likely due to the cementation. These well-cemented layers act as barriers to fluid flow. Although there is a thick section of multistoried braided channel deposits, the erosional surfaces within the formation also create baffles to fluid flow regardless of cementation. Conglomeratic and pebbly sandstone facies (F2 and F3) above erosional scours are moderately sorted, have low permeability, and are ubiquitous within the formation, creating multiple vertical baffles. Siltier sandstone facies with better sorting could create preferential pathways for flow and could act as conduits for fluids. Despite the poor reservoir quality in this location, there was a large amount of original pore space that was later cemented.

Other parts of the formation that exhibit similar lithologic character and are less cemented could have improved reservoir quality. This is seen elsewhere in the Annapolis Valley, where the Wolfville Formation is the most important regional aquifer formation. The Wolfville rocks are highly heterogeneous and form discontinuous lenticular bodies of aquifer/aquitard rocks of high reservoir quality. The finer-grained Blomidon Formation is another important regional aquifer (Rivard et al., 2007).

#### **5.5 Hydrocarbon Producing Analogue for a Braided Channel System**

Braided fluvial deposits tend to form high quality hydrocarbon reservoirs due to the good sorting, high porosity and permeability, and homogenous blocky channel morphologies that can hold large volumes of liquids. However, the heterogeneity created by dynamic fluvial environments poses a challenge for production from these reservoirs.

The Prudhoe Bay field is a giant reservoir located in Alaska with reserves of 22 million barrels of oil and 47 trillion cubic feet of gas (Atkinson et al., 1990). The reservoir formation is the Ivishak Sandstone, which is a Triassic braided-river dominated fluviodeltaic deposit overlying an unconformity surface. The fluvial deposits include channel and bar fill sequences separated by erosive-base surfaces and forming multistoried complexes. These deposits are surrounded by subaerial braided stream and abandoned channel and overbank deposits.

Reservoir quality is primarily controlled by sedimentary textures. Decreasing grain size in sandstone successions is noted from proximal to distal environments. Permeability of these

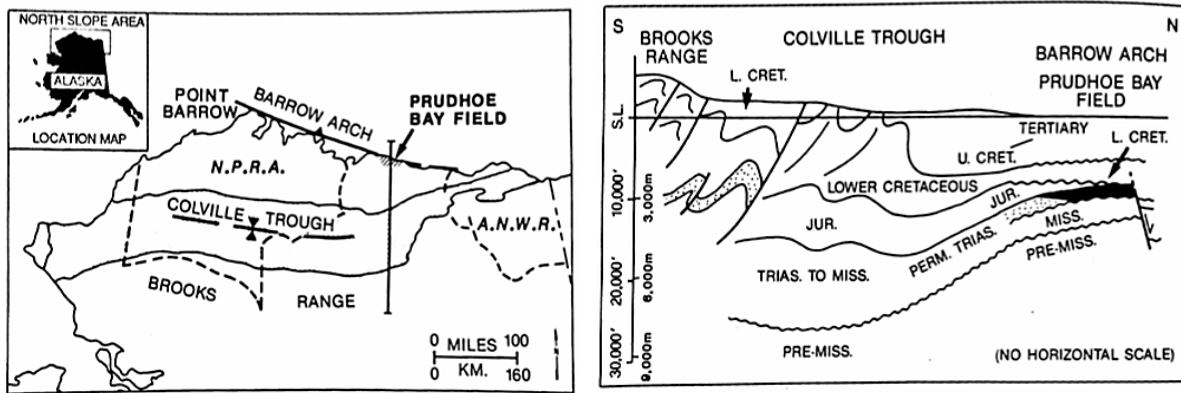


Figure 5.3. Map and geologic cross section of the location of the Prudhoe Bay field and its Permian-Triassic productin reservoir formation (Atkinson et al., 1990).

successions follows a similar trend. The conglomeratic facies that exhibit bimodal grain sorting tend to have lower porosity but higher permeability than the moderately sorted sandstone facies present in the braided streams (Atkinson et al., 1990).

The heterogeneity in reservoir architecture at Prudhoe Bay comes from shale intervals deposited by abandoned channels and intrachannel drapes and from permeability variation between the alternating sandstones and conglomerates in channel fill deposits. To aid in production, the reservoir is separated into mappable “flow units” – volumes displaying consistency of the geological and petrophysical properties that influence fluid flow. The units are generally the coarser grain, braided stream conglomerates (relative to the siltier distal fluvial and deltaic deposits). Diagenetic characteristics in the reservoir include partial cementation and porosity-reducing compaction, followed by later limited dissolution producing secondary porosity. The cements present are quartz, siderite, kaolinite, pyrite, and ferroan carbonate. While there is ferroan carbonate present, it does not have the drastic effect on porosity and permeability reduction as is seen in the Wolfville Formation at Rainy Cove. This may be due to the relatively early emplacement of hydrocarbons, which could inhibit diagenesis. The complicated facies distribution at this field has influenced the development

strategy for hydrocarbon companies in the way that the field is mapped into flow units and in a focus on secondary and tertiary recovery techniques (Atkinson et al., 1990).

ENVIRONMENT TYPE	PREDOMINANT LITHOLOGY	GRAIN SIZE TREND	SORTING TREND	PERMEABILITY TREND	
				LOW	HIGH
MID-BRAIDED STREAM	SANDY CONGLOMERATE CONGLOMERATIC SS COARSE-GRAINED SS	↓ DECREASE	↑ DECREASE		
DISTAL BRAIDED STREAM	MEDIUM-GRAINED SANDSTONE				
DELTA FRONT	FINE- TO VERY FINE-GRAINED SS				

Figure 5.4. Diagram depicting the correlation between grain size and sorting (governed by depositional environment) and permeability observed in the sandstone reservoirs of the Prudhoe Bay field (Atkinson et al., 1990).

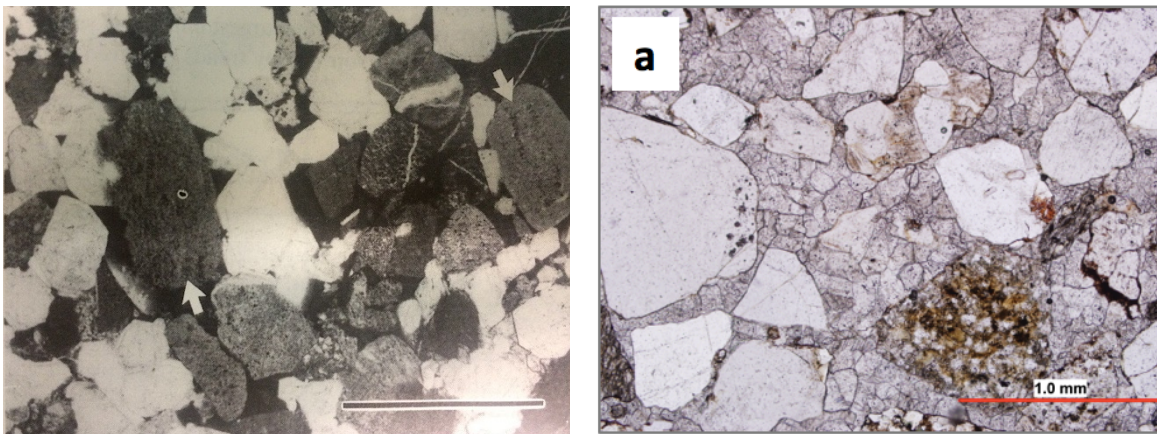


Figure 5.5. Photomicrographs from the Ivishak (left) and Wolfville (right) formations. Both have subangular siliciclastic framework grains, but the prevalent carbonate cementation in the Wolfville sediments is not present in the Ivishak, where black-coloured pore space is visible between grains. White arrow in Ivishak section points to feldspar grain (Atkinson et al., 1990).

## Chapter 6: Conclusions

### 6.1 Conclusions

This study investigated the lithologic characteristics and cementation textures within the Triassic fluvial successions in Rainy Cove, Nova Scotia. The objectives of the study were to use descriptions of lithology and cementation texture across erosional surfaces to interpret the paragenesis of the successions and the effect of cementation style on outcrop erosion, and to connect observations to fluid flow and reservoir quality in the formation.

Six lithofacies were identified in the Wolfville Formation at Rainy Cove above and below the erosional surfaces. Lithofacies are associated with alluvial and fluvial braided channel depositional environments. All lithofacies are well cemented by pore filling carbonate mosaics. The blocky, granular, and dogtooth cement textures and the crystal characteristics under light-polarizing microscopy and cathodoluminescence indicate limited early cementation in a meteoric environment and dominant later cementation in a burial environment. The textural type and grain size variations between cements are minor and indicate that the Triassic successions across the outcrop at Rainy Cove were cemented in the same relative time frame. There is no apparent cementation change between lithofacies that could account for preferential preservation of certain areas of outcrop, specifically the promontory at Rainy Cove.

Cementation fills pore space and prevents permeability in the sediments, creating baffles or barriers to fluid flow. The heterogeneities created by erosional surfaces in the outcrop also produce baffles to vertical flow in this braided channel system due to lower permeability in poorly sorted conglomeratic facies above these erosive surfaces. These factors contribute to low reservoir quality in the Wolfville Formation at this location; however, the amount of cemented pore space and the importance of the Wolfville Formation as an aquifer in the Annapolis Valley indicates that this type of deposit has potential to be a high-quality reservoir rock. Braided channel systems are proven prolific hydrocarbon reservoirs elsewhere in the world, exemplified by the Ivishak Sandstone in the Prudhoe Bay Field, Alaska (Atkinson et al., 1990).

## 6.2 Recommendations and Future Work

This work raises further questions about the cementation of sandstones at Rainy Cove, the timing of their diagenetic history, and their contribution to preferential preservation of coastal outcrop. Further work should include geochemical analyses to determine cement composition. Oxygen and carbon isotope data would be valuable to assess the cementation environment, as different cementation processes would preserve different geochemical signatures from the pore fluids. In order to study the cement composition in greater detail and look for multiple phases of cementation, EDS/SEM mapping could be done for elements such as Fe, Mg, and Ca. These element maps can show where element concentrations change within the cement fabric and may reveal earlier and later cement phases of different chemical composition and improve understanding of cementation environment and sediment paragenesis.

It may also be useful to obtain outcrop and subsurface samples from the Wolfville Formation elsewhere along the Minas Basin and compare the cement texture and composition between locations. There are several promontories along the southern margin of the Minas Basin that may exhibit similar differences in erodibility between lithofacies (Figure 6.1). A study of the Wolfville Formation in these other outcrop locations or in borehole cores (used in previous study by Pothier, 2009) would improve the overall understanding of variability in coastal outcrop preservation and reservoir quality of these successions. Although the Wolfville Formation is well cemented at Rainy Cove, it acts as an aquifer in other locations within the province (Rivard et al., 2007) so there are clearly differences in the diagenetic (cementation, specifically) history between locations. These studies contribute to knowledge about hydrocarbon reservoir and aquifer potential for this formation and as an analogue for other alluvial-fluvial systems.

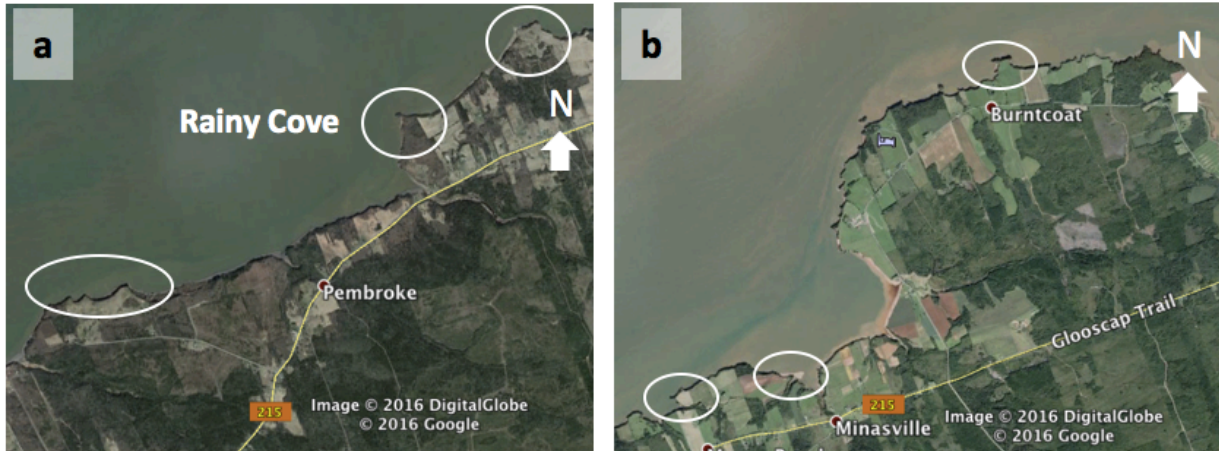


Figure 6.1. Satellite photographs showing circled examples of coastal promontories along the southern margin of the Minas Basin near (a) Rainy Cove and (b) Burntcoat Head (Google Earth Pro, 2016).

## References

- Al-Masrahy, M. and Mountney, N. 2015. A classification scheme for fluvial-aeolian system interaction in desert-margin settings. *Aeolian Research*, **17**: 67-88.
- Atkinson, C., McGowen, J., Block, S., Lundell, L. and Trumbly, P. 1990. Braidplain and Deltaic Reservoir, Prudhoe Bay Field, Alaska. *In Sandstone Petroleum Reservoirs. Edited by Barwis, J., McPherson, J. and Studlick, J. Springer-Verlag New York Inc., New York, NY.* pp. 7-29.
- Blakey, R. Paleogeographic Maps [online]. Available from <http://jan.ucc.nau.edu/rcb7/index.html> [cited 27 October 2016].
- Boggs, S. 2012. *Principles of Sedimentology and Stratigraphy*, 5<sup>th</sup> edition. Pearson Education, Inc., New Jersey, USA.
- Campbell, C. 1967. Lamina, laminaset, bed and bedset. *Sedimentology*, **8(1)**: 7-26.
- Flügel, E. and Axel, M. 2010. *Microfacies of carbonate rocks: analysis, interpretation, and application*, 2<sup>nd</sup> edition. Springer, Heidelberg, NY.
- Gatan, Inc. High spatial resolution cathodoluminescence [online]. Available from <http://www.gatan.com/high-spatial-resolution-cathodoluminescence> [cited 26 October 2016].
- Henry, D. 2016. Cathodoluminescence Theory [online]. Available from [http://serc.carleton.edu/research\\_education/geochemsheets/CLTheory.html](http://serc.carleton.edu/research_education/geochemsheets/CLTheory.html) [cited 09 January 2017].
- Hodych, J. and Dunning, G. 1992. Did the Manicouagan impact trigger end-of-Triassic mass extinction? *Geology* 20: 51–554.
- James, N. and Jones, B. 2016. *Origin of Carbonate Sedimentary Rocks*. Wiley, West Sussex, UK.
- Keppie, J. 1982. The Minas geofracture. *In Major Structural Zones and Faults of the Northern Appalachians*, St-Julien, P. and Beland, J. (eds). Geological Association of Canada, Boulder, CO; Special Paper **24**, 1–34.
- Kettanah, Y., Kettanah, M., and Wach, G. 2013. Provenance, diagenesis, and reservoir quality of the Upper Triassic Wolfville Formation, Bay of Fundy, Nova Scotia, Canada. *Geological Society, London, Special Publications*, **386**: 75-110.
- Klein, G. 1962. Triassic Sedimentation, Maritime Provinces, Canada. *Geological Society of America Bulletin* **73.9**: 1127-1146.



- Larsen, G., and Chilingar, G (ed.). 1979. *Developments in Sedimentology 25A: Diagenesis in Sediments and Sedimentary Rocks*. Elsevier Scientific Publishing Company, New York, NY.
- Leeder, M. 1975. Pedogenic carbonate and flood sediment accretion rates: a quantitative model for alluvial, arid-zone lithofacies. *Geologic Magazine*, **112**: 257-270.
- Leleu, S. and Hartley, A. 2010. Controls on the Stratigraphic Development of the Triassic Fundy Basin, Nova Scotia: implications for the tectonostratigraphic evolution of Triassic Atlantic rift basins. *Journal of the Geological Society, London*, **167**: 437-454.
- McIlreath, I. and Morrow, D., ed. 1990. *Diagenesis*. Geoscience Canada reprint series 4. The Runge Press Ltd., Ottawa, Ontario.
- Mckenzie, D. 1978. Some remarks on the development of sedimentary basins. *Earth and Planetary Science Letters*, **40(1)**: 25-32.
- Mulcahy, P. 2006. Reservoir modeling and simulation of a braided channel complex at Cambridge Cove, Nova Scotia. M.Eng Thesis, Faculty of Engineering, Dalhousie University, Halifax, NS.
- Murphy, J., Waldron, J., Kontak, D., Pe-Piper, G., and Piper, D. 2011. Minas Fault Zone: Late Paleozoic history of an intra-continental orogenic transform fault in the Canadian Appalachians. *Journal of Structural Geology*, **33**: 312-328.
- Nichols, G. 2009. *Sedimentology and Stratigraphy*, Second Edition. Wiley-Blackwell, Oxford, UK.
- Nickerson, J. 2010. Architecture and geometry of braided channel complex in the Triassic Wolfville Formation. BSc. Honours Thesis, Department of Earth Sciences, Dalhousie University, Halifax, NS.
- O'Connor, D. 2016. Facies distribution, fluvial architecture, provenance, diagenesis, and reservoir quality of synrift successions from the breakup of Pangea: examples from the Fundy Basin and Orpheus Graben. MSc. Thesis, Department of Earth Sciences, Dalhousie University, Halifax, NS.
- Ohen, H. and Kersey, D. 1992. Permeability. *Development Geology Reference Manual*, AAPG Methods in Exploration Series No. 10. Tulsa, Oklahoma.
- Olsen, P. 1997. Stratigraphic record of the early Mesozoic breakup of Pangea in the Laurasia-Gondwana rift system. *Annual Review of Earth and Planetary Sciences*, **25(1)**: 337-401.
- Olsen, P. and Schlische, R. 1990. Transtensional arm of the early Mesozoic Fundy rift basin: Penecontemporaneous faulting and sedimentation. *Geology*, **18(8)**: 695-698.

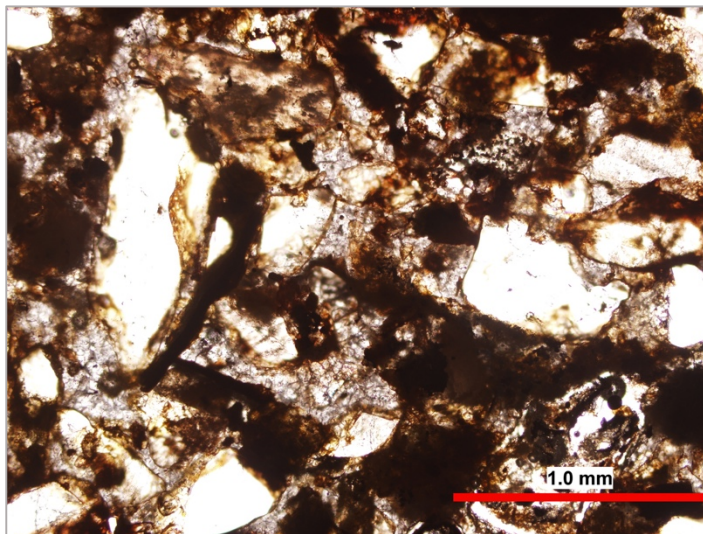
- Pothier, H., 2009. Potential of Uranium mobility in a sandstone aquifer in the Bridgetown area, Nova Scotia. BSc. Honours Thesis, Department of Earth Sciences, Dalhousie University, Halifax, NS.
- Rivard, C., Deblonde, C., Boivin, R., Bolduc, A., Paradis, S., Paradis, D., Liao, S., Gauthier, M., Blackmore, A., Trepanier, S., Castonguay, S., Drage, J., and Michaud, Y. 2007. Canadian groundwater inventory: hydrogeological atlas of the Annapolis Valley, Nova Scotia. Natural Resources Canada, Geological Survey of Canada, open file 5541.
- Reading, H. 2009. Sedimentary environments: processes, facies and stratigraphy. John Wiley & Sons.
- Reineck, H. and Singh, I. 1980. Depositional Sedimentary Environments. Springer-Verlag Berlin Heidelberg, Heidelberg, Germany.
- Sues, H. and Olsen, P. 2015. Stratigraphic and temporal context and faunal diversity of Permian-Jurassic continental tetrapod assemblages from the Fundy rift basin, eastern Canada. *Atlantic Geology*, **51**: 139-205.
- Vaughan, M. 2011. High resolution radar stratigraphy (GPR) of braided channel complexes in the Triassic Wolfville Formation – controls on reservoir heterogeneity. BSc. Honours Thesis, Department of Earth Sciences, Dalhousie University, Halifax, NS.
- Wade, J., Brown, D., Traverse, A. and Fensome, R. 1996. The Triassic-Jurassic Fundy Basin, eastern Canada: regional setting, stratigraphy, and hydrocarbon potential. *Atlantic Geology*, **32**: 189-231.
- White, N. and McKenzie, D. 1988. Formation of the “steer’s head” geometry of sedimentary basins by differential stretching of the crust and mantle. *Geology*, **16**: 250-253.
- Williams, J., Fyffe, L., Wardle, R., Colman-Sadd, S., Boehner, R., and Watt, J. 1985. Lexicon of Canadian Stratigraphy Volume VI Atlantic Region. Canadian Society of Petroleum Geologists. Sentinel Printing Limited, Yarmouth, NS.
- Withjack, M., Olsen, P., and Schlische, R. 1995. Tectonic evolution of the Fundy rift basin, Canada: evidence of extension and shortening during passive margin development. *Tectonics* **14**: 390–405.
- Withjack, M. and Schlische, R. 2005. A review of tectonic events on the passive margin of eastern North America. *Petroleum Systems of Divergent Continental Margin Basins*, Post, P (ed.). 25th Bob S. Perkins Research Conference, Gulf Coast Section of SEPM, 203–235.

Withjack, M., Schlische, R., and Baum, M. 2009. Extensional development of the Fundy rift basin, southeastern Canada. *Geological Journal*, **44**: 631-651.

## Appendix

## Sample Photographs

GW550-2016

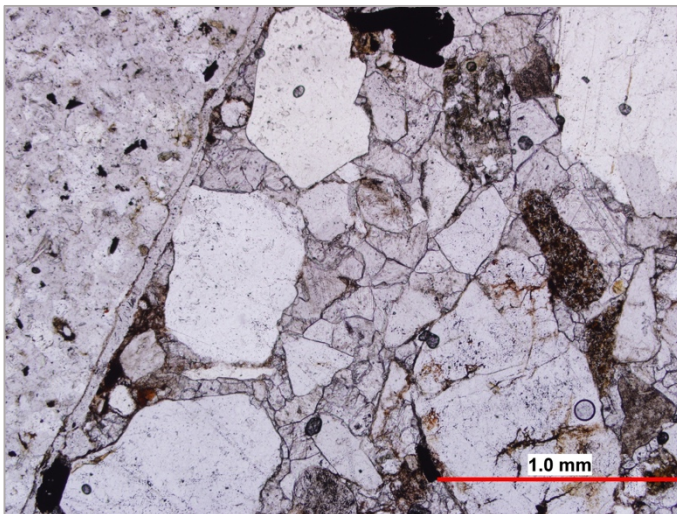


Grain Size: 0.2-1.5 mm

Grain Shape: subangular

Grain Sorting: moderately well  
sorted

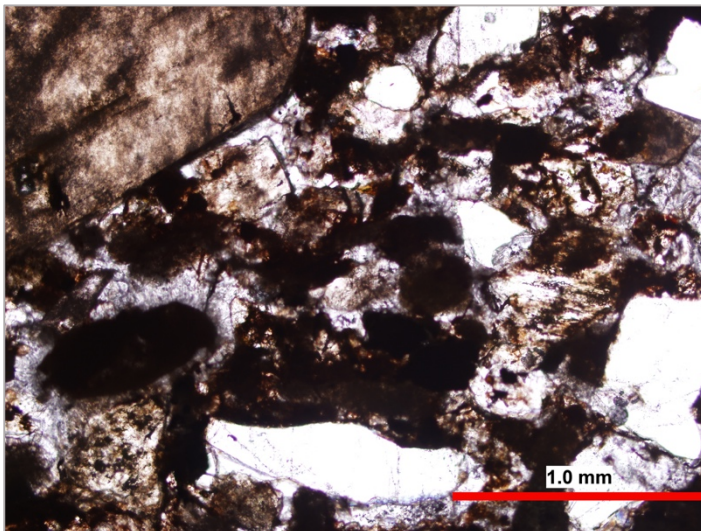
GW551-2016



Grain Size: 0.2-5.0 mm  
Grain Shape: subangular  
Grain Sorting: moderately sorted



GW552-2016



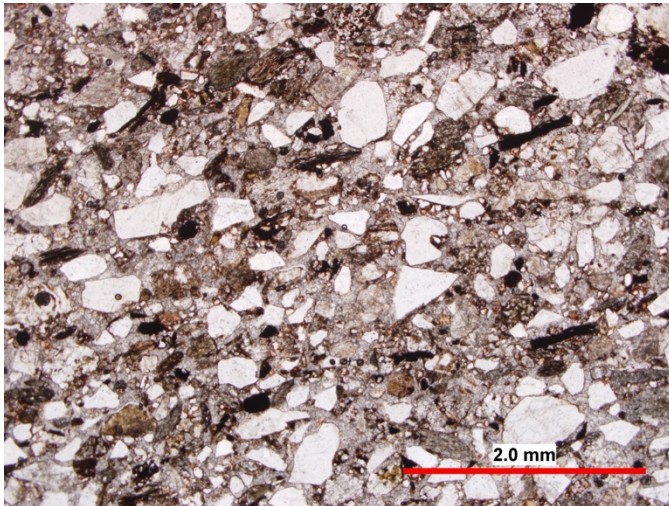
Grain Size: 0.2-4.6 mm

Grain Shape: subangular

Grain Sorting: moderately sorted

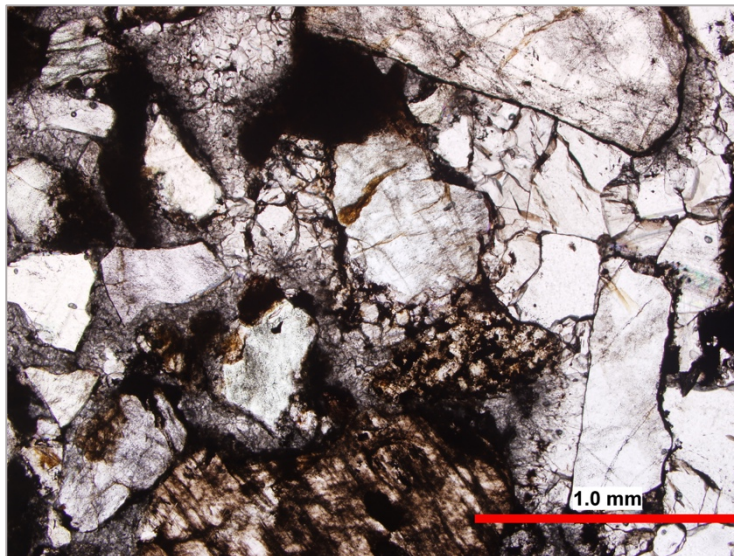


GW553-2016



Grain Size: 0.1-2.5 mm  
Grain Shape: subangular  
Grain Sorting: moderately sorted

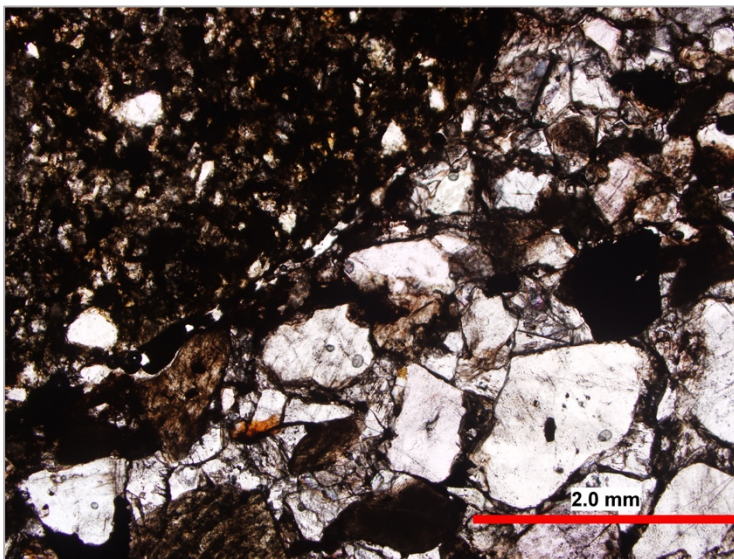
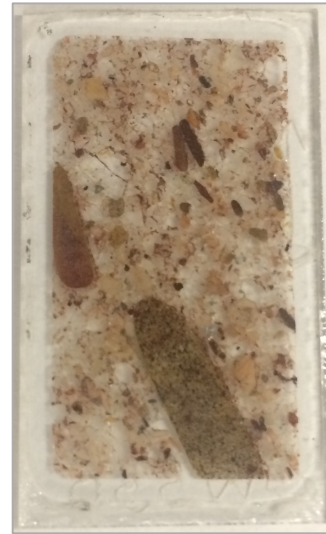
GW554-2016



Grain Size: 0.3-5.5 mm  
Grain Shape: subrounded  
Grain Sorting: moderately sorted

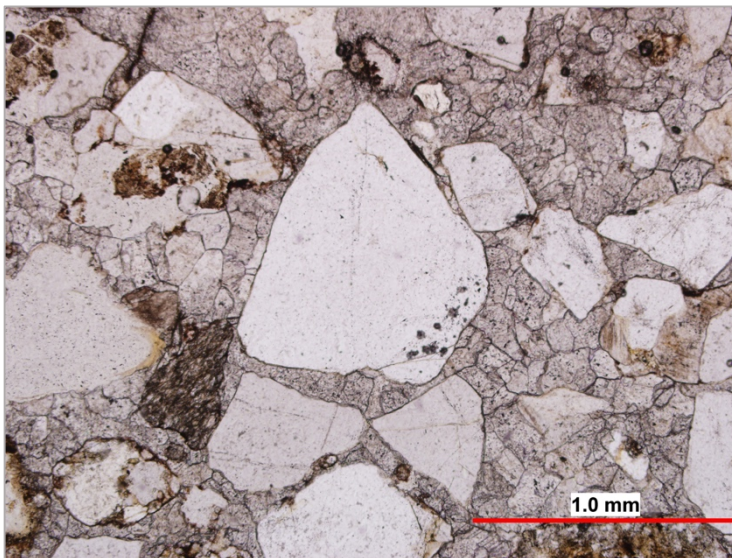


GW556-2016



Grain Size: 0.2-10 mm  
Grain Shape: subrounded  
Grain Sorting: moderately sorted

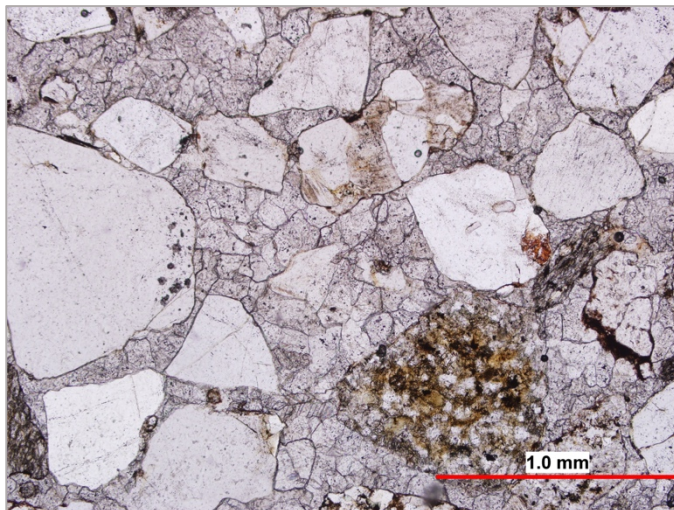
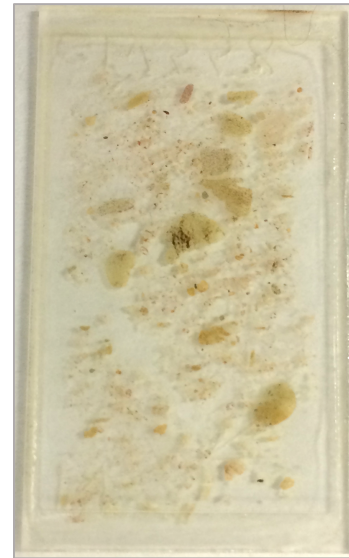
GW557-2016



Grain Size: 0.2-4.4 mm  
Grain Shape: subangular  
Grain Sorting: moderately well sorted

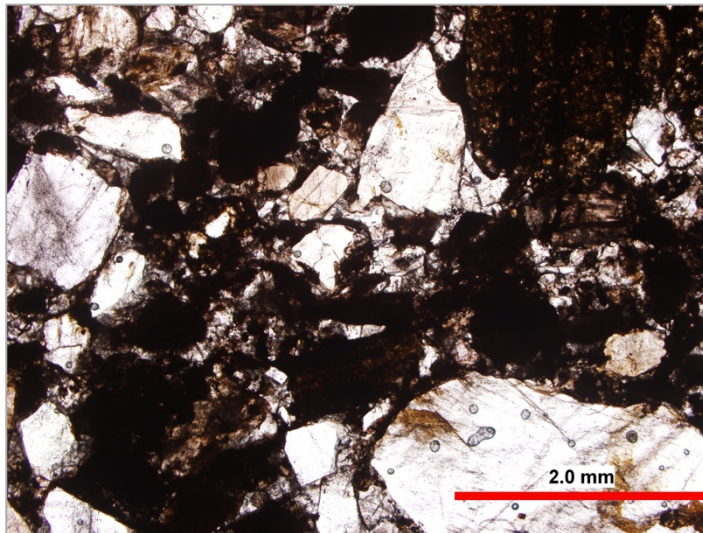


GW558-2016



Grain Size: 0.2-3.2 mm  
Grain Shape: subangular  
Grain Sorting: moderately sorted

GW559-2016



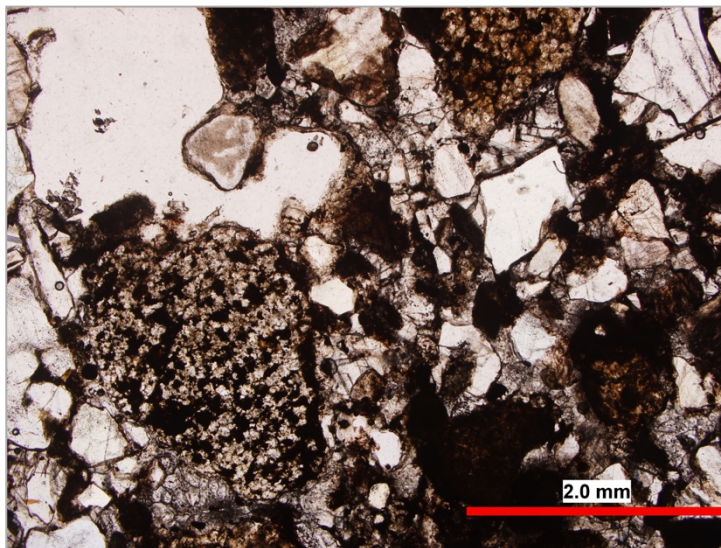
Grain Size: 0.3-5.6 mm

Grain Shape: subangular

Grain Sorting: moderately sorted



GW560-2016

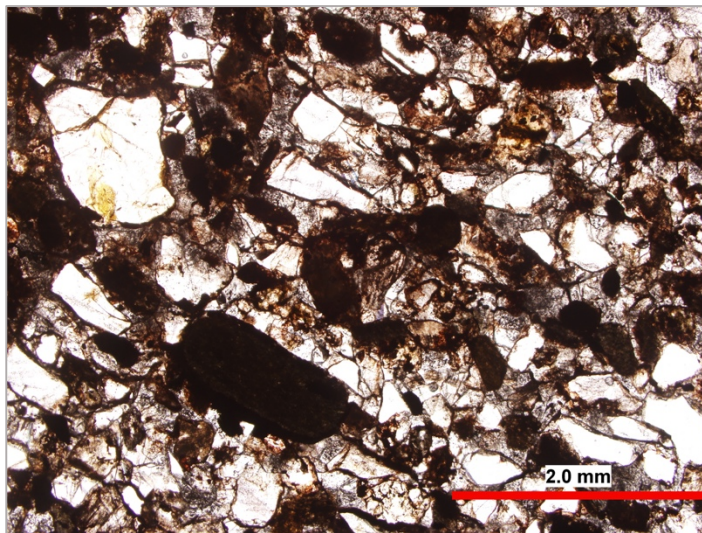


Grain Size: 0.2-6.5 mm

Grain Shape: subangular

Grain Sorting: moderately sorted

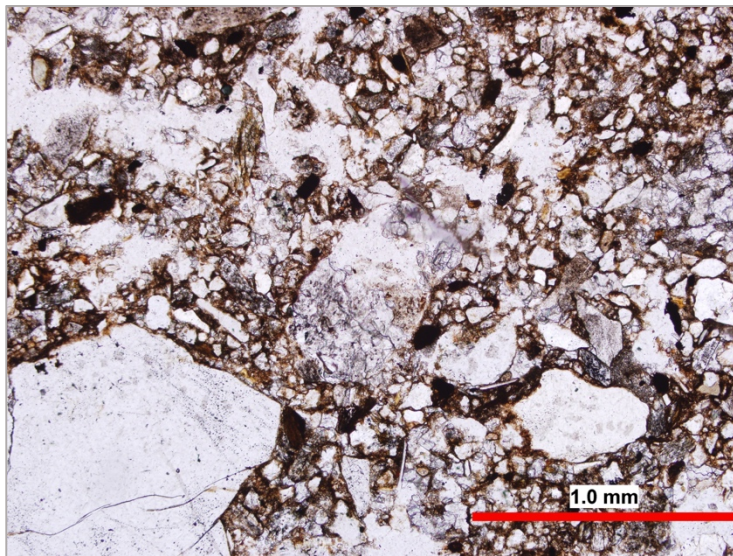
GW561-2016



Grain Size: 0.16-0.9 mm  
Grain Shape: subangular  
Grain Sorting: moderately well sorted

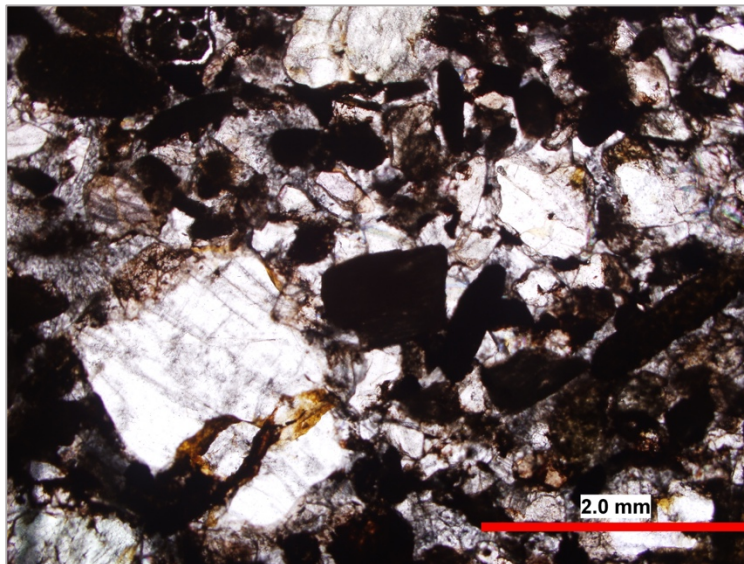


GW562-2016



Grain Size: 0.04-1.6 mm  
Grain Shape: subrounded  
Grain Sorting: poorly sorted

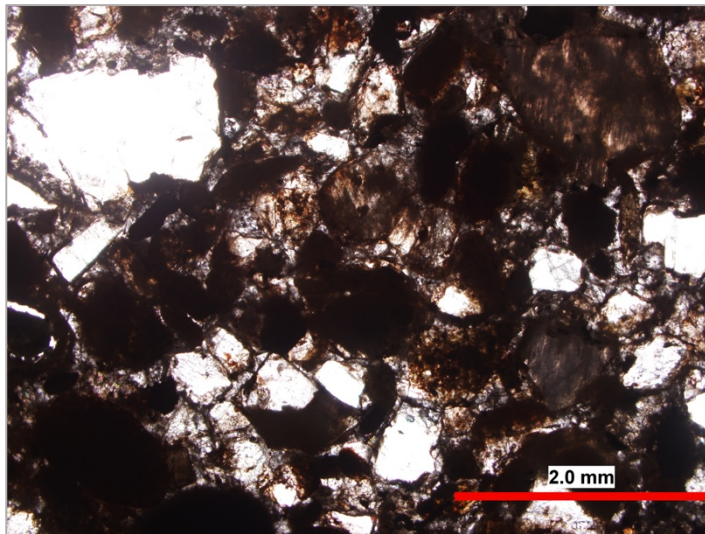
GW563-2016



Grain Size: 0.2-8.9 mm  
Grain Shape: subangular  
Grain Sorting: poorly sorted



GW564-2016

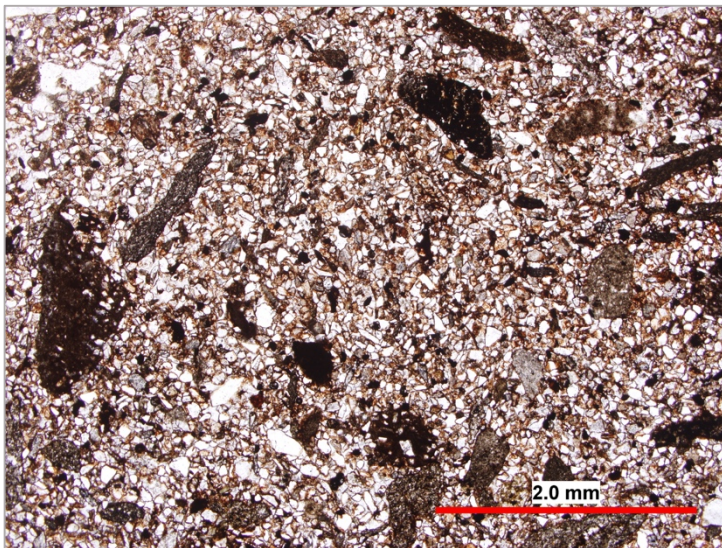


Grain Size: 0.2-3.2 mm

Grain Shape: subangular

Grain Sorting: moderately sorted

GW565-2016



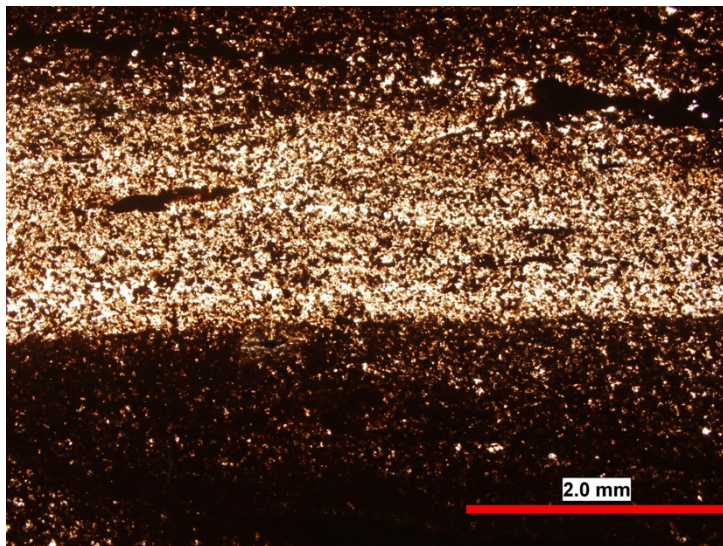
Grain Size: 0.03-1.8 mm

Grain Shape: subangular

Grain Sorting: poorly sorted



GW566-2016



Grain Size: silt  
Grain Shape: subrounded to rounded  
Grain Sorting: very well sorted

### Gamma Ray Scintillometer Data

<b>Section 1: Carboniferous-Triassic Unconformity</b>						
<b>logged section (m from base)</b>	<b>gt-40</b>	<b>K (ppm)</b>	<b>U (ppm)</b>	<b>Th (%)</b>	<b>dose (nSv)</b>	<b>dose rate (nSv/hr)</b>
0.0	125.00	2.9	6.4	9.5	15.0	27
0.1	122.33					
0.2						
0.3						
0.4						
0.5	130.88	2.4	7.0	7.8	15.0	21
0.6						
0.7						
0.8						
0.9						
1.0						
1.0	119.50					
1.1	97.50					
1.2						
1.3						
1.4	103.00					
1.5	94.80	2.3	5.9	8.5	15.0	18
1.6						
1.7						
1.8						
1.9						
1.9						
2.0	84.57	2.2	5.9	8.2	14.0	21
2.1						
2.2						
2.3	87.86					
2.4	95.43	2.3	5.9	8.0	14.0	22
2.5						
2.6						
2.7	93.25					
2.8						
2.9						
3.0	87.38	2.3	4.0	10.0	14.0	24
3.1						
3.2	92.50					

Section 2: Alluvial and Fluvial Contacts						
logged section (m from base)	gt-40	K (ppm)	U (ppm)	Th (%)	dose (nSv)	dose rate (nSv/hr)
0.0	68.00					
0.1						
0.2		2.4	2.9	9.3	7.9	16
0.3						
0.4	65.17					
0.5						
0.6						
0.7	73.40					
0.8	63.80	1.9	3.6	5.7	8.0	13
0.9						
1.0	58.00					
1.0	58.38	1.9	2.8	7.6	8.2	14
1.1		2.0	2.8	7.3	8.3	20
1.2						
1.3	60.20					
1.4						
1.5	53.67	2.1	2.6	6.2	8.4	12
1.6	68.20	2.3	2.3	6.3	8.5	19
1.7						
1.8						
1.9	66.71					
1.9	67.00					
2.0						

Section 3: Intra-Triassic Unconformity						
logged section (m from base)	gt-40	K (ppm)	U (ppm)	Th (%)	dose (nSv)	dose rate (nSv/hr)
0.0	55.20	2.1	2.5	3.9	2.2	13
0.1	57.80	2.1	2.5	9.9	2.2	13
0.2	67.00	2.1	2.5	3.7	2.3	15
0.3	51.60	2.1	2.5	3.7	2.3	15
0.4	56.40					
0.5	55.20	2.2	2.4	3.9	2.5	2
0.6	58.20					
0.7						
0.8	60.00	2.1	2.4	4.1	4.0	13
0.9						
1.0	74.00					
1.0	55.75	2.4	0.9	6.9	4.3	2
1.1	61.60	2.2	1.9	6.4	4.4	12
1.2	39.40					
1.3	56.00					
1.4	49.00					
1.5						
1.6	51.00	2.3	1.9	4.8	4.6	2
1.7						
1.8	52.00					
1.9						
2.0	48.80					



## Permeability Data

Sample No.	Reading 1	Reading 2	Reading 3	Average Permeameter Reading	Permeability (mD)
GW553-2016	11.24	11.23	11.37	11.28	87.52
GW554-2016	11.93	11.53	11.42	11.63	32.78
GW559-2016	11.42	11.9	11.46	11.59	36.67
GW560-2016	10.81	10.91	11.69	11.14	129.64
GW561-2016	10.7	10.88	11.04	10.87	276.53
GW562-2016	10.84	11.17	11	11.00	192.01
GW563-2016	10.25	11.81	11.58	11.21	106.52

# Grain Size Measurements

Sample Count	550		551		552		553		554		556		557		558	
	Framework	Fmwk Phi	Framework	Fmwk Phi	Framework	Fmwk Phi	Framework	Fmwk Phi	Framework	Fmwk Phi	Framework	Fmwk Phi	Framework	Fmwk Phi	Framework	Fmwk Phi
1	0.755	0.405	1.467	-0.553	0.399	1.326	0.422	1.245	1.063	-0.088	1.119	-0.162	0.474	1.077	0.395	1.340
2	0.429	1.221	0.396	1.336	0.749	0.417	0.337	1.569	0.458	1.127	2.012	-1.139	1.362	-0.446	1.107	-0.147
3	0.479	1.062	0.817	0.292	0.309	1.694	0.202	2.308	2.911	-1.542	0.208	0.596	0.747	0.959	0.060	0.747
4	0.373	1.423	2.007	-1.005	0.320	1.644	0.262	1.932	0.495	1.014	0.428	1.224	0.683	0.550	0.190	2.396
5	0.279	1.842	0.526	0.927	0.257	1.960	0.109	3.198	1.041	-0.058	0.783	0.581	0.544	0.878	0.507	0.980
6	0.359	1.478	1.824	-0.867	0.493	1.020	0.657	3.006	5.546	-2.471	1.891	-0.919	1.428	-0.514	0.456	1.133
7	0.324	1.626	0.908	0.139	0.462	1.114	0.455	1.136	1.561	-0.642	0.731	0.452	0.803	0.317	0.428	1.224
8	0.459	1.123	0.900	0.152	0.307	1.704	0.268	1.900	1.325	-0.406	1.339	-0.421	0.190	2.396	1.367	-0.451
9	0.313	1.676	0.328	1.608	0.337	1.569	0.197	2.344	0.589	0.764	1.071	-0.099	0.615	0.701	0.821	0.285
10	0.239	2.065	0.623	0.683	0.352	1.506	1.096	-0.132	0.736	0.442	1.590	-0.669	0.303	1.375	0.385	1.723
11	0.417	1.262	1.180	-0.239	0.966	0.050	0.414	1.272	0.454	1.139	1.115	-0.157	0.493	1.020	0.559	0.839
12	0.354	1.498	0.568	0.816	0.309	1.694	0.199	2.329	0.669	0.580	1.421	-0.507	0.290	1.786	0.568	0.816
13	0.297	1.751	0.608	0.718	0.225	2.152	0.556	0.847	0.365	1.454	0.318	1.653	0.942	0.086	1.026	-0.037
14	0.232	2.108	0.301	1.732	0.400	1.322	0.160	2.644	0.469	1.092	1.680	-0.748	0.687	0.542	0.566	0.821
15	0.288	1.796	0.510	0.971	0.318	1.653	0.202	2.308	0.883	0.180	0.854	0.228	0.484	1.047	1.430	-0.516
16	0.605	0.725	0.899	0.154	0.455	1.136	0.469	1.092	0.884	0.178	4.827	-2.271	0.820	0.286	0.813	0.299
17	0.389	1.362	0.643	0.637	0.607	0.720	0.277	1.852	1.602	-0.680	0.552	0.857	0.534	0.905	0.447	1.162
18	0.242	2.047	0.667	0.584	0.305	1.713	0.213	2.231	0.586	0.771	1.836	-0.877	0.648	0.626	0.985	0.022
19	0.766	0.385	0.373	1.423	0.286	1.806	0.157	2.671	1.892	-0.920	0.971	0.042	0.385	1.377	0.417	1.262
20	0.336	1.573	0.238	2.071	0.250	2.000	0.323	1.630	0.463	1.111	0.559	0.839	0.448	1.158	0.833	0.264
21	0.542	0.884	1.068	-0.095	0.945	0.082	0.335	1.578	2.335	-1.223	0.709	0.496	0.510	0.971	0.620	0.690
22	0.472	1.083	1.921	-0.942	0.410	1.286	0.250	2.000	2.508	-1.327	1.557	-0.639	0.561	0.834	0.851	0.233
23	0.524	0.932	0.876	0.191	0.493	1.020	0.270	1.889	1.594	-0.673	0.463	1.111	0.317	1.657	0.455	1.136
24	0.272	1.878	0.511	0.969	0.290	1.786	0.377	1.407	0.616	0.699	2.680	-1.422	0.398	1.329	0.464	1.108
25	0.299	1.742	0.343	1.544	0.928	0.108	0.234	2.095	0.750	0.415	1.617	-0.693	0.637	0.651	1.466	-0.552
26	0.487	1.038	2.556	-1.354	2.343	-1.228	0.678	0.561	0.977	0.034	1.291	-0.368	0.980	0.029	0.798	0.326
27	0.324	1.626	1.116	-0.158	0.601	0.735	0.277	1.852	1.153	-0.205	0.936	0.095	0.704	0.506	0.328	1.608
28	1.214	-0.280	0.419	1.255	0.302	1.727	0.178	2.490	0.471	1.086	0.546	0.873	0.415	1.269	0.473	1.080
29	0.674	0.569	0.383	1.385	0.296	1.756	0.153	2.708	0.292	1.776	0.318	1.653	0.245	2.029	0.295	1.761
30	0.377	1.407	0.518	0.949	0.664	0.591	0.191	2.388	0.536	0.900	2.033	-1.024	0.956	0.065	0.469	1.092
31	0.708	0.498	1.027	-0.038	2.602	-1.380	0.440	1.184	0.893	0.163	1.045	-0.064	1.557	-0.639	0.406	1.300
32	0.366	1.450	0.626	0.676	0.404	1.308	0.199	2.329	1.589	-0.668	0.724	0.466	0.516	0.955	0.381	1.392
33	0.591	0.759	0.291	1.781	0.673	0.571	0.124	3.012	0.598	0.742	1.525	-0.609	0.884	0.178	1.585	-0.664
34	0.388	1.366	0.876	0.191	0.337	1.569	0.163	2.617	3.025	-1.597	7.649	-2.935	0.801	0.320	0.616	0.699
35	0.344	1.540	0.250	2.000	0.354	1.498	0.393	1.347	0.503	0.991	1.381	1.074	0.384	1.381	0.693	0.529
36	0.336	1.573	0.705	0.504	0.541	0.886	0.239	2.065	1.053	-0.075	2.127	-1.089	0.645	0.633	2.003	-1.002
37	0.521	0.941	0.489	1.032	0.228	2.133	0.223	2.165	1.478	-0.564	1.900	-0.926	0.426	1.231	0.607	0.720
38	0.181	2.466	0.471	1.086	0.359	1.478	0.313	1.676	0.908	0.139	1.325	-0.406	0.527	0.924	0.493	1.020
39	0.220	2.184	0.277	1.852	0.254	1.977	0.176	2.506	0.410	1.286	0.932	0.102	0.911	0.134	1.818	-0.862
40	0.547	0.870	0.433	1.208	0.210	2.252	0.164	2.608	0.754	0.407	0.985	0.022	0.601	0.735	0.657	0.606

GRAIN SIZE MEASUREMENTS (mm)		550		551		552		553		554		556		557		558		
Sample Count	Framework	Fmwk Phi	Framework	Fmwk Phi	Framework	Fmwk Phi	Framework	Fmwk Phi	Framework	Fmwk Phi	Framework	Fmwk Phi	Framework	Fmwk Phi	Framework	Fmwk Phi	Framework	Fmwk Phi
40	0.547	0.870	1.208	0.210	2.252	0.164	2.608	0.407	0.985	0.022	0.601	0.735	0.601	0.601	0.601	0.657	0.606	
41	0.555	0.849	1.642	0.594	0.751	0.214	2.224	-2.238	3.466	-1.793	0.369	1.438	0.369	0.369	0.369	0.426	1.231	
42	0.405	1.304	0.683	0.373	1.423	0.164	2.608	0.750	2.123	-1.086	0.499	1.003	0.499	0.499	1.111	1.111	-0.152	
43	0.309	1.694	0.469	0.316	1.662	0.221	2.178	1.096	0.519	0.946	0.633	0.660	0.633	0.633	0.343	0.343	1.544	
44	0.639	0.646	0.396	1.336	1.816	0.236	2.083	0.806	0.617	0.795	0.795	0.331	0.795	0.795	0.746	0.746	0.423	
45	0.180	2.474	0.388	1.366	0.900	0.141	2.826	0.969	1.332	-0.414	0.724	0.466	0.724	0.724	0.594	0.594	0.751	
46	0.571	0.808	1.089	0.672	0.573	0.290	1.786	-0.726	0.406	1.300	0.615	0.701	0.615	0.615	0.891	0.891	0.167	
47	0.574	0.801	0.847	0.378	1.404	0.225	2.152	-0.589	0.642	0.639	0.585	0.773	0.585	0.585	0.381	0.381	1.392	
48	0.553	0.855	0.504	0.989	0.602	0.316	1.662	1.102	0.220	2.184	1.158	-0.212	1.158	1.158	0.795	0.795	0.331	
49	0.311	1.685	0.277	1.852	0.917	0.125	0.545	0.876	1.036	-0.051	0.852	0.231	0.852	0.852	0.272	0.272	1.878	
50	0.239	2.065	0.402	1.315	0.346	1.531	0.216	2.211	0.691	0.533	0.572	0.806	0.572	0.572	0.631	0.631	0.664	
51	0.367	1.446	0.721	0.472	1.438	1.027	-0.038	0.919	0.764	0.388	0.786	0.347	0.786	0.786	2.922	2.922	-1.547	
52	0.729	0.456	0.489	1.032	0.311	1.685	1.523	1.450	1.597	-0.675	0.546	0.873	0.546	0.546	0.708	0.708	0.498	
53	0.541	0.886	0.272	1.878	0.214	2.224	0.238	2.071	1.273	-0.348	0.455	1.136	0.455	0.455	0.470	0.470	1.089	
54	0.908	0.139	0.730	0.454	0.590	0.761	0.594	0.692	0.727	0.460	0.708	0.498	0.708	0.708	0.904	0.904	0.146	
55	0.304	1.718	5.642	-2.496	1.624	-0.700	3.012	1.852	0.784	0.351	0.316	1.662	0.316	0.316	0.362	0.362	1.466	
56	1.577	-0.657	0.814	0.297	2.144	-1.100	0.392	-2.097	0.904	0.146	0.962	0.056	0.962	0.962	0.331	0.331	1.595	
57	0.471	1.086	0.421	1.248	0.318	1.653	-0.947	0.715	0.768	0.381	0.837	0.257	0.837	0.837	0.264	0.264	0.664	
58	0.391	1.355	0.533	0.908	0.321	1.639	0.292	1.776	0.801	0.320	0.436	1.198	0.436	0.436	0.527	0.527	0.924	
59	0.182	2.458	0.280	1.837	0.342	1.548	0.180	2.474	4.156	-2.055	0.449	1.155	0.449	0.449	1.099	1.099	-0.136	
60	0.272	1.878	0.811	0.302	0.260	1.943	0.134	2.900	0.697	0.521	0.440	1.184	0.440	0.440	0.341	0.341	1.552	
61	0.466	1.102	0.835	0.260	0.676	0.565	0.907	-1.875	0.988	0.017	0.307	1.704	0.307	0.307	0.346	0.346	1.531	
62	0.246	2.023	5.055	-2.338	0.309	1.694	0.227	2.139	1.122	-0.166	0.840	0.252	0.840	0.840	1.044	1.044	-0.062	
63	0.505	0.986	0.669	0.580	0.418	1.258	0.142	2.816	0.941	0.088	0.682	0.552	0.682	0.682	0.527	0.527	0.924	
64	0.225	2.152	0.643	0.637	0.277	1.852	0.268	1.900	0.930	0.105	0.369	1.438	0.369	0.369	1.833	1.833	-0.874	
65	0.357	1.486	0.923	0.116	0.227	2.139	0.261	1.938	1.668	-0.738	0.286	1.806	0.286	0.286	0.989	0.989	0.016	
66	0.430	1.218	0.837	0.257	1.451	-0.537	0.337	1.569	1.559	-0.641	0.508	0.977	0.508	0.508	0.928	0.928	0.108	
67	0.377	1.407	0.647	0.628	0.266	1.911	0.153	2.708	0.802	0.318	0.701	0.513	0.701	0.701	0.294	0.294	1.766	
68	0.447	1.162	0.579	0.788	0.533	0.908	0.336	1.573	0.419	1.255	4.414	-2.142	4.414	4.414	0.811	0.811	0.302	
69	0.193	2.373	0.429	1.221	0.366	1.450	0.291	1.781	1.622	-0.698	0.447	1.162	0.447	0.447	1.369	1.369	-0.453	
70	0.288	1.796	0.735	0.444	0.294	1.766	0.327	1.613	0.559	0.839	0.350	1.515	0.350	0.350	2.178	2.178	-1.123	

Sample Count	550		551		552		553		554		555		556		557		558	
	Framework	Fmwk Phi	Framework	Fmwk Phi	Framework	Fmwk Phi	Framework	Fmwk Phi	Framework	Fmwk Phi	Framework	Fmwk Phi	Framework	Fmwk Phi	Framework	Fmwk Phi	Framework	Fmwk Phi
71	0.597	0.744	0.944	0.083	0.607	0.720	0.482	1.053	1.110	-0.151	10.202	-3.351	0.385	1.377	1.407	-0.493		
72	0.650	0.621	0.344	1.540	0.301	1.732	0.143	2.806	0.834	0.262	0.866	0.208	0.624	0.680	0.735	0.444		
73	0.240	2.059	0.536	0.900	0.851	0.233	0.336	1.573	0.462	1.114	0.949	0.076	1.557	-0.639	0.360	0.360		
74	0.287	1.801	0.290	1.786	0.298	1.747	0.221	2.178	0.960	0.059	0.967	0.048	0.328	1.608	2.078	-1.055		
75	0.210	2.252	0.327	1.613	0.221	2.178	0.615	0.701	0.835	0.260	1.284	-0.361	0.557	0.844	0.290	1.786		
76	1.415	-0.501	0.683	0.550	4.608	-2.204	0.701	0.513	1.717	-0.780	0.887	0.173	0.527	0.924	1.163	-0.218		
77	0.646	0.630	0.825	0.278	1.755	-0.811	0.279	1.842	0.988	0.017	1.052	-0.073	0.689	0.537	1.138	-0.187		
78	0.377	1.407	0.534	0.905	0.481	1.056	0.260	1.943	0.656	0.608	2.661	-1.412	0.336	1.573	0.492	1.023		
79	0.344	1.540	0.986	0.020	0.216	2.211	0.235	2.089	5.083	-2.346	0.740	0.434	0.723	0.468	3.194	-1.675		
80	0.352	1.506	0.395	1.340	0.276	1.857	2.466	-1.302	4.064	-2.023	1.346	-0.429	0.366	1.450	0.708	0.498		
81	0.904	0.146	2.369	-1.244	0.948	0.077	0.337	1.569	0.963	0.054	2.227	-1.155	0.520	0.943	0.578	0.791		
82	0.769	0.379	0.321	1.639	0.635	0.655	0.340	1.556	0.981	0.028	1.111	-0.152	0.540	0.889	0.959	0.060		
83	0.473	1.080	0.660	0.599	0.378	1.404	1.429	-0.515	0.598	0.742	1.563	-0.644	0.402	1.315	0.363	1.462		
84	0.342	1.548	0.292	1.776	4.205	-2.072	0.527	0.924	0.858	0.221	0.661	0.597	0.157	2.671	1.163	-0.218		
85	0.385	1.377	0.679	0.559	0.198	2.336	0.198	2.336	0.526	0.927	1.258	-0.331	0.749	0.417	0.477	1.068		
86	0.406	1.300	1.684	-0.752	1.075	-0.104	0.583	0.778	1.221	-0.288	1.113	-0.154	0.503	0.991	0.419	1.255		
87	0.254	1.977	1.705	-0.770	0.597	0.744	0.407	1.297	0.941	0.088	1.546	-0.629	0.676	0.565	0.660	0.599		
88	0.369	1.438	0.699	0.517	0.320	1.644	0.213	2.231	0.593	0.754	0.821	0.285	0.306	1.708	0.414	1.272		
89	0.352	1.506	0.467	1.099	0.269	1.894	0.232	2.108	0.575	0.798	0.762	0.392	0.436	1.198	0.973	0.039		
90	0.516	0.955	0.514	0.960	0.356	1.490	0.406	1.300	0.383	1.385	1.582	-0.662	0.527	0.924	0.305	1.713		
91	0.230	2.120	2.180	-1.124	0.940	0.089	0.689	0.537	0.545	0.876	0.966	0.050	0.475	1.074	1.628	-0.703		
92	0.360	1.474	0.989	0.016	0.224	2.158	0.373	1.423	0.493	1.020	1.777	-0.829	0.343	1.544	0.467	1.099		
93	0.250	2.000	0.572	0.806	0.283	1.821	0.216	2.211	0.520	0.943	0.923	0.116	0.616	0.699	0.911	0.134		
94	0.251	1.994	0.714	0.486	0.921	0.119	0.180	2.474	1.822	-0.866	0.679	0.559	0.556	0.847	0.768	0.381		
95	0.227	2.139	3.108	-1.636	0.407	1.297	0.290	1.786	1.034	-0.048	0.889	0.170	0.385	1.377	0.298	1.747		
96	0.605	0.725	0.765	0.386	0.574	0.801	0.533	0.908	0.444	1.171	2.929	-1.550	0.436	1.198	0.540	0.889		
97	0.402	1.315	0.505	0.986	0.408	1.293	0.213	2.231	0.619	0.692	1.385	-0.470	0.847	0.240	0.893	0.163		
98	0.445	1.168	1.184	-0.244	0.473	1.080	0.288	1.796	0.908	0.139	1.585	-0.664	0.943	0.085	1.033	-0.047		
99	0.339	1.561	1.066	-0.092	0.205	2.286	0.240	2.059	0.954	0.068	0.560	0.837	1.676	-0.745	0.454	1.139		
100	0.178	2.490	5.063	-2.340	0.314	1.671	1.536	-0.619	0.768	0.381	1.951	-0.964	0.343	1.544	1.856	-0.892		

Sample Count	559		560		561		562		563		564		565	
	Framework	Fmwk Phi	Framework	Fmwk Phi	Framework	Fmwk Phi	Framework	Fmwk Phi	Framework	Fmwk Phi	Framework	Fmwk Phi	Framework	Fmwk Phi
1	1.067	-0.094	0.877	0.189	0.572	0.806	0.198	2.336	2.524	-1.336	1.387	-0.472	0.425	1.234
2	2.857	-1.515	0.284	1.816	0.354	1.498	0.238	2.071	0.516	0.955	0.427	1.228	0.059	4.083
3	0.779	0.360	1.195	-0.257	0.292	1.776	0.288	1.796	0.309	1.694	2.133	-1.093	0.123	3.023
4	1.101	-0.139	1.171	-0.228	0.389	1.362	0.086	3.540	0.840	0.252	0.717	0.480	0.058	4.108
5	0.723	0.468	0.377	1.407	0.258	1.955	0.082	3.608	0.402	1.315	0.713	0.488	0.074	3.756
6	5.605	-2.487	0.445	1.168	0.336	1.573	0.243	2.041	0.251	1.994	0.926	0.111	1.333	-0.415
7	0.613	0.706	0.268	-0.066	0.451	1.149	0.116	3.108	0.466	1.102	0.507	0.980	0.414	1.272
8	0.423	1.241	0.605	0.725	0.319	1.648	0.325	1.621	1.850	-0.888	0.206	2.279	0.093	3.427
9	0.671	-9.390	1.051	-0.072	0.197	2.344	0.089	3.490	1.058	-0.081	0.510	0.971	0.066	3.921
10	0.631	0.664	0.362	1.466	0.264	1.921	0.280	1.837	0.355	1.494	2.544	-1.347	0.083	3.591
11	3.232	-1.692	0.852	0.231	0.342	1.548	0.917	0.125	2.105	-1.074	0.896	0.158	0.109	3.198
12	0.673	0.571	0.891	0.167	0.365	1.454	0.122	3.035	1.342	-0.424	0.605	0.725	0.426	1.231
13	0.328	1.608	1.396	-0.481	0.422	1.245	0.319	1.648	0.358	1.482	0.436	1.198	0.251	1.994
14	0.663	0.593	0.940	0.089	0.234	2.095	0.086	3.540	4.329	-2.114	0.411	1.283	0.074	3.756
15	0.597	0.744	0.325	1.621	0.298	1.747	0.139	2.847	0.384	1.381	0.407	1.297	0.071	3.816
16	0.612	0.708	3.167	-1.663	0.908	0.139	0.542	0.884	1.385	-0.470	1.589	-0.668	0.086	3.540
17	1.057	-0.080	0.538	0.894	0.355	1.494	0.422	1.245	1.947	-0.961	0.464	1.108	0.066	3.921
18	1.262	-0.336	0.347	1.527	0.250	2.000	0.157	2.671	2.458	-1.297	0.723	0.468	0.370	1.434
19	1.172	-0.229	0.667	0.584	0.160	2.644	0.090	3.474	0.762	0.392	0.695	0.525	0.082	3.608
20	0.440	1.184	0.660	0.660	0.213	2.231	0.049	4.351	2.443	-1.289	0.858	0.221	0.066	3.921
21	1.942	-0.958	0.767	0.383	0.512	0.966	0.224	2.158	1.048	-0.068	0.869	0.203	0.469	1.092
22	0.451	1.149	0.582	0.781	0.305	1.713	0.429	1.221	0.429	1.221	0.322	1.635	0.098	3.351
23	0.724	0.466	0.984	0.023	0.223	2.165	0.086	3.540	1.390	-0.475	0.575	0.798	0.065	3.943
24	1.609	-0.686	3.122	-1.642	0.489	1.032	0.066	3.921	0.395	1.340	0.520	0.943	0.116	3.108
25	0.395	1.340	0.325	1.621	0.296	1.756	0.057	4.133	0.695	0.525	1.254	-0.327	0.049	4.351
26	1.183	-0.242	0.898	0.155	0.780	0.358	0.276	1.857	2.094	-1.066	0.896	0.158	0.710	0.494
27	0.630	0.667	0.448	1.158	0.327	1.613	0.068	3.878	1.020	-0.029	0.422	1.245	0.116	3.108
28	0.760	0.396	0.486	1.041	0.264	1.921	0.074	3.756	0.373	1.423	1.709	-0.773	0.175	2.515
29	0.503	0.991	1.268	-0.343	0.231	2.114	0.130	2.943	0.807	0.309	0.406	1.300	0.082	3.608
30	1.394	-0.479	0.470	1.089	0.369	1.438	0.141	2.826	0.637	0.651	0.745	0.425	1.448	-0.534
31	1.124	-0.169	0.869	0.203	0.637	0.651	1.634	-0.708	3.883	-1.957	0.568	0.816	0.041	4.608
32	0.493	1.020	0.515	0.957	0.366	1.450	0.269	1.894	1.063	-0.088	0.432	1.211	0.093	3.427
33	0.403	1.311	1.311	-0.391	0.352	1.506	0.066	3.921	0.699	0.517	1.039	-0.055	0.106	3.238
34	0.921	0.119	0.388	1.366	0.205	2.286	0.117	3.095	0.344	1.540	0.511	0.969	0.101	3.308
35	0.441	1.181	2.529	-1.339	0.520	0.943	0.082	3.608	2.029	-1.021	1.303	-0.382	0.139	2.847
36	2.672	-1.418	2.776	-1.473	0.448	1.158	0.189	2.404	0.759	0.398	1.458	-0.544	0.393	1.347
37	1.320	-0.401	0.984	0.023	0.208	2.265	0.098	3.351	1.362	-0.446	0.654	0.613	0.082	3.608
38	0.575	0.798	0.484	1.047	0.377	1.407	0.272	1.878	1.407	0.402	0.721	0.472	0.092	3.442
39	0.419	1.255	2.686	-1.425	0.249	2.006	0.100	3.322	2.396	-1.261	0.575	0.798	0.145	2.786
40	0.568	0.816	0.568	0.816	0.425	1.234	0.198	2.336	0.298	1.747	0.684	0.548	0.102	3.293

GRAIN SIZE MEASUREMENTS (mm)		559		560		561		562		563		564		565		
Sample Count	Framework	Fmwk Phi	Framework	Fmwk Phi	Framework	Fmwk Phi	Framework	Fmwk Phi	Framework	Fmwk Phi	Framework	Fmwk Phi	Framework	Fmwk Phi	Framework	Fmwk Phi
40	0.568	0.816	0.568	0.816	0.425	1.234	0.198	2.336	0.298	1.747	0.684	0.548	0.102	3.293		
41	0.620	0.690	1.654	-0.726	0.258	1.955	0.507	0.980	8.891	-3.152	0.728	0.458	0.397	1.333		
42	3.408	-1.769	1.526	-0.610	0.372	1.427	0.127	2.977	0.586	0.771	0.549	0.865	0.178	2.490		
43	1.148	-0.199	0.716	0.482	0.180	2.474	0.135	2.889	1.980	-0.986	0.484	1.047	0.221	2.178		
44	1.511	-0.596	0.310	1.690	0.214	2.224	0.188	2.411	1.800	-0.848	0.948	0.077	0.329	1.604		
45	0.650	0.621	0.313	1.676	0.249	2.006	0.098	3.351	1.615	-0.692	0.364	1.458	0.077	3.699		
46	1.918	-0.940	1.201	-0.264	0.470	1.089	0.322	1.635	2.027	-1.019	0.567	0.819	1.719	-0.782		
47	1.056	-0.079	0.770	0.377	0.286	1.806	0.057	4.133	0.492	1.023	1.083	-0.115	0.193	2.373		
48	0.437	1.194	1.219	-0.286	0.303	1.723	0.098	3.351	2.068	-1.048	0.482	1.053	0.087	3.523		
49	1.171	-0.228	0.433	1.208	0.194	2.366	0.091	3.458	0.320	1.644	0.786	0.347	0.107	3.224		
50	0.500	1.000	0.723	0.468	0.474	1.077	0.083	3.591	0.337	1.569	0.678	0.561	0.090	3.474		
51	3.045	-1.606	1.896	-0.923	0.316	1.662	0.143	2.806	2.086	-1.061	0.591	0.759	0.069	3.857		
52	1.020	-0.029	1.112	-0.153	0.395	1.340	0.191	2.388	0.827	0.274	0.366	1.450	0.246	2.023		
53	0.376	1.411	0.469	1.092	0.228	2.133	0.107	3.224	0.516	0.955	0.527	0.924	0.082	3.608		
54	1.007	-0.010	0.788	0.344	0.246	2.023	0.059	4.083	0.650	0.621	1.217	-0.283	0.213	2.231		
55	0.615	0.701	0.292	1.776	0.238	2.071	0.152	2.718	0.884	0.178	0.634	0.657	0.068	3.878		
56	1.821	-0.865	1.191	-0.252	0.870	2.021	0.157	2.671	1.911	-0.934	0.780	0.358	0.205	2.286		
57	0.505	0.986	0.930	0.105	0.270	1.889	0.100	3.322	0.862	0.214	0.431	1.214	0.070	3.837		
58	0.914	-9.836	0.406	1.300	0.359	1.478	0.092	3.442	0.795	0.331	0.781	0.357	0.075	3.737		
59	0.907	0.141	0.404	1.308	0.403	1.311	0.311	1.685	0.642	0.639	0.616	0.699	0.156	2.680		
60	0.348	1.523	1.221	-0.288	0.503	0.991	0.191	2.388	0.540	0.889	0.333	1.586	0.471	1.086		
61	2.980	-1.575	1.449	-0.535	0.520	0.943	0.459	1.123	2.019	-1.014	1.538	-0.621	0.514	0.960		
62	0.992	0.012	0.980	0.029	0.509	0.974	0.227	2.139	2.641	-1.401	0.424	1.238	0.098	3.351		
63	0.705	0.504	0.549	0.865	0.260	1.943	0.081	3.626	0.323	1.630	0.824	0.279	0.082	3.608		
64	0.597	0.744	0.695	0.525	0.224	2.158	0.074	3.756	1.656	-0.728	2.248	-1.169	0.057	4.133		
65	0.367	1.446	0.232	2.108	0.423	1.241	0.070	3.837	0.724	0.466	0.306	1.708	1.821	-0.865		
66	1.393	-0.478	0.520	0.943	0.432	1.211	0.581	0.783	1.627	-0.702	0.842	0.248	0.175	2.515		
67	0.538	0.894	0.354	1.498	0.533	0.908	0.131	2.932	0.873	0.196	0.567	0.819	0.623	0.683		
68	0.458	1.127	0.548	0.868	0.343	1.544	0.082	3.608	0.648	0.626	0.574	0.801	0.051	4.293		
69	0.926	0.111	0.791	0.338	0.444	1.171	0.044	4.506	0.389	1.362	0.286	1.806	0.087	3.523		
70	0.515	0.957	1.122	-0.166	0.415	1.269	0.127	2.977	0.362	1.466	0.545	0.876	0.104	3.265		

Sample Count	GRAIN SIZE MEASUREMENTS (mm)													
	559		560		561		562		563		564		565	
	Framework	Fmwk Phi	Framework	Fmwk Phi	Framework	Fmwk Phi	Framework	Fmwk Phi	Framework	Fmwk Phi	Framework	Fmwk Phi	Framework	Fmwk Phi
71	0.712	0.490	1.898	-0.924	0.602	0.732	0.402	1.315	2.482	-1.312	3.187	-1.672	0.083	3.591
72	0.507	0.980	0.585	0.773	0.404	1.308	0.264	1.921	0.538	0.894	0.454	1.139	0.362	1.466
73	0.365	1.454	0.508	0.977	0.298	1.747	0.127	2.977	0.805	0.313	0.982	0.026	0.090	3.474
74	0.352	1.506	1.418	-0.504	0.488	1.035	0.043	4.540	0.505	0.986	0.992	0.012	0.117	3.095
75	0.579	0.788	0.687	0.542	0.429	1.221	0.119	3.071	0.377	1.407	0.469	1.092	0.109	3.198
76	1.475	-0.561	1.701	-0.766	0.497	1.009	0.419	1.255	1.363	-0.447	1.653	-0.725	0.631	0.664
77	1.115	-0.157	0.518	0.949	0.289	1.791	0.059	4.083	0.593	0.754	0.486	1.041	0.224	2.158
78	0.378	1.404	1.069	-0.096	0.434	1.204	0.124	3.012	0.623	0.683	1.266	-0.340	0.049	4.351
79	0.855	0.226	0.570	0.811	0.249	2.006	0.049	4.351	2.759	-1.464	0.392	1.351	0.091	3.458
80	2.480	-1.310	0.578	0.791	0.327	1.613	0.056	4.158	0.270	1.889	0.941	0.088	0.053	4.238
81	0.790	0.340	5.611	-2.488	0.949	0.076	0.496	1.012	0.796	0.329	0.394	1.344	0.149	2.747
82	0.673	0.571	0.672	0.573	0.574	0.801	0.120	3.059	0.400	1.322	0.556	0.847	0.098	3.351
83	0.451	1.149	0.579	0.788	0.374	1.419	0.101	3.308	0.329	1.604	1.046	-0.065	0.219	2.191
84	3.801	-1.926	1.077	-0.107	0.270	1.889	0.074	3.756	0.249	2.006	0.507	0.980	0.070	3.837
85	1.380	-0.465	1.579	-0.659	0.366	1.450	0.117	3.095	0.761	0.394	0.623	0.683	0.033	4.921
86	0.883	0.180	0.508	0.977	0.307	1.704	0.534	0.905	0.944	0.083	2.881	-1.527	1.346	-0.429
87	2.135	-1.094	0.694	0.527	0.261	1.938	0.183	2.450	0.344	1.540	0.716	0.482	0.254	1.977
88	0.447	1.162	0.639	0.646	0.287	1.801	0.081	3.626	0.630	0.667	0.945	0.082	0.045	4.474
89	0.605	0.725	1.231	-0.300	0.254	1.977	0.042	4.573	0.329	1.604	0.415	1.269	0.065	3.943
90	2.691	-1.428	5.202	-2.379	0.354	1.498	0.107	3.224	1.841	-0.880	0.492	1.023	0.090	3.474
91	0.915	0.128	1.336	-0.418	0.696	0.523	0.142	2.816	0.631	0.664	0.956	0.065	0.058	4.108
92	2.802	-1.486	0.934	0.099	0.362	1.466	0.117	3.095	0.388	1.366	2.345	-1.230	0.542	0.884
93	0.617	0.697	0.510	0.971	0.351	1.510	0.179	2.482	0.947	0.079	0.448	1.158	0.092	3.442
94	0.473	1.080	0.414	1.272	0.225	2.152	0.083	3.591	0.417	1.262	0.538	0.894	0.262	1.932
95	1.287	-0.364	0.788	0.344	0.459	1.123	0.141	2.826	0.309	1.694	0.846	0.241	0.069	3.857
96	0.624	0.680	6.545	-2.710	0.363	1.462	0.167	2.582	1.024	-0.034	1.139	-0.188	0.077	3.699
97	0.706	0.502	0.497	1.009	0.418	1.258	0.176	2.506	0.484	1.047	0.515	0.957	0.648	0.626
98	0.648	0.626	0.555	0.849	0.433	1.208	0.389	1.362	0.443	1.175	1.035	-0.050	0.092	3.442
99	0.290	1.786	1.349	-0.432	0.240	2.059	0.123	3.023	0.956	0.065	0.449	1.155	0.038	4.718
100	0.993	0.010	0.564	0.826	0.425	1.234	0.009	6.796	0.246	2.023	0.286	1.806	0.046	4.442